



Project Title:

## Innovative compact HYbrid electrical/thermal storage systems for low energy BUILDings

Project Acronym:

**HYBUILD**

# Deliverable Report

Deliverable number:

**D2.2**

Deliverable title:

## Low & high temperature latent storage realized

<b>Related task:</b>	2.2
<b>Lead beneficiary:</b>	CNR
<b>Authors and institutions:</b>	UDL - Gabriel Zsembinski, David Vérez, Luisa F. Cabeza AIT - Tilman Barz, Klemens Marx, Judit Aizpuru, Johann Emhofer AKG - Andreas Strehlow, Birgo Nitsch, Katerina Hatesuer CNR - Andrea Frazzica, Valeria Palomba
<b>Due date:</b>	30 <sup>th</sup> of September 2019

### DISSEMINATION LEVEL

PU	Public, fully open, e.g. web	X
CO	Confidential, restricted under conditions set out in Model Grant Agreement	
CI	Classified, information as referred to in Commission Decision 2001/844/EC.	



*This project has received funding from the European Union's Horizon 2020 research and innovation programme under grant agreement No 768824.*

*The content of this document reflects only the author's view and the Commission is not responsible for any use that may be made of the information it contains.*

DOCUMENT STATUS HISTORY		
Date	Description	Partner
2019/08/28	Draft v1	AKG
2019/08/29	Draft v2	UDL
2019/08/29	Draft v3	AKG
2019/08/30	Draft v4	AIT
2019/09/03	Finalized version	CNR
2021/03/25	Reviewed	AIT, CNR, AKG, UDL
2021/03/31	Accepted	COMSA

# Table of contents

<b>Publishable executive summary</b> .....	<b>5</b>
<b>Acronyms and Abbreviations</b> .....	<b>7</b>
<b>1 Introduction</b> .....	<b>8</b>
1.1 Aims and objectives .....	8
1.2 Relations to other activities in the project .....	8
1.3 Report structure .....	8
1.4 Contributions of partners .....	8
<b>2 Description of the latent storage concept</b> .....	<b>9</b>
<b>3 Identification of suitable PCMs</b> .....	<b>11</b>
3.1 Introduction .....	11
3.2 Identification of PCM for low temperature storage .....	11
3.3 Identification of PCM for high temperature storage .....	14
<b>4 Basic components design</b> .....	<b>20</b>
4.1 Detailed model-based design .....	20
4.1.1 Calculation of heat transfer .....	22
4.1.2 Calculation of pressure drop:.....	22
4.1.3 Design considerations for an RPW-HEX .....	24
4.2 Lab-scale latent storages manufacturing.....	26
4.2.1 2-Fluid water/PCM for SOC analysis .....	27
4.2.2 3-fluid RPW-HEX-1, first MED design .....	27
4.2.3 3-fluid RPW-HEX-2, first CON design 2 PCM .....	27
4.2.4 3-fluid RPW-HEX-3, second MED design .....	28
4.2.5 2-fluid W/PCM storage .....	29
4.2.6 2-fluid Water-PCM test cubes .....	30
4.3 Lab-scale latent storage testing.....	30
4.3.1 Low temperature latent storage lab-testing.....	30
4.3.2 High temperature latent storage lab-testing.....	41
<b>5 Full-scale latent storages design and manufacturing</b> .....	<b>55</b>
5.1.1 Low temperature full-scale latent storage design .....	55
5.1.2 High temperature full-scale latent storage design .....	56
5.1.3 Full-scale latent storages manufacturing.....	58
<b>6 Latent storage advanced monitoring algorithms</b> .....	<b>62</b>

6.1 Analysis of RPW-HEX storage capacity as a function of its charging/discharging operating range.....	63
6.1.1 PCM solid/liquid phase transition temperature range .....	63
6.1.2 RPW-HEX energy absorption/release .....	64
6.1.3 PCM density changes .....	65
6.1.4 Experimental tests for the monitoring of the SOC with the low temperature lab-scale 2-fluid HEX.....	66
6.1.5 Experimental tests for the monitoring of the SOC with the full-scale lab prototype for the CONT system.....	68
6.1.6 Conclusions/ recommendations .....	72
<b>7 Conclusions.....</b>	<b>75</b>
<b>8 References.....</b>	<b>76</b>

## Publishable executive summary

HYBUILD is an EU Horizon 2020 - funded project, led by COMSA Corporación, which will develop two innovative compact hybrid electrical/thermal storage systems for stand-alone and district connected buildings.

The present deliverable describes the activity of T2.2, regarding the development of high-temperature and low-temperature thermal storages in the HYBUILD solution. The high temperature heat storage was specifically developed for the application in the Continental HYBUILD system, and is integrated in the hot refrigerant flow exiting the compressor of a compression HP on the primary side and in the process water flow on the secondary side. The main purpose of the storage is to deliver Domestic Hot Water (DHW) to decentralized DHW storages located in the individual apartments of a multi-family house. Furthermore, it adds the necessary flexibility by decoupling the high temperature high power energy streams (for DHW generation) and the low temperature and low power energy stream (for space heating).

The low temperature heat storage, specifically developed for the Mediterranean HYBUILD system, is meant to store the cooling energy at the evaporator of the Heat Pump (HP), thus extending the operating hour of the cooling system or allowing to shift the operation of heat pump in hours where electricity production is cheaper or more efficient. The RPW-HEX is integrated as a secondary evaporator unit in the HP.

The heat storage technology selected is latent heat thermal energy storage. The key idea is to optimally use the available exergy of the refrigerant during operation all over the year. This goal is accomplished by the optimal assignment of high and low temperature heat during conventional HP operation. It is realized by a refrigerant (R)/water (W) heat exchanger (HEX) with phase (P) change material – in short: RPW-HEX.

The first phase in the development of the RPW-HEX was the selection of the most adequate PCMs for the two applications by UDL, by defining the constraints and requirements for the operation in the two cases. A research on available PCMs both in the literature and on the market, was carried out. Next, a decision matrix was developed taking into account the following parameters related to the PCM candidates: phase change range, melting enthalpy, availability, and price. These parameters were chosen because of their direct impact on the system viability from the operational and economic points of view, and the relative easiness in obtaining their values. A score was given to each of the PCM candidate for each of the above decision parameter, and a total score was calculated based on a weighted average. RT4 from Rubitherm was the PCM selected for the Mediterranean low temperature storage, whereas for the Continental high temperature storage RT64HC from Rubitherm was chosen.



Subsequently, several small-scale RPW-HEXs were manufactured by AKG and shipped to UDL and AIT for lab testing. Heat transfer and pressure drops in several designs were calculated by using literature or specific equations developed by AKG and used to optimise the lab-scale storages manufactured. The

tests done were focused on three main different aspects:

- Evaluate the behaviour of the RPW-HEX in different operating conditions;
- Identify the most appropriate methodology to measure the state of charge (SOC) of the storage;

- Guide the design, manufacturing and operation of the full-scale storages to be installed in the demo sites.

The main features of the full-scale low temperature storage are:

	refrigerant	coolant	PCM (RT4)
Number of passages	20	20	42
Fin #	73	18	33
Fluid volume in /	5.34	4.6	46
core length x width x depth in <i>mm</i>	1000 x 585 x 160		
empty weight in <i>kg</i> (Al)	190		

Instead, the main features of the full-scale high temperature storage are:

	refrigerant	coolant	PCM (RT64HC)
Number of passages	21	22	42
Fin #	73	18	33
Fluid volume in /	5,6	5	46
core length x width x depth in <i>mm</i>	1000 x 594 x 160		
Empty weight in <i>kg</i> (Al)	110		

Regarding the evaluation of the SOC, 4 different methods were tested and analysed. Outcome of the analysis was that the method based on pressure measurements inside the PCM cavity can be applied to estimate the SOC of the HEX because there is a direct relation between the pressure and the state of the PCM.

## Acronyms and Abbreviations

<b>Nomenclature</b>	
$d_h$	Hydraulic diameter, m
E	Energy, J
f	Friction factor
Fr	Froude Number
g	Gravity constant, m <sup>2</sup> /s
$\dot{G}$	Mass flow density, kg/(s m <sup>2</sup> )
h	Enthalpy, J
j	Colburn factor
L	Length, m
M	Mass, kg
Nu	Nusselt Number
p	Pressure, bar
Pr	Prandtl Number
Re	Reynolds Number
t	Time, s
T	Temperature, °C
V	volume
$\alpha$	Heat Transfer Coefficient, W/(m <sup>2</sup> K)
$\varepsilon$	displacement
$\lambda$	Thermal conductivity, W/(mK)
$\xi$	Liquid mass fraction
$\eta$	Viscosity, Pa s
$\rho$	Density, kg/m <sup>3</sup>
$\Theta_{ref}$	Reference temperature, °C
<b>Subscripts and superscripts</b>	
in	inlet
l	liquid
out	outlet
ref	reference
s	solid
<b>Abbreviations</b>	
CONT	Continental
DSC	Differential Scanning Calorimeter
HEX	Heat Exchanger
HTF	Heat Transfer Fluid
MED	Mediterranean
PCM	Phase Change Material
RPW	Refrigerant-PCM-Water
SOC	State of Charge

## 1 Introduction

### 1.1 Aims and objectives

The present deliverable describes the overall development of the latent thermal energy storage system for low temperature (Mediterranean HYBUILD solution) and high temperature (Continental HYBUILD solution). At first, the constraints and requirements for PCMs were identified and, according to a specific methodology, the PCM candidates for both applications were identified and characterized. The design of the latent heat storage was accomplished by coupling modelling through numerical correlations and experimental activity on different test modules. Finally, advanced process monitoring algorithms for online estimation of state of charge (SOC) were developed, with the aim of providing key variables for the smart high-level control strategy (BEMS) of the complete building system.

### 1.2 Relations to other activities in the project

The activity presented here was done in the framework of Task 2.2. The full-scale storages developed will be tested in the framework of WP3 and subsequently used for the installation in demo sites (WP6). The monitoring procedure developed will be used for the implementation of the low-level and high-level controls in WP4.

### 1.3 Report structure

The present report is structured as follows:

- Section 2 presents the description of the latent storage developed;
- Section 3 presents the methodology used for the selection of the PCMs for the Mediterranean and Continental system;
- Section 4 presents the design and manufacturing of the various storages tested;
- Section 5 presents the design of the full-scale latent storage for installation in demo sites;
- Section 6 presents the activity for the calculation of the State of Charge of the storage from measurable data.

### 1.4 Contributions of partners

UDL selected the PCMs and characterized the materials chosen for the application in the Mediterranean and Continental system and tested the lab-scale systems for Mediterranean application. AKG manufactured all the heat exchangers for the latent storages in both lab-scale and full-scale size; AIT tested the lab-scale system for Continental applications. CNR supervised the development activity and supported the deliverable preparation.

## 2 Description of the latent storage concept

Today's commercially available air source HPs work highly efficient and make a valuable contribution to reach climatic goals as the reduction of CO<sub>2</sub> in our atmosphere. To further increase the efficiency of HPs many different concepts using latent heat thermal energy storage technologies were proposed recently. The aim is to decrease the size of buffer tanks and to avoid the oversizing of HPs reducing thermal peak loads by shifting heating and cooling demands in time [1], to optimize integration of solar thermal collectors[2], to enhance the storage density of DHW storages [3] or to enhance the defrosting performance of air source HPs [4]. Recent studies showed further that a wide spectrum of PCMs are available to be used in such storages at different temperature levels [5].

Within HYBUILD, latent heat thermal energy storage technology is employed to increase the efficiency of HP systems in multi-family houses. The key idea is to optimally use the available exergy of the refrigerant during operation all over the year. This goal is accomplished by the optimal assignment of high and low temperature heat during conventional HP operation. It is realized by a refrigerant (R)/water (W) heat exchanger (HEX) with phase (P) change material – in short: RPW-HEX.

For the MED system this means that the cooling energy at the evaporator of the HP can be stored for extending the operating hour of the HP or to shift the operation of the HP in hours where electricity production is cheaper or more efficient. The RPW-HEX is integrated as a secondary evaporator unit in the HP. On the primary (refrigerant) side, 3-way motorised valves allow switching from the standard evaporator to the RPW-HEX. On the secondary side, the evaporator is connected to the chilled water circuit of the fan coils, representing the user to which cooling energy has to be provided.

For the CONT system this means that, high temperature thermal energy delivered at the superheated section of the HP cycle is stored in a PCM. Rather than using this energy at intermediate temperatures for heating (state-of-the-art) or even wasting it in case of HP cooling operation, this energy is stored and used later for high temperature DHW generation.

The compact RPW-HEX is integrated in the hot refrigerant flow exiting the compressor of a compression HP on the primary side and in the process water flow on the secondary side. From the secondary side of the RPW-HEX, the process water delivers the thermal energy to decentralized DHW storages located in the individual apartments of a multi-family house. The RPW-HEX also manages flexible DHW demands and by this minimizes the operation of the air source HP in the highly non-efficient direct DHW operating mode. Furthermore, it adds the necessary flexibility by decoupling the high temperature high power energy streams (for DHW generation) and the low temperature and low power energy stream (for heating). To guarantee high heat transfer coefficients between the hot gaseous refrigerant and the PCM, between the PCM and the process water and between the refrigerant and the process water, with a minimum of refrigerant mass, a plate and fin aluminium heat exchanger design is used.

Figure 1 exemplarily shows the concept for the CONT system for an application with three apartments located in average climate conditions in Europe and an air source HP.

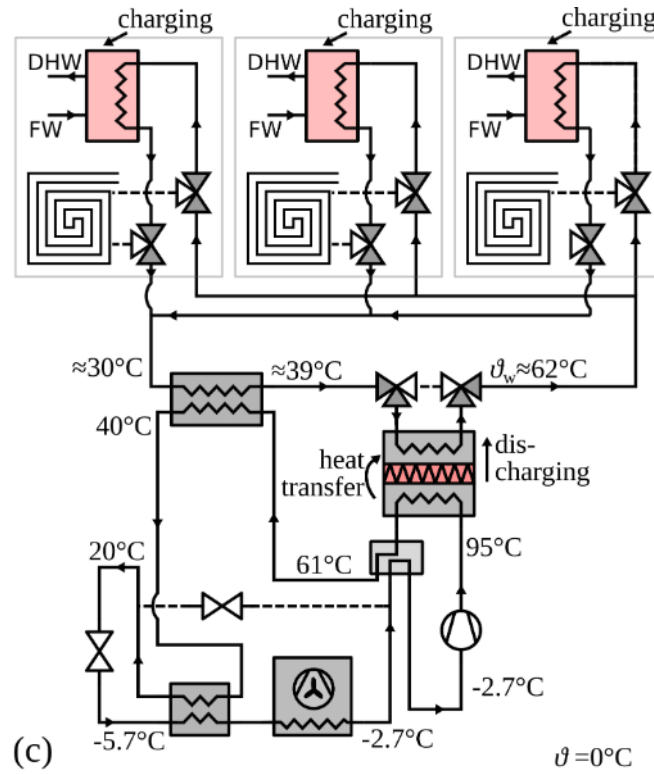


Figure 1. Concept for the integration of the latent thermal energy storage for the CONT system for a scenario with three apartments. The main purpose is heating in winter and DHW generation all over the year. Through switching into reverse mode, cooling during summer is also possible. Valve positions indicate the operation for energy efficient DHW generation by discharging the RPW-HEX. Temperatures refer to the system state shortly after switching from heating operation to the operation shown in this figure. The ambient temperature is assumed equal  $0^\circ\text{C}$ . [6]

### 3 Identification of suitable PCMs

#### 3.1 Introduction

The PCM selection procedure becomes a crucial step for the optimum operation of any TES component and the associated thermal processes. An important aspect within this procedure is the identification of the critical parameters and requirements, which are not always easy to identify and are sometimes in conflict with each other. In latent heat TES systems, the values of the phase change temperature and enthalpy are the most widely used selection criteria. However, other properties such as health hazard, corrosion, cost, availability of the material, and thermal and cycling stability should also be taken into account to broaden the abovementioned selection criteria [7,8]

Gasia et al. [7] and Miró et al. [8] proposed a methodology for a proper PCM selection. This methodology needs a high number of experiments such as thermal and cycling stability tests. Therefore, a preliminary selection based on information provided by the PCM supplier was needed before a deeper experimental analysis of the most promising PCM candidates was performed.

On one hand, the system requirements restrict the phase change temperature of the possible PCM candidates, the maximum temperature that the PCM must stand, and its compatibility with aluminium. On the other hand, the general features that should usually be fulfilled by a PCM should also be taken into account: high phase change enthalpy, narrow phase change range, low or no subcooling, no hysteresis, high thermal conductivity, high density, availability, no or low toxicity, and low cost.

At the very incipient stage of the project, the characteristics of the boundary conditions and the operating temperatures of the latent heat TES components in both systems required that the selected PCM should have a phase change temperature ranged between 0 °C and 7 °C for the Mediterranean concept, and between 48 °C and 68 °C for the Continental concept.

The objective of this section is to present the methodology applied for the selection of the most appropriate PCM to be used in the latent heat TES of the Mediterranean and of the Continental systems, as well as the main results obtained.

#### 3.2 Identification of PCM for low temperature storage

Currently, there are few reviews in the literature covering the temperature range for the Mediterranean system [9,10]. Moreover, not all existing PCM within this range are available in these reviews. Therefore, in order to broaden and update the list of all PCM available with a phase change temperature between 0 °C and 7 °C, a new literature review was done.

Around 60 PCM candidates potentially suitable to be used in the low temperature storage were found. Given the relatively large number of possible PCM candidates, a pre-selection was performed in order to exclude those PCM that could not be selected taking into account some properties such as health hazard, corrosion with aluminium, availability, or phase change enthalpy. To further reduce the number of most promising PCM candidates, only those PCM with phase change temperature close to the most desirable phase change temperature range (around 2 °C to 4 °C) were taken into account. The list pre-selected PCM candidates for the Mediterranean system are shown in Table 1.

**Table 1. List of pre-selected available PCM for the Mediterranean system and some of their thermophysical properties according to the literature**

Commercial name/Composition	Type	T <sub>m</sub> (°C)	ΔH (kJ/kg)	k (W/m·K)	ρ (kg/m <sup>3</sup> )	Reference
RT3HC_1	Organic (paraffin)	1-3	190	0.20 (l) 0.20 (s)	770 (l) 880 (s)	[11]
A3	Organic (n.a.)	3	200	0.210	765	[12]
0200- Q2 BioPCM	Organic (bioPCM)	2	200-230	0.2-0.7 (l) 0.25-2.5 (s)	850-1300 (l) 900-1250 (s)	[13]
PCM-PDR03P	Organic (n.a.)	3.5	185	n.a. <sup>1</sup>	570	[14]
savE OM 03	Organic (n.a.)	3.5	229	0.224 (l) 0.146 (l)	835 (l) 912 (s)	[15]
Caprylic acid + lauric acid (9:1 by mol)	Organic eutectic (fatty acid)	3.8	151.5	n.a.	n.a.	[16]
RT4	Organic (paraffin)	2-4	175	0.20 (l) 0.20 (s)	770 (l) 880 (s)	[11]
0200- Q4 BioPCM	Organic (bioPCM)	4	200-230	0.2-0.7 (l) 0.25-2.5 (s)	850-1300 (l) 900-1250 (s)	[13]
PureTemp 4	Organic (biobased)	4	195	n.a.	n.a.	[17]
Tetrahydrofuran clathrate hydrate	Inorganic (clathrate hydrate)	4.4	255	n.a.	n.a.	[18]

Next, a decision matrix was developed taking into account the following parameters related to the PCM candidates: phase change range, melting enthalpy, availability, and price. These parameters were chosen because of their direct impact on the system viability from the operational and economic points of view, and the relative easiness in obtaining their values. A score was given to each of the PCM candidate for each of the above decision parameter, and a total score was calculated based on a weighted average. The weight assigned to each parameter was selected based on the importance that the researchers from UDL considered that they could have on the final decision. However, a sensibility analysis is recommended to study the influence of varying the different weights on the results, which is currently being performed and it is intended to be published in a journal paper that is in preparation.

The weights assigned to the decision parameters are listed in Table 2. The score given to each of the decision parameter was calculated taking into account the criteria shown in Table 3.

<sup>1</sup> n.a. – not available

**Table 2. Weights assigned to each decision parameter of the Mediterranean system.**

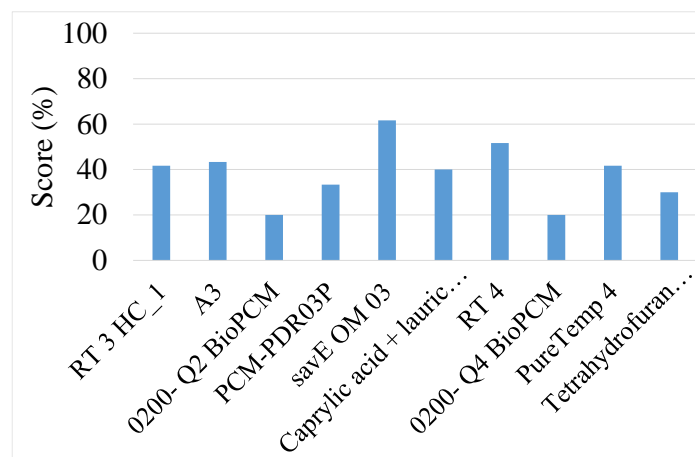
Decision parameter	Weight (%)
Phase change temperature range (Cp-T curve)	25
Enthalpy	30
Availability	15
Price	30
Total	100

**Table 3. Scoring criteria applied to each decision parameter of the Mediterranean system.**

Temperature range (°C)		Enthalpy (kJ/kg)		Availability		Price (€/kg)	
<2	3	>250	3	Yes	3	<2.5	3
2<T<3	2	200<h<250	2	No	0	2.5<P<5	2
3<T<4	1	150<h<200	1	---	---	5<P<10	1
>4 or n.a.	0	<150 or n.a.	0	---	---	>10 or n.a.	0

The results of applying the decision matrix described in Table 2 and the scoring criteria of Table 3 are shown in Figure 2 [19]. For the temperature range of interest, the best candidate is the save OM 03 commercial product from PLUS<sup>®</sup> [15], a manufacturer from India. However, since the transportation costs and any potential additional costs were not taken into consideration in the decision matrix, the results may be different and the best solution can consequently also change. A promising alternative to the save OM 03 candidate is RT4 from Rubitherm.

Furthermore, both PCM from Rubitherm (RT3HC and RT4) were characterized in the laboratory and the results of the Differential Scanning Calorimeter (DSC) analysis are shown in Figure 3 [19].


**Figure 2. Score obtained by each of the pre-selected PCM candidates for the Mediterranean system [19]**

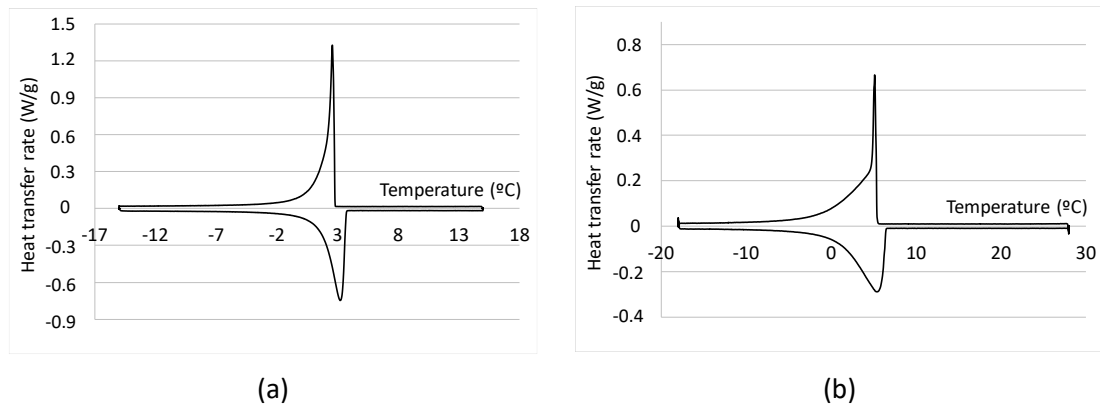


Figure 3. DSC analysis of the Rubitherm PCM for the Mediterranean system obtained at UDL laboratory. (a) RT3HC; (b) RT4 [19]

### 3.3 Identification of PCM for high temperature storage

A literature review was also done to find suitable PCM candidates for the Continental latent heat TES component, with melting temperature in the range between 48 °C and 68 °C. As a result, more than 120 potential PCM candidates were initially found, which is even much higher than the number found in the Mediterranean case. Therefore, a pre-selection was also applied in this case to first exclude those PCM candidates that were either corrosive with aluminium, or had very low phase change enthalpy, or bad thermo-physical properties, or were not available. Likewise, in the case of different PCM of the same type or with similar thermophysical properties, only the most suitable of them was chosen. To further reduce the number of suitable PCM candidates, only those PCM with phase change temperature around different values (50 °C, 55 °C, 60 °C, and 65 °C) were included. After applying all these criteria, the pre-selected PCM candidates for the Continental system are shown in Table 4.

Table 4. Pre-selected available PCM for the Continental system and some of their thermophysical properties as given by the manufacturer

Commercial name/Composition	Type	$T_m$ (°C)	$\Delta H$ (kJ/kg)	$k$ (W/m·K)	$\rho$ (kg/m <sup>3</sup> )	Ref.
A50	Organic (n.a.)	50	218	0.18	810	[12]
0500- Q50 BioPCM	Organic (bioPCM)	50	200-230	0.2-0.7 (l) 0.25-2.5 (s)	850-1300 (l) 900-1250 (s)	[13]
save OM50	Organic (fatty acids mixture)	50-51	223	0.14 (l) 0.21 (s)	859 (l) 961 (s)	[15]
RT54HC	Organic (paraffin)	53-54	200	0.2	800 (l) 850 (s)	[11]
Stearic acid (CH <sub>3</sub> (CH <sub>2</sub> ) <sub>16</sub> -COOH)	Organic (fatty acid)	54	157	0.17 (l) 0.29 (s)	940 (s)	[20]

Cetyl stearate	Organic (ester)	54.6	212.1–216.3	n.a.	n.a.	[18]
savE OM 55	Organic (mixture of fatty acids)	55	208	0.16 (l) 0.1 (s)	841 (l) 935 (s)	[15]
0500- Q56 BioPCM	Organic (bioPCM)	56	200-230	0.2-0.7 (l) 0.25-2.5 (s)	850-1300 (l) 900-1250 (s)	[13]
Tristearin ((C <sub>17</sub> H <sub>35</sub> COO) <sub>3</sub> C <sub>3</sub> H <sub>5</sub> )	Organic	56	190.8	n.a.	862 (l)	[18]
PureTemp 58	Organic (bio-based)	58	225	0.15 (l) 0.25 (s)	810 (l) 890 (s)	[17]
A58H	Organic (n.a.)	58	243	0.18	820	[12]
66.7% Polyethylene oxide 10000 + 33.3% Myristic acid	Organic (plastic + fatty acid)	58.7	191	n.a.	n.a.	[21]
Climsel C58	Inorganic (salt hydrate)	58	259	1.46	n.a.	[22,23]
		55-58	260	0.47 (l) 0.57 (s)	1400	[24]
		58	80	0.5–0.7	1460	[25]
THP 5860	Organic (paraffin)	55–60	153	n.a.	n.a.	(own measurements)
Paraffin C27	Organic (paraffin)	58.8	236	n.a.	n.a.	[26]
RT60	Organic (paraffin)	58–60	214	0.2	n.a.	[25]
Stearyl stearate	Organic (ester)	59.2	214.75 – 214.93	n.a.	n.a.	[18]
PureTemp 63	Organic (bio based)	63	206	0.15 (l) 0.25 (s)	840 (l) 920 (s)	[17]
RT64HC	Organic (n.a.)	63-65	250	0.2	780 (l) 880 (s)	[11]
Stearyl arachidate (C <sub>38</sub> H <sub>76</sub> O <sub>2</sub> )	Organic (ester)	64.9 6	226	n.a.	2350 (l) 1930 (s)	[18]

50% CH <sub>3</sub> CONH <sub>2</sub> + 50% C <sub>17</sub> H <sub>35</sub> COOH	Organic (eutectic)	65	218	n.a.	n.a.	[26]
0500- Q65 BioPCM	Organic (bioPCM)	65	200- 230	0.2-0.7 (l) 0.25-2.5 (s)	850-1300 (l) 900-1250 (s)	[13]
savE FS 65	Organic (blend of organic material in polymer matrix)	66- 68	218	0.25 (s)	842 (s)	[15]
PureTemp 68	Organic (bio based)	68	213	0.15 (l) 0.25 (s)	870 (l) 960 (s)	[17]
0500- Q68 BioPCM	Organic (bioPCM)	68	200- 235	0.2-0.7 (l) 0.25-2.5 (s)	850-1300 (l) 900-1250 (s)	[13]

Following the same methodology as in the Mediterranean case, a decision matrix was developed taking into account the following parameters: phase change range, melting enthalpy, availability, price, and maximum temperature that the PCM can stand. This last criterion is particularly important in this system because the latent storage of the Continental system is located at the compressor outlet, so that the PCM may be heated by the hot vapour refrigerant to around 120 °C, which is the maximum temperature of the refrigerant at the compressor exit. A score was given to each of the PCM candidate for each of the above decision parameter, and a total score was calculated based on a weighted average.

The weights assigned to the decision parameters of the Continental system are listed in Table 5. The score given to each of the decision parameter was calculated taking into account the criteria shown in Table 6.

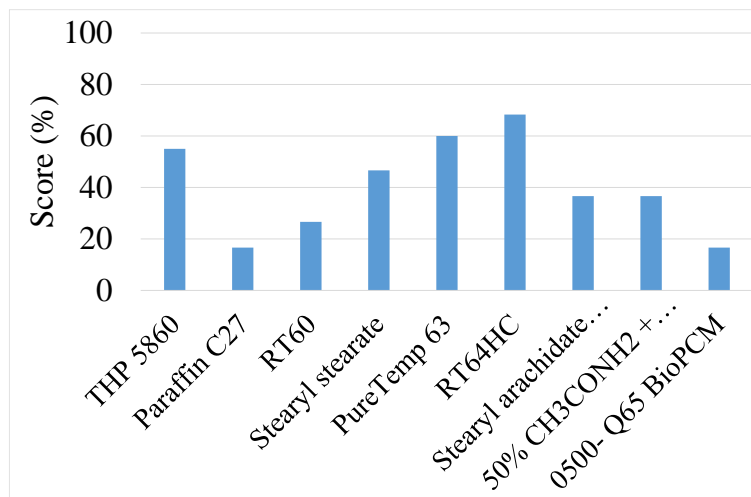
**Table 5. Weights assigned to each decision parameter of the Continental system.**

Decision parameter	Weight (%)
Phase change temperature range (Cp-T curve)	20
Enthalpy	25
Availability	10
Price	25
Maximum working temperature	20
Total	100

**Table 6. Scoring criteria applied to each decision parameter of the Continental system.**

Temperature range (°C)		Enthalpy (kJ/kg)		Availability		Price (€/kg)		Maximum temperature (°C)	
<2	3	>250	3	Yes	3	<2.5	3	>120	3
2<T<3	2	200<h<250	2	No	0	2.5<P<5	2	<120 or n.a.	0
3<T<4	1	150<h<200	1	---	---	5<P<10	1	---	---
>4 or n.a.	0	<150 or n.a.	0	---	---	>10 or n.a.	0	---	---

According to the latest simulations performed within WP3 activities, the most promising phase change temperature range for the PCM to be used in the Continental latent heat TES is between 60°C and 65 °C. Therefore, the decision matrix described in Table 5 and the scoring criteria of Table 6 were only applied to those PCM candidates with phase change temperature within this range, and the results are shown in Figure 4 [19].


**Figure 4. Score obtained by each of the pre-selected PCM candidate for the Continental system [19]**

The best three PCM candidates, RT64HC, PureTemp63, and TH5860, were characterized in the laboratory. Figure 5 shows the results of the DSC analysis of different cycled PCM samples after 0, 10, 100, 1000, and 8000 cycles.

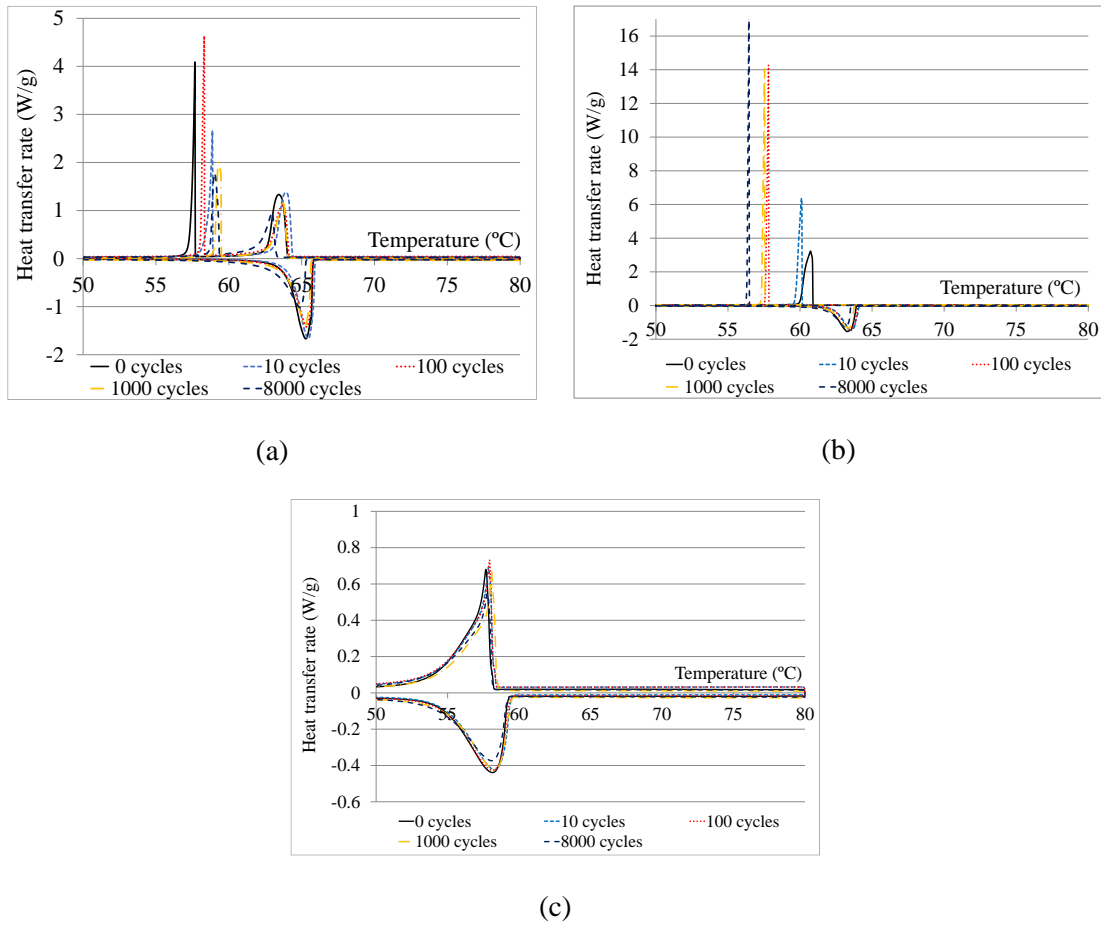
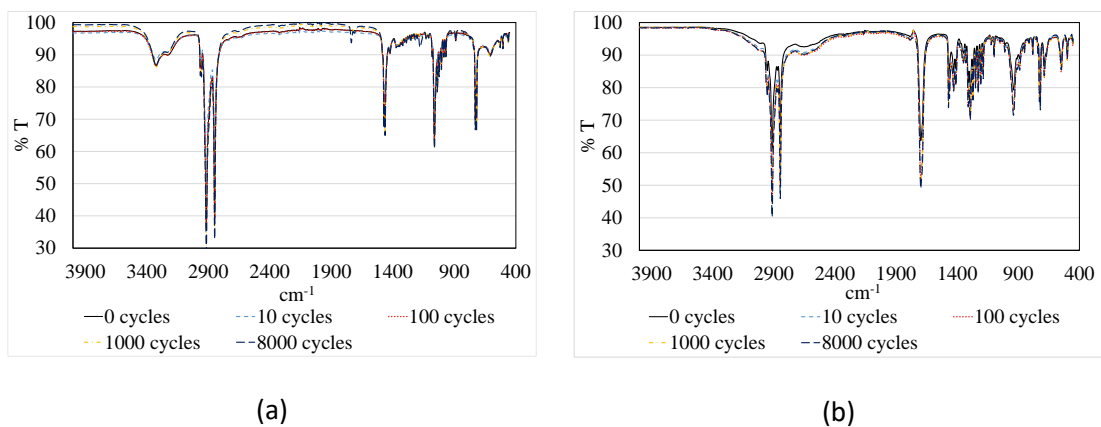
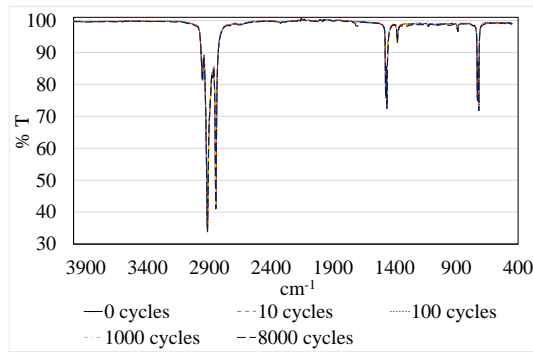


Figure 5. DSC analysis of the cycled PCM at the UDL laboratories. (a) RT64HC; (b) PureTemp 63; (c) THP5860 [19].

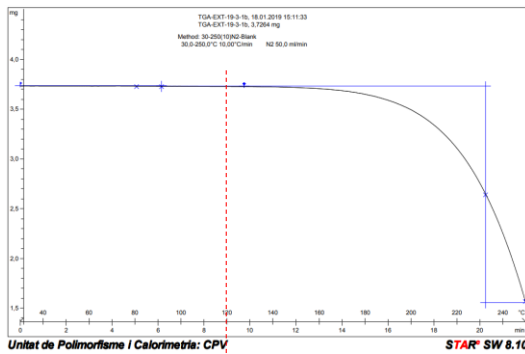
Figure 6 and Figure 7 show, respectively, the results of the Fourier transformed-infrared analysis (FT-IR) and thermogravimetric analysis (TGA) of the same PCM candidates and for the different cycled samples after 0, 10, 100, 1000, and 8000 cycles.



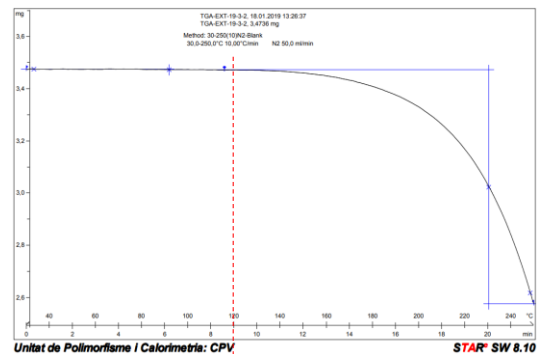


(c)

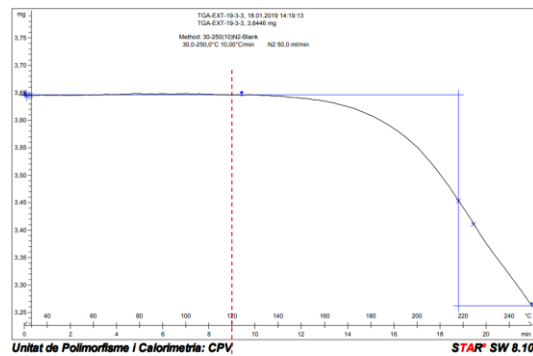
Figure 6. FT-IR analysis of the cycled PCM at UDL laboratories. (a) RT64HC; (b) PureTemp 63; (c) THP5860 [19].



(a)



(b)



(c)

Figure 7. TGA analysis of the cycled PCM at UDL laboratories. (a) RT64HC; (b) PureTemp 63; (c) THP5860 [19].

The mass loss of RT64 and PureTemp 63 at 120 °C are 0.13% and 0.09%, respectively, while THP5860 does not lose weight until the temperature reaches around 135 °C.

In view of the results of the decision matrix and the characterization carried out in the laboratory, the most suitable PCM candidate for the Continental system is RT64HC from Rubitherm.

## 4 Basic components design

### 4.1 Detailed model-based design

AKG is manufacturing heat exchangers with integrated PCM-passages since several years. Best results were achieved with an offset-fin that is dense enough to allow good contact to the PCM and high enough to hold as much PCM as possible. The chosen fin 33 is shown in Figure 8. The dense geometry and rather strong material also provide good mechanical stability to withstand stresses from density changes resulting from the phase change of the PCM.

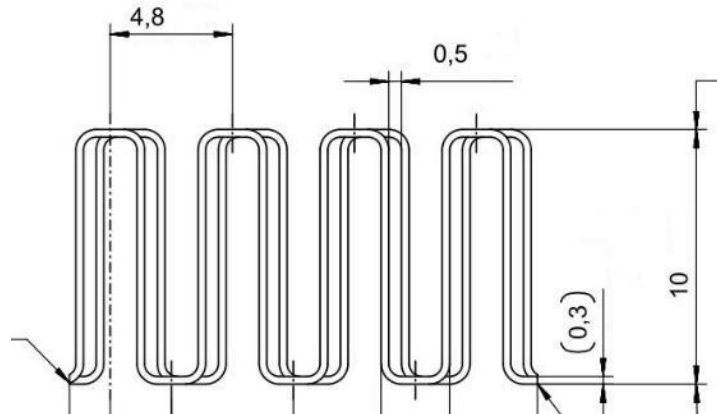


Figure 8: PCM-fin 33

The requirement for the refrigerant passage is dominated by the mechanical stability to withstand the operating pressures of the refrigerant. One option is AKG's offset-fin 43 (Figure 9), which also provides a very good thermal performance at moderate pressure losses. An even stronger alternative for the refrigerant side is fin 73, which uses even thicker material (Figure 10).

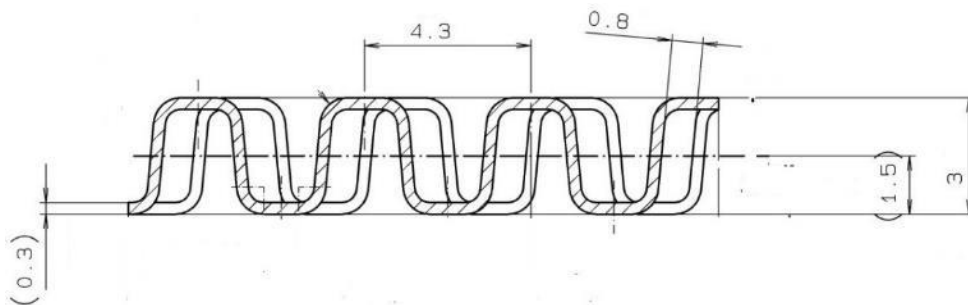


Figure 9: Fin 43 used for refrigerant and water passages

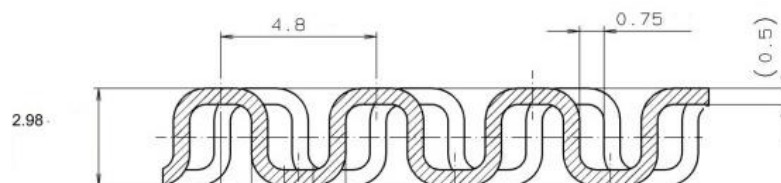


Figure 10: Fin 73 used for refrigerant

Fin 43 may also be used for the coolant passages. But if the flow rates are not high also the more compact 2mm high fin 18 (Figure 11) may be used.

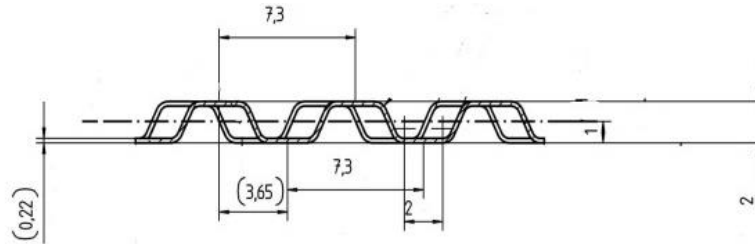


Figure 11: Fin 18 used for refrigerant and water passages

Table 7 shows the boundary conditions for the different versions of the RPW-HEX for the applications. The parameters for the continental system changed because of changes on the heat pump side.

Table 7: Pre-defined boundary conditions for the RPW-HEX

Boundary conditions			Continental high temp. (first trial)	Continental high temp. (new cond.)	Mediterranean low temp.
Refrigerant		unit	R32	R32	R410a
Heat transfer rate to PCM in RPW-HEX	$Q$	kW	0,93	0,59	13,20
Inlet temperature	$T_{R,in}$	°C	91,3	95,0	5,0
Outlet temperature	$T_{R,out}$	°C	62,0	69,0	9,3
Inlet volume flow	$V_{R,in}$	m <sup>3</sup> /h	1,89	1,41	---
Inlet mass flow	$m_{R,in}$	kg/h	90	67	280
Maximum pressure in HEX	$p_{R,max}$	bar	---	---	42
Maximum allowed pressure loss	$\Delta p_{R,max}$	kPa	59	29	10
PCM			Rubitherm RT64HC	Rubitherm RT64HC	Rubitherm RT4
Storage capacity	$C_{PCM}$	Wh/kg	70	70	49
Density solid	$\rho_s$	kg/m <sup>3</sup>	880	880	880
Density liquid	$\rho_L$	kg/m <sup>3</sup>	780	780	770
Water					
Mass flow	$m_{W,in}$	kg/s	0,6	0,6	0,6
Inlet temperature	$T_{W,in}$	°C	30 - 60	???	12

Maximum allowed pressure loss	$\Delta p_{W,max}$	kPa	4,8	???	60,0
Core Dimensions					
Height in mm	H	mm	600	600	590
Width in mm	W	mm	1000	1000	1000
Depth in mm	D	mm	160	160	160

#### 4.1.1 Calculation of heat transfer

The heat transfer coefficient can be calculated as:

$$\alpha = \frac{Nu \lambda}{d_h}$$

Where the Nusselt Number is given by:

$$Nu = j Re Pr^{1/3}$$

The Colburn factor  $j$  can be derived for the used fins by means of special equations developed by AKG<sup>2</sup>:

$$j = A + B \cdot Re^C$$

For new fins an equation from the literature [27] can be used:

$$j = 0,6522 Re^{-0,5403} \left(\frac{s}{h'}\right)^{-0,1541} \left(\frac{\delta_f}{l_f}\right)^{0,1499} \left(\frac{\delta_f}{s}\right)^{-0,0678} \left[1 + 5,269 \cdot 10^{-5} Re^{1,34} \left(\frac{s}{h'}\right)^{0,504} \left(\frac{\delta_f}{l_f}\right)^{0,456} \left(\frac{\delta_f}{s}\right)^{-1,055}\right]^{0,1}$$

#### 4.1.2 Calculation of pressure drop:

Frictional pressure drop in the core (without fittings) in single phase flow can be calculated as:

$$\Delta p_{1ph} = 4 \cdot f \cdot \frac{\rho u^2}{2 d_h} \Delta L$$

Where the friction factor  $f$  is calculated by special equations developed by AKG<sup>3</sup>:

$$f = X + Y \cdot Re^Z$$

For new fins an equation from the literature [27] can be used:

$$f = 9,6243 Re^{-0,7422} \left(\frac{s}{h'}\right)^{-0,1856} \left(\frac{\delta_f}{l_f}\right)^{0,3053} \left(\frac{\delta_f}{s}\right)^{-0,2659} \left[1 + 7,669 \cdot 10^{-8} Re^{4,429} \left(\frac{s}{h'}\right)^{0,92} \left(\frac{\delta_f}{l_f}\right)^{3,767} \left(\frac{\delta_f}{s}\right)^{0,236}\right]^{0,1}$$

The definition of the geometry parameters is shown in Figure 12. Some key numbers for the fins investigated in this project are listed in Table 8.

<sup>2</sup> The coefficients A,B,C are confidential and specific for the different strip fins

<sup>3</sup> The coefficients X,Y,Z are confidential and specific for the different strip fins

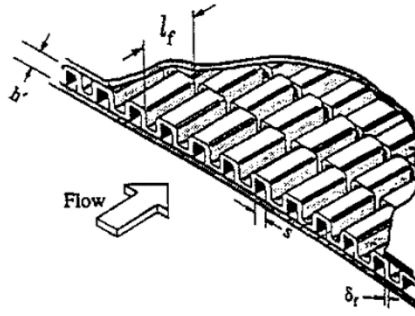


Figure 12: An offset strip fin geometry [27]

 Table 8: Geometry parameters for the calculation of  $j$  and  $f$ 

Offset strip fins:			43	73	18
height	$h'$	mm	3,00	3,00	2,00
pitch	$t$	mm	4,50	5,00	7,50
thickness	$\delta_f$	mm	0,30	0,50	0,22

Frictional pressure drop in the core (without fittings) in **two phase flow** (evaporation) are calculated according to Grønnerud:<sup>4</sup>

$$\Delta p_{2ph} = \Delta p_L \cdot \Phi_{Gd}$$

$$\Delta p_L = 4 \cdot f \cdot \frac{\rho_L u_L^2}{2 d_h} \Delta L$$

The two phase multiplier developed by Grønnerud is :

$$\Phi_{Gd} = O \left( \frac{\Delta p}{\Delta L} \right)_{fr} + 1$$

$$O = \left( \frac{\rho_L}{\rho_G} \right) \left( \frac{\eta_L}{\eta_G} \right)^{-0,25} - 1$$

$$\left( \frac{\Delta p}{\Delta L} \right)_{fr} = f_{Fr} [x^* + 4(x^{*1,8} - x^{*10} f_{Fr}^{0,5})]$$

$$f_{Fr} = Fr_L^{0,3} + 0,0055 \left( \ln \frac{1}{Fr_L} \right)^2$$

Where  $Fr$  is the Froude number:

$$Fr_L = \frac{\dot{G}^2}{\rho_L^2 d g}$$

In which  $\dot{G}$  is the mass flow density

<sup>4</sup> Steimle, F, Stephan,K: Handbuch der Kältetechnik, sechster Band/Teil B, Wärmeaustauscher, Springer Verlag, 1988

#### 4.1.3 Design considerations for an RPW-HEX

When integrating PCM in a thermal system, the PCM is often in a separate compartment, where heat or cold is introduced via more or less sophisticated heat exchangers. The simplest application is to fill PCM in a tank and add some heat exchanger tubes to heat or cool it. While the heat transfer is sufficient while the PCM is liquid, the heat transfer is dramatically reduced to thermal conductivity alone once the PCM starts to solidify on the cold surfaces.

This situation is improved by filling one side of a (liquid-to-liquid) heat exchanger with PCM. The maximum distances for thermal conductivity are much shorter and the storage can be charged and discharged much faster.

One very flexible type of heat exchangers are AKG's bar-and-plate heat exchangers, which are forming passages for multiple fluids by stacking aluminium-plates as separators of the fluids and bars and fins to form a rectangular tube. The designs allow a flexible combination of fluid passages at low tooling costs. Figure 13 shows a cut version of an air-liquid heat exchanger identifying the single components of the heat exchanger.

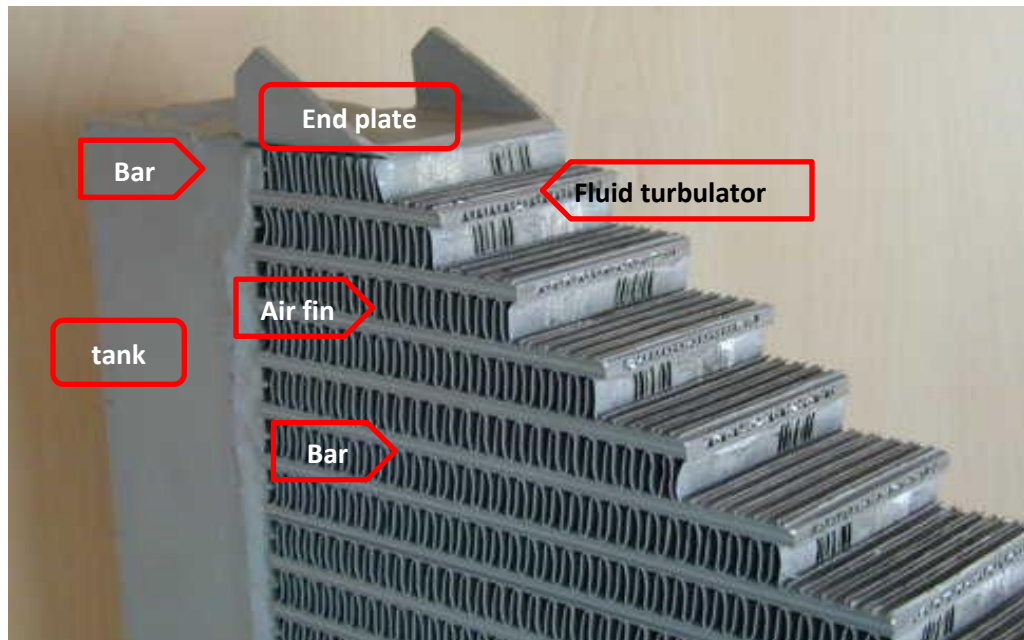


Figure 13: Example of bar-plate heat exchanger [28]

The possibility to integrate three different fluids in AKG's heat exchanger design allows the elimination of an additional PCM-heat exchanger to store heat or cold. Since the thermal process already includes a heat exchanger to cool and heats the process fluids, the storage could be directly integrated in the existing heat exchanger. Therefore, the PCM-heat-exchanger was modified to handle three different fluids in one core. For that purpose, an additional passage for PCM is added, which contains the fin structure from Figure 8, which not only helps distribute the heat from the fin into the PCM fluid but also thermally connects the adjacent passages for coolant and refrigerant. Figure 14 shows the arrangement of the different passages for the lab-scale RPW-HEX manufactured for UDL. In this case the three passages were arranged as triples of the three fluid passages. For better analysis of the operating behaviour the core was equipped with multiple ports for thermal sensors.

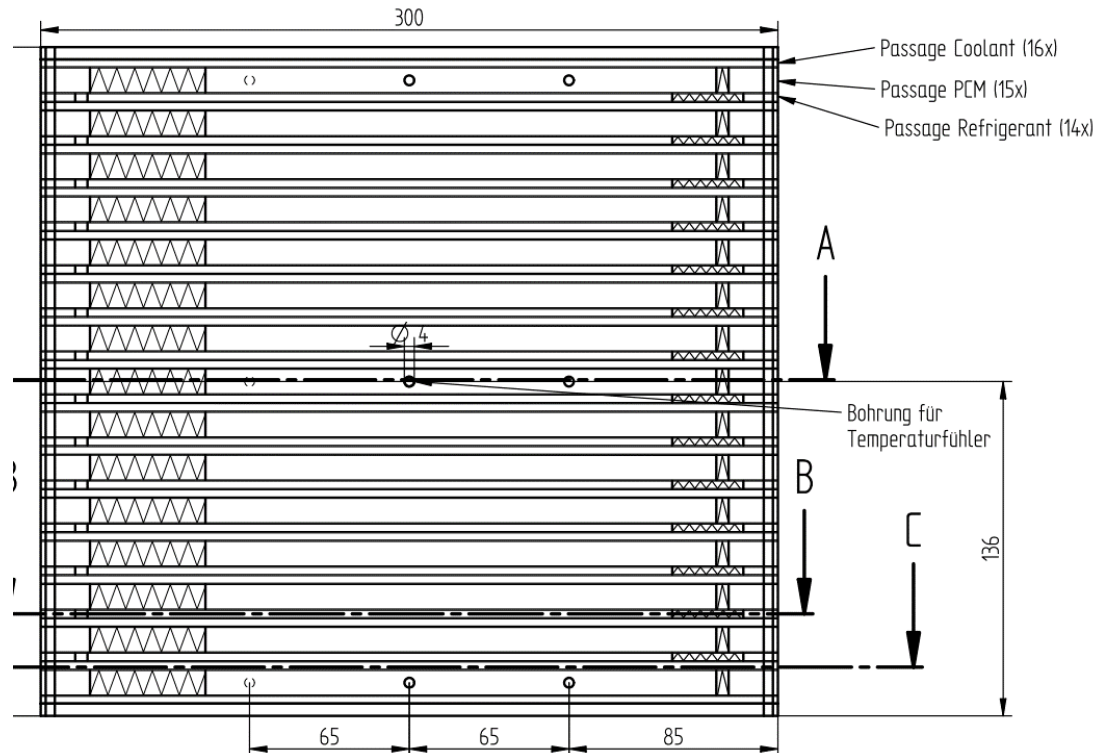


Figure 14: Lab-scale RPW-HEX for Udl (NP 4012093)

The design and size of such a heat exchanger is influenced by additional factors compared to sizing a conventional two-fluid heat exchanger. The minimum thermodynamic requirements are defined by the processes of its application as shown in Table 7. Compact design, low pressure loss, low weight, mechanical strength, etc. are typical parameters to observe during design. When a certain amount of thermal PCM-storage capacity has to be added the impact on the overall dimensions can be dominating. If the sizing is led by the thermodynamics the simplest design is then to size the cooler for the heat transfer requirements (number and size of passages for coolant and refrigerant) and add a passage for the PCM next to the passages as shown in Figure 14. Depending on the storage capacity of the PCM used (see section 3) the total storage capacity may be sufficient or not.

If the requested storage capacity is the leading requirement additional passages of PCM have to be introduced. This can be done according to the system shown in Figure 14 by adding as many triples of passages until the needed storage capacity is needed. This will lead to an over-performance of the heat exchanger functionality, which might be welcome. But especially with respect to the heat exchanger's charge with environmentally relevant refrigerant the heat exchangers should be further adjusted. A big benefit of the bar-and-plate design is that the aluminium structures in the PCM-passage connect the coolant and refrigerant passages thermally so that heat flows preferably between those passages and sizing can be done for that requirement. Only when there is an imbalance between refrigerant and coolant thermal energy has to be transferred into the PCM-passages. Figure 15 shows an example of a RPW-HEX with four PCM-passages per coolant-refrigerant-couple, which allows a significant increase of storage capacity without decreasing the thermal performance of the heat exchanger.

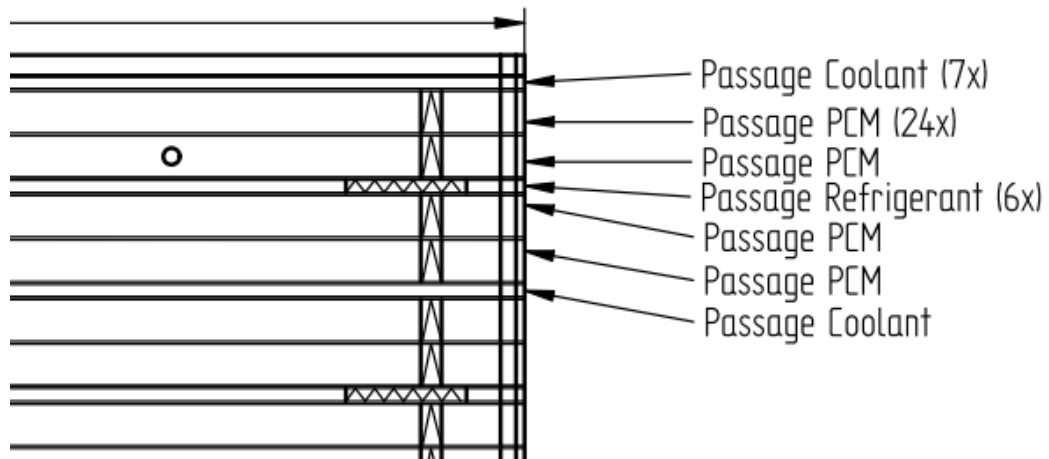


Figure 15: RPW-HEX design with extra PCM-passages

Multiple combinations of refrigerant, coolant and PCM-passages were built and investigated in lab- and full-scale to identify the limits and possibility of the design. The results are shown in the following sections.

#### 4.2 Lab-scale latent storages manufacturing

All RPW-HEX were manufactured in AKG’s bar-and-plate design as described in section 4.1. The heat exchangers are fully made from aluminium. The cores are mainly made from 3000 aluminium alloys, which were brazed in AKG’s unique dip-brazing process at about 600°C. Leaving the three different types of passages open in different areas of the core it is possible to put collector tanks (6000 aluminium alloys) for each fluid. Figure 16 shows the finished RPW-HEX with three pairs of collector tanks to provide inlets and outlets for all three fluids.

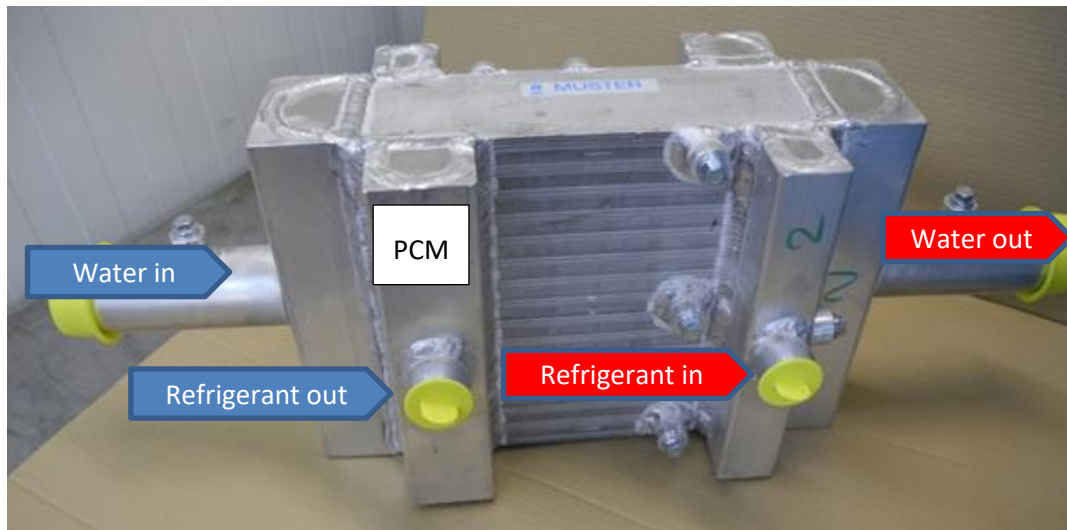


Figure 16: Photo of lab-scale RPW-HEX for UDL (NP 4012093)

In the following sections, the different components, produced for UDL and AIT for the various purposes are shown in detail.

#### 4.2.1 2-Fluid water/PCM for SOC analysis

In a first proof of concept a heat exchanger with PCM was manufactured for UDL, where water could be used to charge and discharge the PCM and run first analyses. The heat exchanger is shown in Figure 17 and the main design data are listed in Table 9.

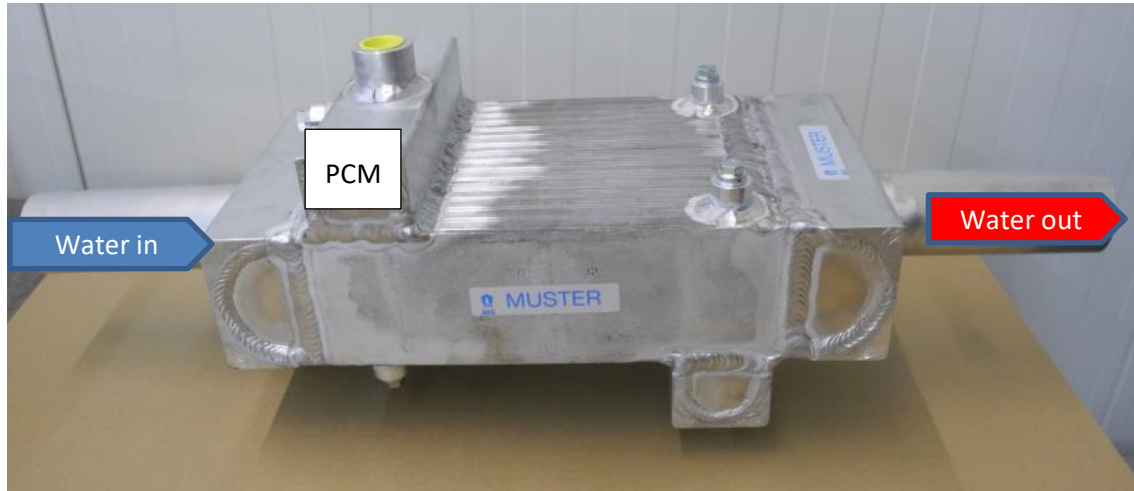


Figure 17: Photo of lab-scale PCM-Water-HEX for Udl (NP 4011467)

Table 9: Characteristics of 2-Fluid water/PCM for SOC analysis (NP 4011467)

	refrigerant	coolant	PCM
Number of passages	0	14	15
Fin #	-	43	33
Fluid volume in ltr	0	0.7	3.72
core length x width x depth in mm	300 x 216 x 94		

#### 4.2.2 3-fluid RPW-HEX-1, first MED design

The first 3-fluid RPW-HEX was manufactured with the concept of one PCM-passage being next to coolant and refrigerant as shown in Figure 14. The design was preferred by UDL for the Mediterranean demo sites. The heat exchanger is shown in Figure 16 and the main design data are listed in Table 9.

Table 10: Characteristics of 3-Fluid RPW-HEX-1 (NP 4012093)

	refrigerant	coolant	PCM
Number of passages	14	16	15
Fin #	43	43	33
Fluid volume in ltr	0.65	0.8	3.72
core length x width x depth in mm	300 x 272 x 94		

#### 4.2.3 3-fluid RPW-HEX-2, first CON design 2 PCM

For the Continental design options with more PCM-passages were investigated. One version has four PCM-passages, which are distributed in pairs of two passages between the coolant and

refrigerant passages as shown in Figure 15. The heat exchanger is shown in [Figure 18](#) and the main design data are listed in Table 11.

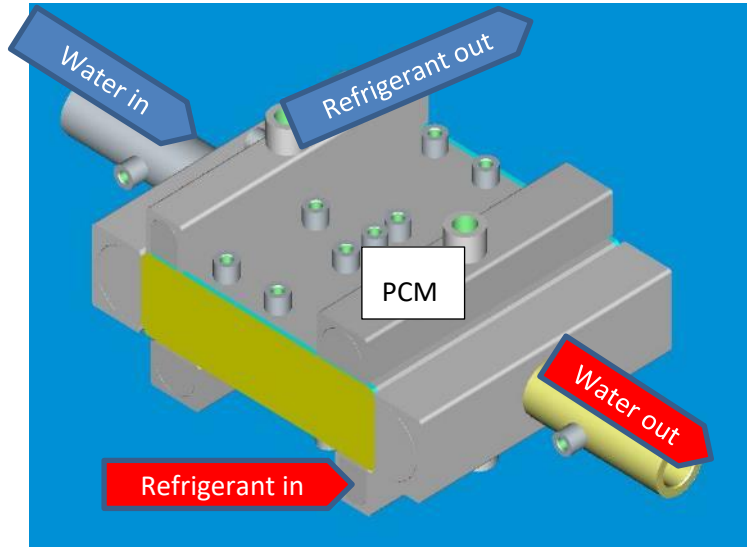


Figure 18: Lab-scale PCM-Water-HEX-2 for UdL (NP 4013450)

Table 11: Characteristics of 3-Fluid RPW-HEX-2 (NP 4013450)

	refrigerant	coolant	PCM
Number of passages	6	7	24
Fin #	43	43	33
Fluid volume in ltr	0.28	0.35	5.5
core length x width x depth in mm	300 x 313 x 94		

#### 4.2.4 3-fluid RPW-HEX-3, second MED design

Since for the Mediterranean version the coolant and refrigerant passages are preferred to have direct contact the four PCM-passages were located as groups of four next to the coolant-refrigerant- couples as shown in [Figure 19](#). The heat exchanger is shown in [Figure 20](#) and the main design data are listed in Table 12.

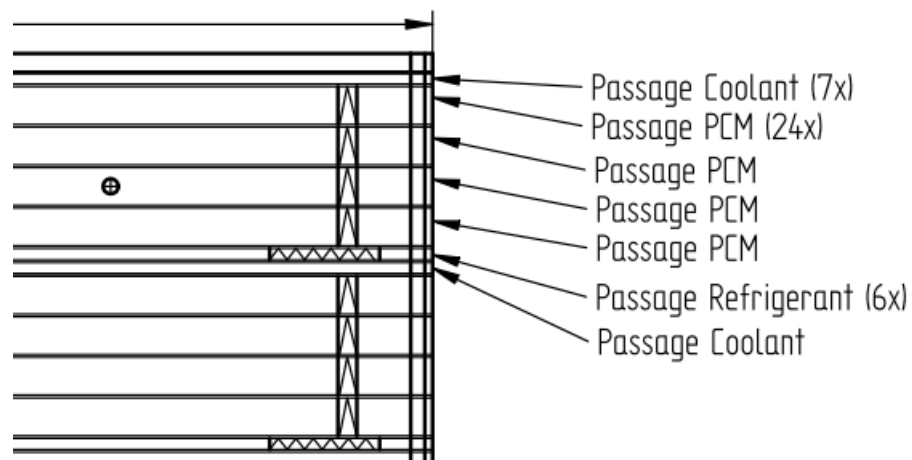


Figure 19: Arrangement of 4 adjacent PCM-passages per coolant and refrigerant passage

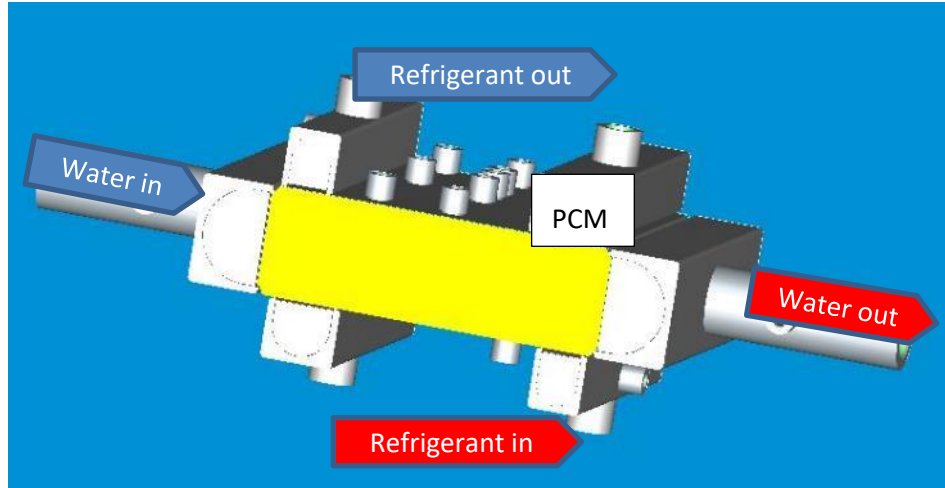


Figure 20: Lab-scale PCM-Water-HEX-3 for UDL (NP 4013449)

Table 12: Characteristics of 3-Fluid RPW-HEX-3 (NP 4013449)

	refrigerant	coolant	PCM
Number of passages	6	7	24
Fin #	43	43	33
Fluid volume in ltr	0.28	0.35	5.5
core length x width x depth in mm	300 x 313 x 94		

#### 4.2.5 2-fluid W/PCM storage

For tests at AIT a 2-fluid water-PCM heat exchanger was built. A special feature was a removable cover enclosing the PCM. This allowed easy filling of the system with solid PCM at ambient temperature and visualisation of the melting process. The heat exchanger is shown in [Figure 21](#) and the main design data are listed in [Table 13](#).

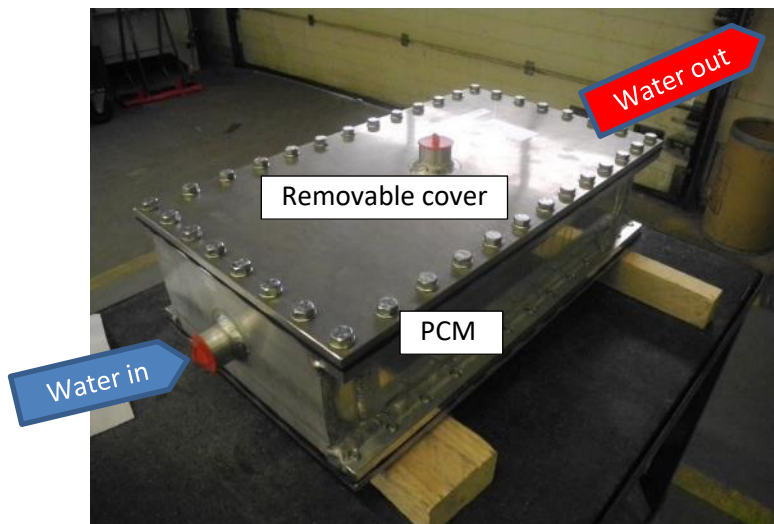


Figure 21: 2-Fluid Water-PCM-HEX for AIT (NP 4011050)

Table 13: Characteristics of 2-Fluid Water-PCM-HEX for AIT (NP 4011050 )

	refrigerant	coolant	PCM

Number of passages	0	19	20
Fin #	-	43	33
Fluid volume in ltr	0	4.23	11.4
core length x width x depth in mm	500 x 286 x 140		

#### 4.2.6 2-fluid Water-PCM test cubes

For studies on the solidification process of PCM four small samples were manufactured, where different structures were arranged between two MPE-tubes. **Figure 22** shows two examples filled with PCM, and with no fins and with straight fins between the tubes. The other samples differ in the distance between the tubes (1 cm versus 3 cm distance). Main design data is given in Table 14.



Figure 22: PCM-samples filled with RT64HC with no fins (left) and straight fins (right) and 1 cm distance between MPE-tubes.

Table 14: Characteristics of 2-Fluid Water-PCM test cubes (AIT)

Sample number	1	2	3	4
<b>Water side</b>	MPE tubes			
Free volume [mm <sup>3</sup> ]	7040			
Amount of aluminium [kg]	0.02475			
Heat transfer area [m <sup>2</sup> ]	0.0224			
<b>PCM side</b>				
Amount of aluminium [kg]	0	0.0154	0	0.0463
Heat transfer area [m <sup>2</sup> ]	0	0.0589	0	0.1767

### 4.3 Lab-scale latent storage testing

#### 4.3.1 Low temperature latent storage lab-testing

Several experimental tests were carried out in the laboratory using different lab-scale prototypes to assist the design of the full-scale latent storage and to identify possible difficulties or improvements in some of the key parts of this component of the Mediterranean system. One of the critical points in the development of an optimization strategy of the entire system is the

knowledge of the state-of-charge (SOC) of the latent heat TES tank. Therefore, the first experimental tests focused on defining a reliable method to determine the SOC of the latent heat TES [29]. A two-fluid (water/PCM) prototype manufactured by AKG was used for that purpose.

The commercial RT4 product provided by Rubitherm was used as PCM material in all experimental tests. Some of the relevant thermophysical properties of RT4 according to the literature were shown in Table 1. However, the partial specific enthalpy of the PCM was determined experimentally using a DSC 3+ Mettler Toledo equipment available at the GREiA research group at the University of Lleida. Figure 23 shows the partial specific enthalpy of RT4, which indicates that the phase change temperature is around 5 °C. Since this property is a key input for the determination of the SOC of the PCM, experimental values were used in the present study.

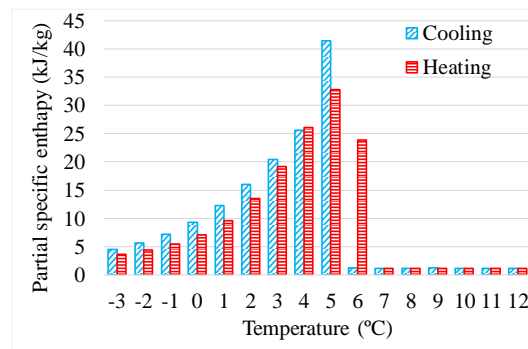


Figure 23. Partial specific enthalpy of RT4 according to DSC analysis at UDL laboratories [29]

A mixture of 70% water and 30% mono ethylene glycol was used as heat transfer fluid (HTF) for charging or discharging the PCM. Some of the relevant thermophysical properties of the HTF are shown in Table 15, which were calculated by interpolating the values provided by the manufacturer at different temperatures [30].

Table 15. Properties of the HTF used, as given by the manufacturer [30]

Properties	At T = -2 °C	At T = 12 °C	Units
Density	1052.7	1047.4	kg/m <sup>3</sup>
Viscosity	4.5	2.8	mPa·s
Specific heat	3585	3624	J/kg·K
Conductivity	0.421	0.437	W/m·K

The experimental test rig shown in Figure 24 was built in the laboratory of the GREiA research group at the University of Lleida to perform different PCM charging and discharging processes in different configurations. It consisted of a two HTF tanks able to provide warm or cold HTF, the two-fluid HEX filled with 2.49 kg of RT4 connected to a DAB VA 65/180 wet rotor pump to recirculate the HTF through the HEX, a Badger Meter Primo Advanced flow meter, with an accuracy of  $\pm 0.25\%$ , two three-way valves to select connection either to the warm or to the cold tank, 0.5" copper pipes insulated with 18x0.9 mm polyurethane tubes, and several valves. The cold and warm HTF tanks had a capacity of 12 L and 20 L, respectively. Auxiliary units such as two JP SELECTA FRIGEDOR refrigerated cooling coils, an OVAN TH100E immersion thermostat, and a JP SELECTA Termotronic immersion thermostat were used to control the temperature in

both the cold and the warm HTF tanks. Table 16 summarizes the characteristics of the warm and cold HTF tanks equipment.

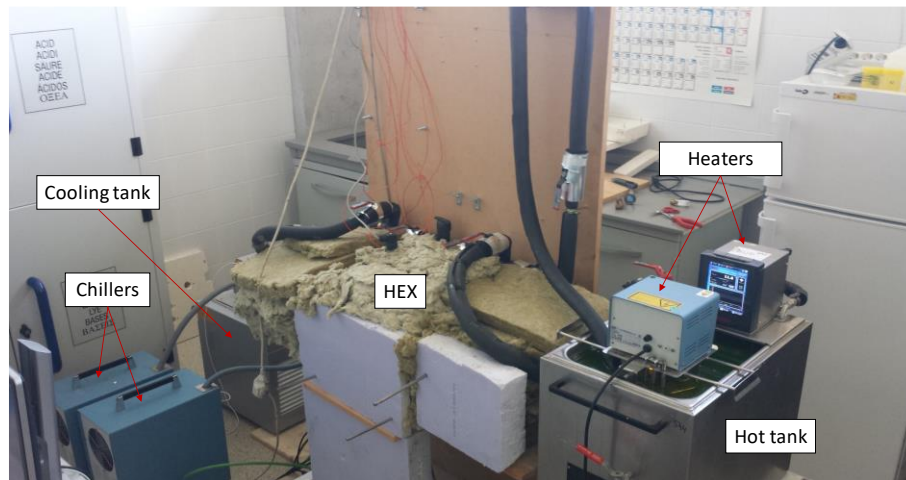


Figure 24. Picture of the experimental set-up [29]

Table 16. Cooling and heating HTF tank equipment

	Equipment	Brand	Function	Heating/cooling power (kW)
Cooling tank equipment	Tank	Ovan	Cooling	0.30
	Chiller	Selecta		0.05
	Chiller with temperature control	Selecta		0.05
	Thermostat	Ovan	Heating	1.60
Heating tank equipment	Tank	Huber	Cooling	0.35-0.40*
	Thermostat	Selecta	Heating	1.00
	Thermostat	Huber		2.00

\* Huber tank data at 0-20 °C, it is lower at lower temperatures

The test rig was equipped with different sensors to measure temperature and pressure at relevant positions. Seven Pt-100 class B temperature sensors were used, five of them within the HEX to measure the PCM temperature at different locations, and two of them at the inlet and outlet of the HEX to measure the HTF temperature. Furthermore, a FG 10S20 WIKA pressure sensor with an accuracy  $\pm 0.25\%$  was used to measure the pressure inside the HEX cavity where the PCM was placed. The temperature in the tanks and mass flow in the system were monitored as well. A data acquisition system consisting of a STEP DL-01 data logger connected to a personal computer was used to record the experimental measurements at a time interval of 30 seconds. Figure 25 shows the details regarding the HEX configuration and the location of temperature and pressure sensors within the heat exchanger. Sensors  $T_1$  and  $T_2$ , as well as  $T_4$  and  $T_5$  were placed symmetrically with respect to the symmetry axis of the HEX, while sensor  $T_3$  was located right at the center of the HEX.

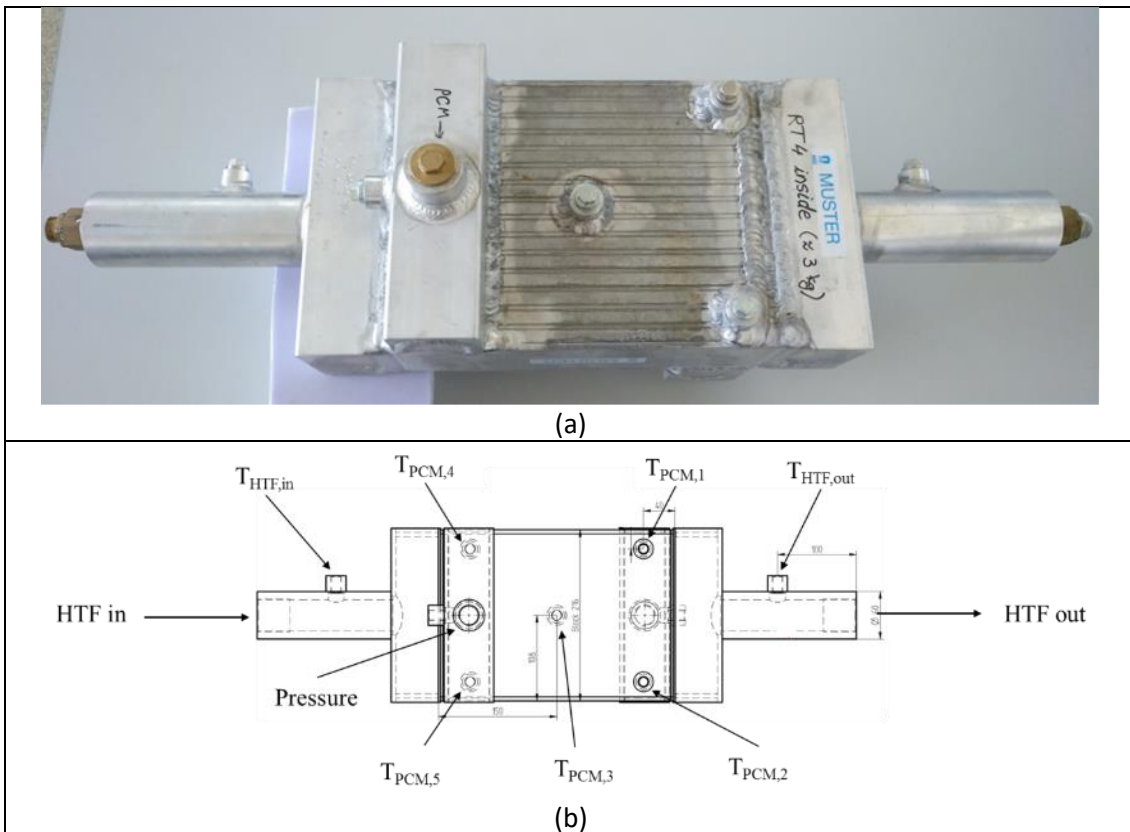


Figure 25. (a) Picture of the HEX; (b) top view of the location of temperature and pressure sensors in the HEX

Several experiments were performed to assess the system performance under different operating conditions, which should allow evaluating the proposed methods for determining the SOC parameter. Two types of experiments were performed, by varying the HTF flow rate for a fixed temperature range and by varying the temperature range for a fixed HTF flow rate. The complete set of experiments performed is summarized in Table 17.

Table 17. Experimental plan

Type	Temperature range for the charging process (°C)	Temperature range for the discharging process (°C)	HTF flow rate (L/min)	Repetitions [-]
Variable HTF flow rate	12 → -2	-2 → 12	2.0	3
			1.5	3
			1.0	3
			0.5	3
Variable temperature range variation	14 → -3	-3 → 14	0.5	3
	12 → -2	-2 → 12	0.5	3
	10 → 1	1 → 10	0.5	3

All experimental tests shown in Table 17 were performed three times to ensure data reliability and robustness of the results. Figure 26 shows the inlet ( $T_{in}$ ) and outlet ( $T_{out}$ ) HTF temperature evolution of three experiments for PCM charging (a) and discharging (b) processes for a HTF flow

rate of 1.0 L/min. The results show that the temperature evolution is similar among the different experiments.

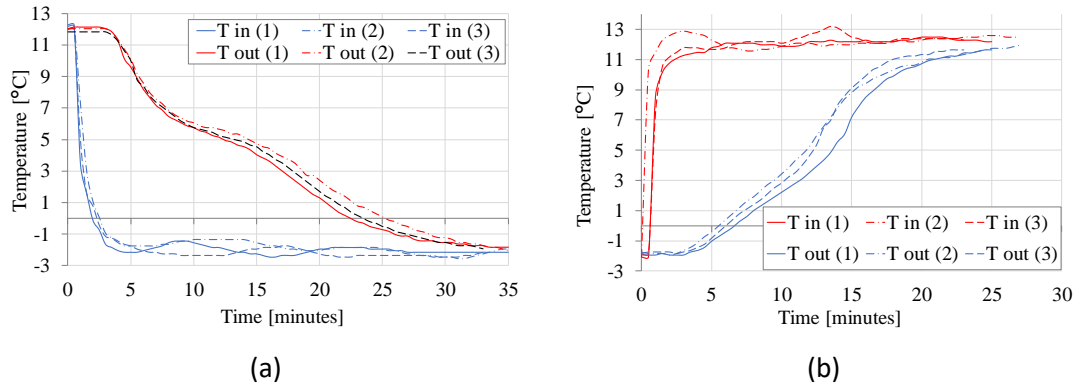


Figure 26. Results of repeatability of inlet and outlet temperature at a flow of 1 L/min for (a) charging and (b) discharging of PCM [29]

Figure 27 shows the PCM temperature evolution of three experiments for PCM charging (a) and discharging (b) processes for a HTF flow rate of 1.0 L/min. Since the pair of temperature sensors positioned at the same distance from the symmetry axis of the HEX (i.e.  $T_1$  and  $T_2$ , and  $T_4$  and  $T_5$ ) had very similar values in all the experiments performed, the data of only one sensor of each pair is shown in all the figures for the sake of simplicity. Here again the temperature evolution is similar among the different experiments.

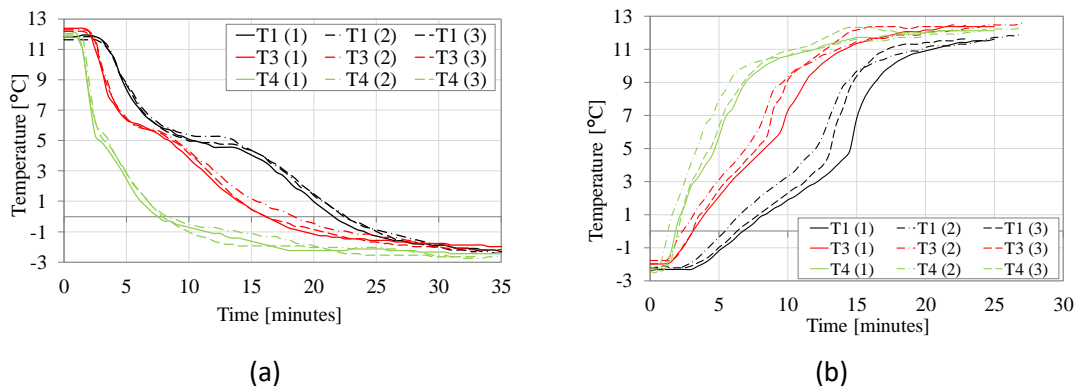


Figure 27. Results of repeatability of PCM temperature at a flow of 1 L/min for (a) charging and (b) discharging of PCM [29]

Figure 28a shows the evolution of the PCM temperature at the relevant locations during the charging process at different HTF flow rates. The sensors located at a position closer to the inlet of the HEX ( $T_4$ ) show an earlier and quicker temperature drop from the initial value of around 12 °C towards the final value around -2 °C for all flow rates. The effect of the PCM solidification process can hardly be noticed at this location. The sensor located in the middle of the HEX ( $T_3$ ) also shows a fast change in temperature, although in this case the effect of the PCM solidification can be observed when the temperature reaches about 6 °C, when the slope of the temperature drop is reduced during a short time interval. This effect is more evident as the flow rate is lower. The sensors located closer to the outlet of the HEX ( $T_1$ ) show a delayed and slower temperature

drop, and the phase change effect is evident around 5 °C at which the temperature remained almost constant for a certain time period depending on the HTF flow rate.

Figure 28b shows the temperature evolution of the PCM during charging processes for different temperature ranges and for a fixed flow rate of 0.5 L/min. The higher temperature range corresponds to a PCM temperature variation from 14 °C to -3 °C (denoted by  $\Delta T \pm 8$  in the legend), while the lower temperature range corresponds to a PCM temperature variation from 10 °C to 1 °C (denoted by  $\Delta T \pm 4$  in the legend). One can notice that both charging processes have similar durations, although the process corresponding to a wider temperature range ( $\Delta T \pm 8$  °C) occurs faster to cross the wider temperature interval in the same period of time.

Figure 28c shows the evolution of the PCM temperature at the relevant locations during discharging process at different HTF flow rates. Similar to the charging process, the change in temperature occurs faster for higher values of the HTF flow rate. The sensors located closer to the inlet of the HEX ( $T_4$ ) show a faster change in temperature towards 12°C. Unlike the charging process, the sensors located in the middle ( $T_3$ ) and closer to the outlet of the HEX ( $T_1$ ) do not show a significant reduction of the slope of temperature increase around the phase change temperature. This difference can be attributed to the different shape of the PCM specific heat capacity for solidification and melting processes.

Figure 28d shows the temperature evolution of the PCM during discharging processes for different temperature ranges and for a fixed flow rate of 0.5 L/min. The higher temperature range corresponds to a PCM temperature variation from -3 °C to 14 °C (denoted by  $\Delta T \pm 8$  in the legend), while the lower temperature range corresponds to a PCM temperature variation from 1 °C to 10 °C (denoted by  $\Delta T \pm 4$  in the legend). Similar to the charging process, the two discharging processes have similar durations, and at a higher temperature range the PCM temperature variation is higher.

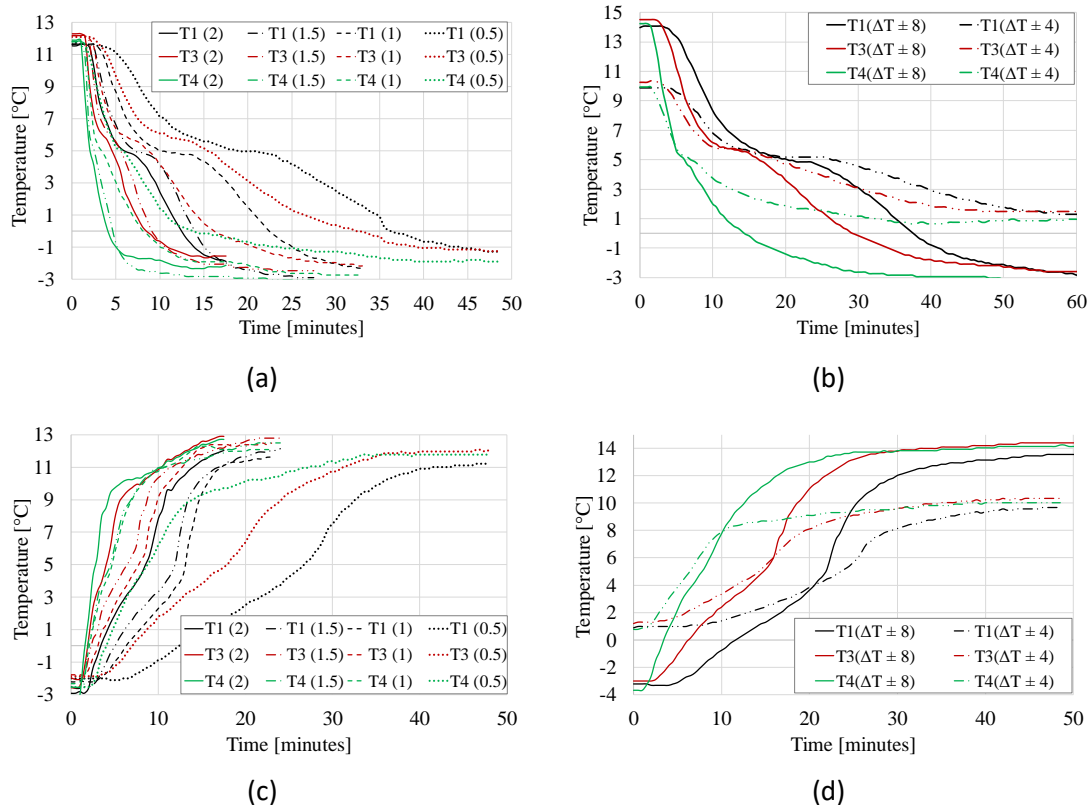


Figure 28. PCM temperature evolution at (a) different flow rates during the charging process, (b) different temperature ranges during the charging process, (c) different flow rates during the discharging process, and (d) different temperature ranges during the discharging process – Note that flow rate values (in L/min) and temperatures ( $^{\circ}\text{C}$ ) are shown inside brackets in the legends [29].

Different experimental tests were also performed at UDL laboratory with the first lab-scale RPW-HEX manufactured by AKG. This prototype was built according to the configuration initially proposed for the Mediterranean system, which considers direct heat transfer between the refrigerant and the water, and only one 1-cm-thick PCM layer, as shown in Figure 29. Further details regarding the RPW-HEX prototype design and features can be found in sections 4.1 and 4.2.

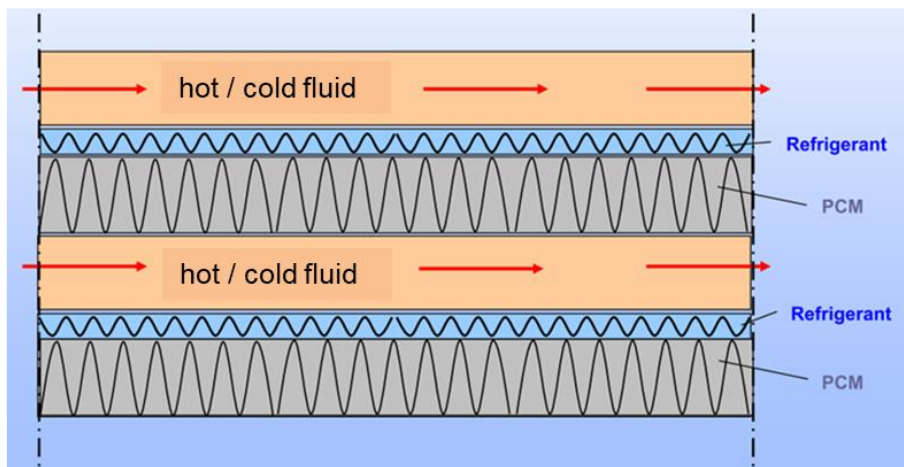


Figure 29. Schematic of the configuration of the RPW-HEX tested at UDL laboratory

The main purpose of the experimental tests was to study the charging and discharging of the RPW-HEX under different working conditions. For that, a dedicated test rig was built at the UDL laboratory, as shown in Figure 30. It consisted of a variable capacity condensing unit from Zannoti, with hermetic scroll digital compressor with a nominal maximum cooling power of 4.768 kW, working with R449A refrigerant, connected to the RPW-HEX filled with 3.15 kg of RT4 that acts as the evaporator of the refrigeration cycle, an electronic expansion valve, a solenoid valve, a flow meter to measure the refrigerant flow rate, a Badger Meter Primo Advanced flow meter to measure the HTF flow rate, with an accuracy of  $\pm 0.25\%$ , piping, insulation, and several valves. Auxiliary units such as two JP SELECTA FRIGEDOR refrigerated cooling coils, an OVAN TH100E immersion thermostat, and a JP SELECTA Termotronic immersion thermostat were used to control the temperature of the HTF in the thermal bath. The same mixture of 70% water and 30% mono ethylene glycol as in the experiments with the 2-fluid lab-scale prototype was used as heat transfer fluid (HTF) for discharging the RPW-HEX. Some of the relevant thermophysical properties of the HTF were shown in Table 15.

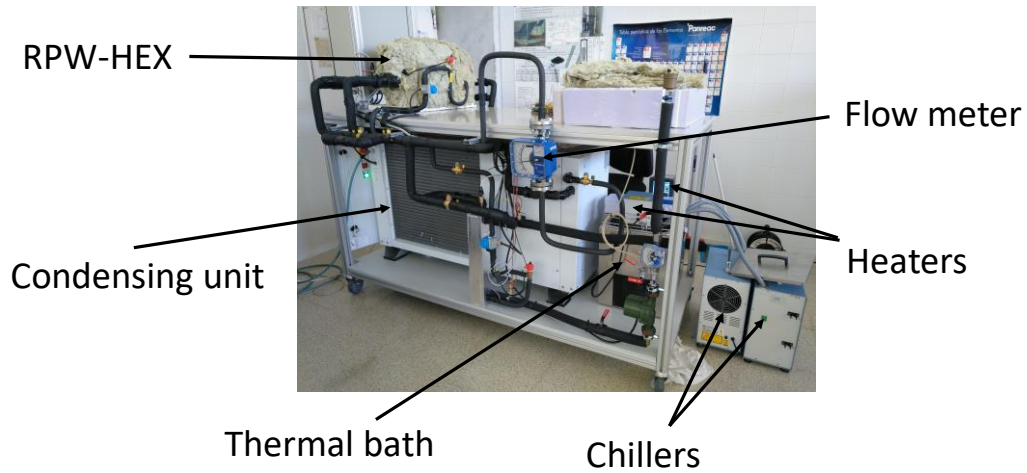


Figure 30. Photo of the test rig at UDL laboratory

The test rig was equipped with 13 Pt-100 class B temperature sensors to measure the temperature distribution inside the PCM, at the HTF inlet and outlet, and at the refrigerant inlet and outlet. A data acquisition system consisting of a STEP DL-01 data logger connected to a personal computer with the Indusoft SCADA software was used to record the experimental measurements at a time interval of 10 seconds.

Figure 31 shows the regarding the inlet and outlet ports of the different fluids and also temperature sensors locations.

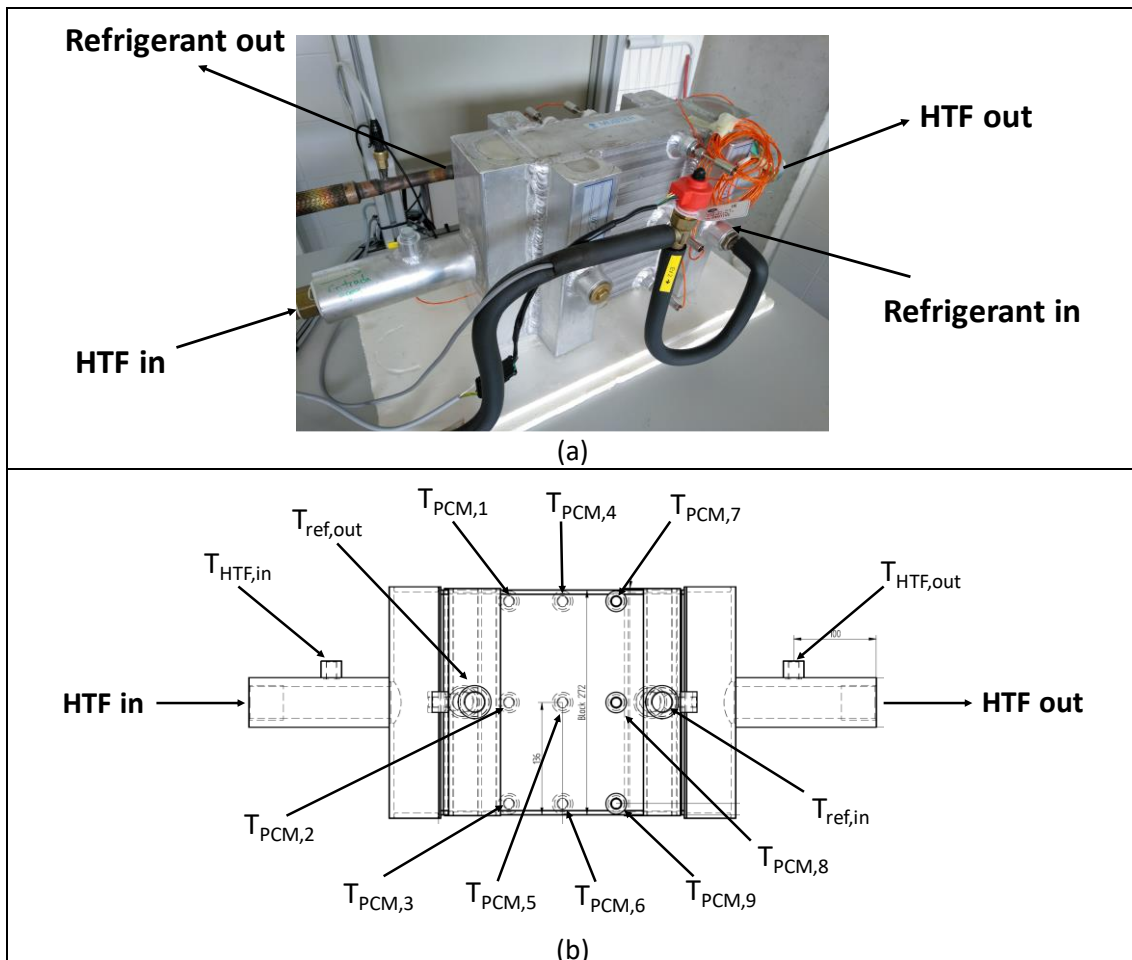


Figure 31. (a) Picture of the RPW-HEX; (b) location of temperature sensors in the RPW-HEX

Three types of experiments can be performed to test the different possible operating modes such as only charging (mode 1), only discharging (mode 2), and simultaneous charging and discharging (mode 3) of the RPW-HEX. For each of the three modes, different working conditions will be tested.

With respect to mode 1, several charging tests were already performed to assess the RPW-HEX performance at different values of the cooling capacity of the condensing unit. In some cases, several repetitions were done. The complete set of experiments performed in mode 1 (charging of the PCM by the refrigerant) are shown in Table 18.

**Table 18. Experiments for PCM charging (mode 1)**

Initial PCM temperature (°C)	Cooling capacity (%)	Repetitions (-)
12	15	4
12	30	1
12	45	4
12	60	2
12	75	1

The cooling capacity is represented as a percentage of the cooling capacity with respect to the maximum value, which depends on the evaporation and condensation temperatures. The performance of the condensing unit is shown in Table 19 for a fixed evaporation temperature of -10 °C and different ambient temperatures.

**Table 19. Performance of the condensing unit**

Evaporation temperature (°C)	Ambient temperature (°C)	Cooling power (kW)	COP (-)
-10	5	6.354	4.08
-10	15	5.903	3.36
-10	25	5.371	2.61
-10	32	4.956	2.12
-10	43	4.237	1.46

Each charging process started with the PCM temperature at 12 °C so that the RPW-HEX was initially completely discharged. The charging process was considered completed when the highest PCM temperature was -3 °C, at which point the condensing unit was switched off. In case the PCM temperature at any location reached -18 °C, the condensing unit was also switched off to avoid freezing of the HTF inside the RPW-HEX, even though there were some regions inside the PCM where the PCM temperature was above -3 °C. The results of the charging experiments at different cooling capacities are shown in Figure 32 [31].

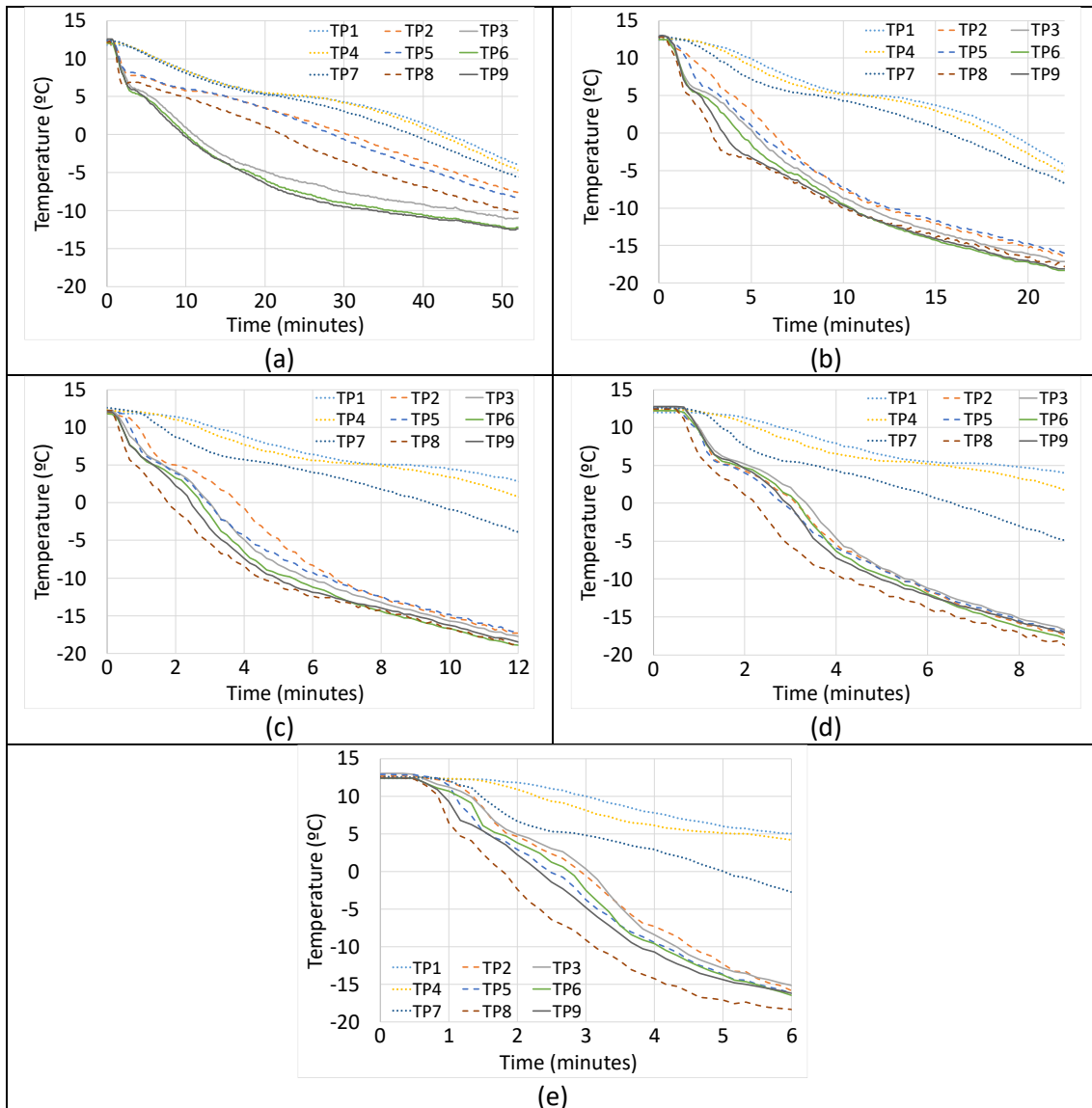


Figure 32. PCM temperature during charging at (a) 15% cooling capacity; (b) 30% cooling capacity; (c) 45% cooling capacity; (d) 60% cooling capacity; (e) 75% cooling capacity [31]

The results show that, at low cooling capacities between 15% and 30%, the RPW-HEX could be completely charged before the temperature at any point reached  $-18\text{ }^{\circ}\text{C}$ . However, at higher cooling capacities, in some regions of the RPW-HEX the PCM was not able to completely solidify because of the fast charging process, which did not allow enough time for the cooling to be uniformly distributed inside the PCM. The higher the cooling capacity, the higher the temperature differences between different parts of the PCM inside the RPW-HEX.

To check the temperature evolution inside the RPW-HEX below the complete charging point, an additional test was performed at 15% cooling capacity to see if the PCM temperature was able to become more homogenized until the lowest point reached  $-18\text{ }^{\circ}\text{C}$ . Figure 33 shows that the temperature difference inside the PCM reduced with time and it reached a value of  $2\text{ }^{\circ}\text{C}$  at the end of 300 minutes, which was the duration of the long charging experiment.

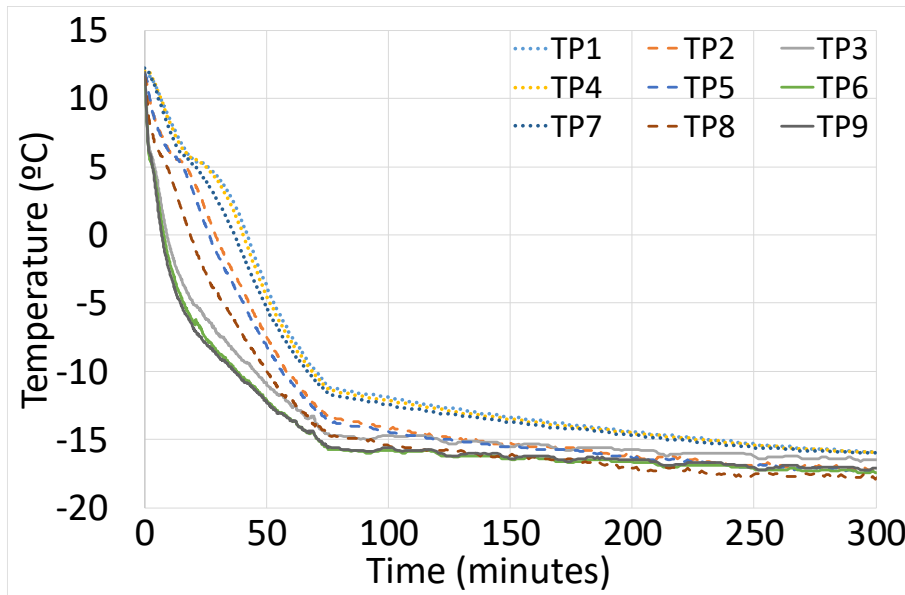


Figure 33. Long charging process at 15% cooling capacity [31]

Regarding mode 2, several discharging tests were also performed to assess the RPW-HEX performance at different values of the HTF flow rate and inlet temperature. The complete set of experiments performed in mode 2 (discharging of the PCM by the HTF) are shown in Table 20.

Table 20. Experiments for PCM discharging (mode 2)

Initial PCM temperature (°C)	HTF temperature (°C)	HTF flow rate (L/h)
-4	9	50
-4		100
-4		150
-4	12	50
-4		100
-4		150
-4	15	50
-4		100
-4		150

Each discharging process started with the PCM temperature around -4 °C to ensure that the RPW-HEX was initially completely charged. The initial PCM temperature distribution was uniformly distributed, being the maximum temperature difference generally less than 1 °C. The discharging process was considered completed when the lowest PCM temperature reached the HTF inlet temperature within the experimental error interval.

The results of the discharging process for an inlet HTF temperature of 12 °C and at different flow rates are shown in Figure 34.

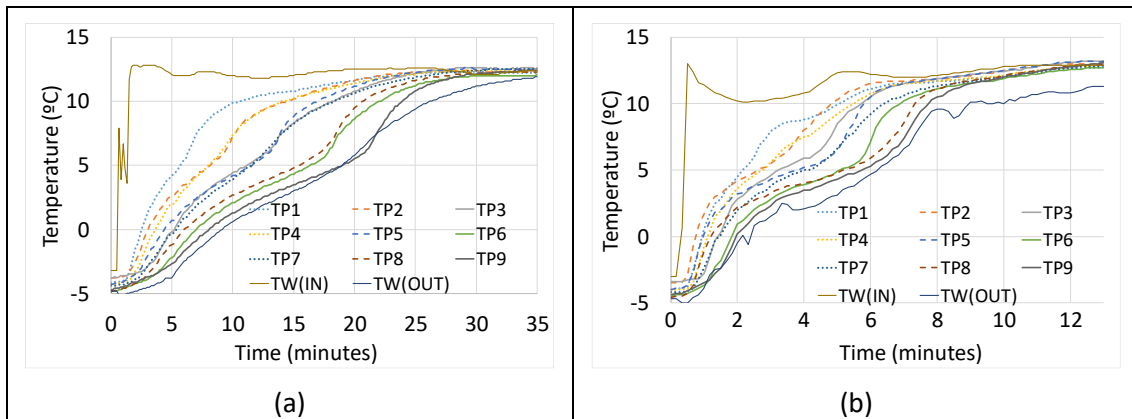


Figure 34. PCM temperature during discharging at an HTF flow rate of (a) 50 L/min; (b) 150 L/min [31]

The results of the discharging process for a constant HTF flow rate of 100 L/min and at different inlet HTF temperatures are shown in Figure 35.

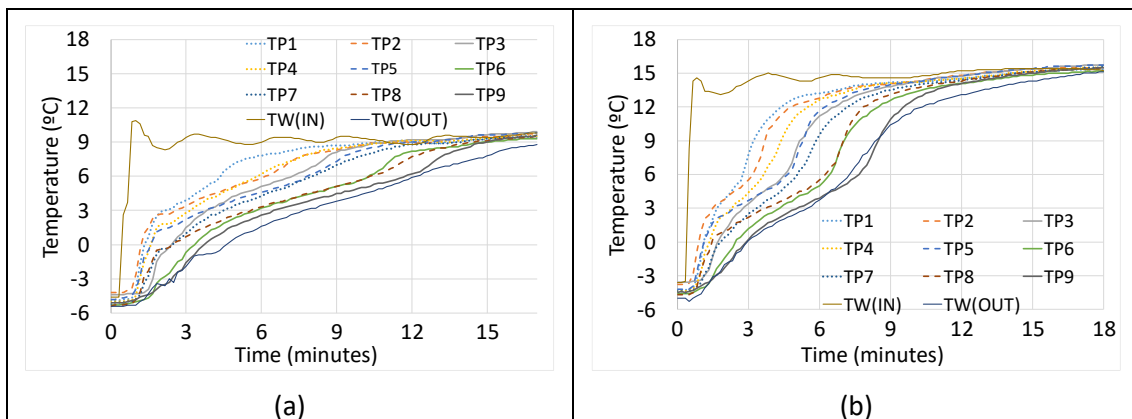


Figure 35. PCM temperature during discharging at HTF inlet temperature of (a) 9 °C; (b) 15 °C [31]

#### 4.3.2 High temperature latent storage lab-testing

Lab-scale storages are operated for the analysis of the heat transfer between water/PCM during charging and discharging operation and give reference data for comparison with results obtained with the full-scale CONT prototype. The focus of the analysis is on the influence of the PCM RT64HC phase transition (melting/solidification) behaviour and different storage-internal fin geometries on the PCM side on the heat transfer characteristics.

Two different lab-scale storages have been studied:

- **2-fluid Water-PCM test cubes:** Are useful to study the state of charge through image processing techniques and compare how different geometries and setups affect the heat transfer process.
- **2-fluid W/PCM storage:** Used to recreate the process of thermal energy storage with different PCMs. This prototype is useful to understand how the process of charging/discharging is, for both complete and partial load cycles.

Due to the temperature requirements for domestic hot water and in order to store considerable amounts of thermal energy, the melting/solidification temperatures of the tested PCMs are around 60°C. The following PCM have been tested and corresponding manufacturer data is given:

PCM [Rubitherm]	Melting range [°C]	Solidification range [°C]	Heat storage capacity [kJ/kg]
RT54HC	53-54	54-53	200
RT55	51-57	57-56	170
RT64HC	63-65	64-61	250

### 2-fluid Water-PCM cubical test samples

The small samples have been used for analysing how different setups of the heat exchangers affect the heat transfer and to get an estimation of the state of charge using image processing techniques.

**Experimental setup:** The experiments realized can be grouped into two categories: visual monitoring and temperature monitoring tests. For both, the basic setup is composed of the small samples from AKG filled with RT54HC PCM and connected to the Julabo F51 heater by simple plastic pipes. The connectors for the water through the MPE-tubes can be seen in Figure 37.

The small storages have been thermally insulated and an external heater was added which compensates the heat losses through the plexiglass which is in one of the sides of the storage - the side which is visually monitored. In Figure 36 this setup can be seen.

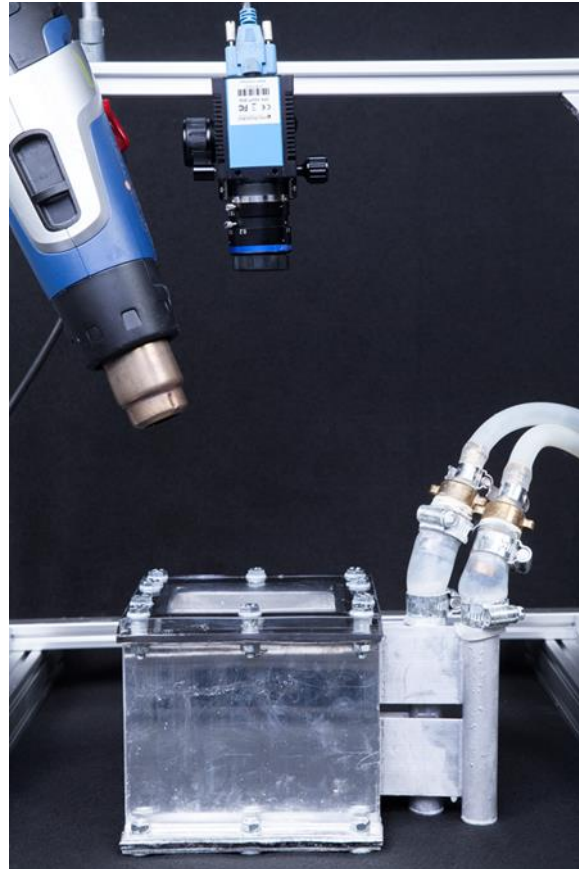


Figure 36: Experimental setup for the visual monitoring of the phase change of PCM inside of the small samples. External heater, camera, storage sample and connection pipes are shown.

For the temperature monitoring setup, three PT100 temperature sensors have been introduced through the plexiglass as shown in Figure 37.

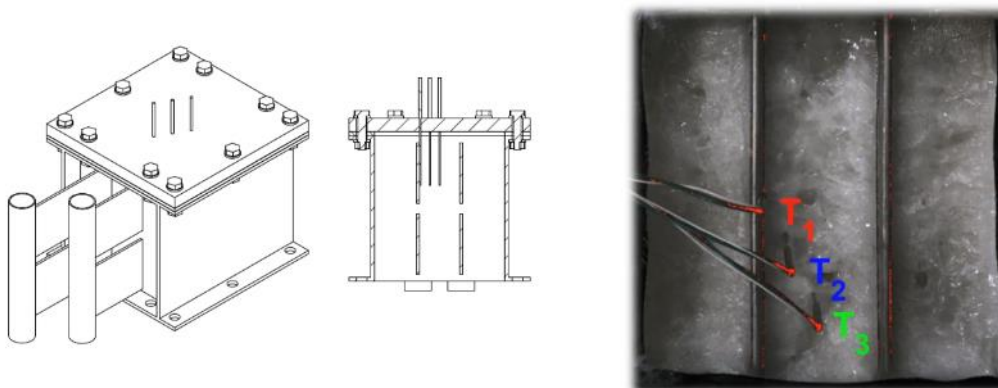


Figure 37: 3 cm separation small sample without fins and with integrated PT100 temperature sensors located between the water channels

**Experimental results:** For the visual monitoring of the phase change of the PCM, pictures of the small samples have been taken with a frequency of 1pic/15s. Monitoring of the propagation of the phase front gives insights on the heat transfer characteristics for different distances between water MPE-tubes and having different fin setups, i.e. fins or not. Therefore, the attention has been focused in the volume between channels, i.e. just the middle part of the storages has been analysed.

Image processing has been carried out with Matlab and the OpenCV library. The procedure to obtain the state of charge (SOC) and the energy (and power) stored/released (given/required) from the sequence of images is the following: After isolating the middle part, as said, a threshold value has been established for the pixel intensity in order to be able to distinguish if it corresponds to the liquid or the solid state of the PCM. Then, counting the pixels contained in the selected area, is straightforward to calculate the percentage of the PCM melted/solidified.

On the other side, the energy and power stored/released has been calculated with the following equations:

$$E_n = \sum_{i=1}^n \Delta N_{Liq_i} m_{pixel} \Delta h_{S-L} \cdot 10^3 \quad [J]$$

$$P_i = \frac{\Delta N_{Liq_i} m_{pixel} \Delta h_{S-L}}{\Delta T_{image}} \cdot 10^3 \quad [W]$$

Where  $n$  is the number of images used,  $\Delta N_{liq}$  is the number of images that became liquid in the last analysed image,  $m_{pixel}$  is the mass correspondent to a pixel,  $\Delta h_{s-L}$  is the latent heat for melting and  $\Delta T_{image}$  is the time interval between consecutive images.

The experiments carried out can be seen in the following table, where the samples studied, the process and the maximum power are shown:

Sample	Acronym	Process	Max. power [W]
1cm separation without fins	1cmNF	Solidification	7.5
		Melting	5.6
3cm separation without fins	3cmNF	Solidification	7.0
		Melting	5.0
1cm separation with fins	1cmF	Solidification	25.4
		Melting	22.3
3cm separation with fins	3cmF	Solidification	47.5
		Melting	45.0

As examples, the monitorization processes for solidification for the 1cm and 3cm samples can be seen below.

**Results for solidification of the samples with 1 cm distance between MPE-tubes:** In Figure 38 the results obtained for the solidification and melting process of the 1 cm separation small samples are shown, where the images of the initial and intermediate states can be seen in combination with the corresponding energy and power calculations (Figure 39, Figure 40).

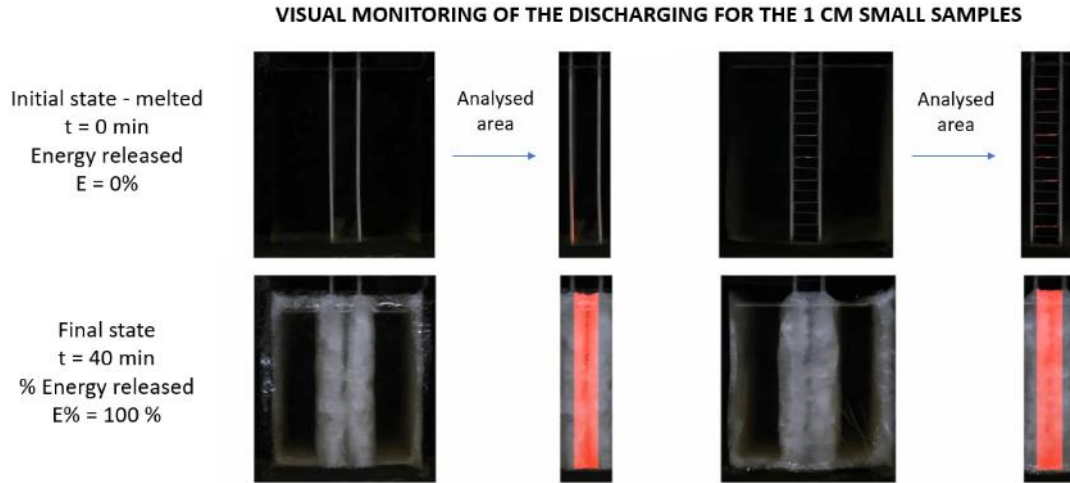


Figure 38: Image processing of solidification for the 1 cm separation samples - Initial and final states.

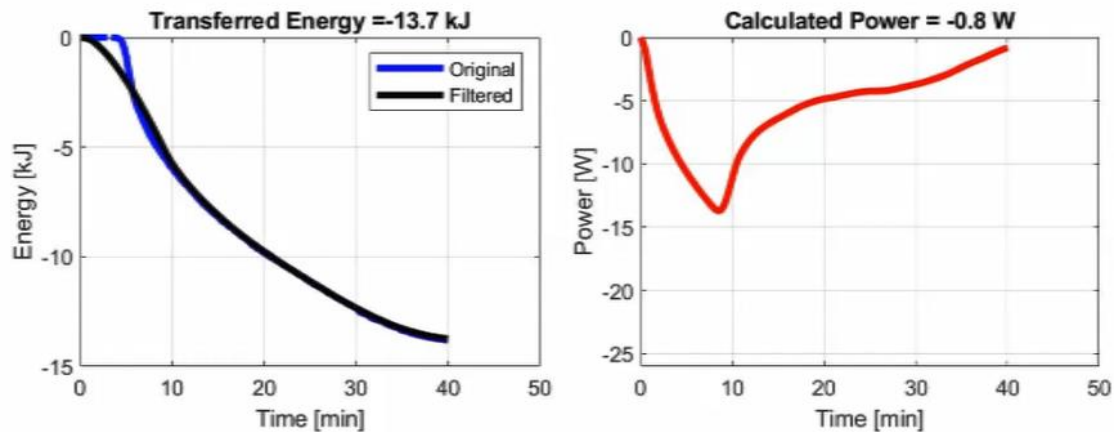


Figure 39: Released energy and required power for the 1 cm separation and no fin sample

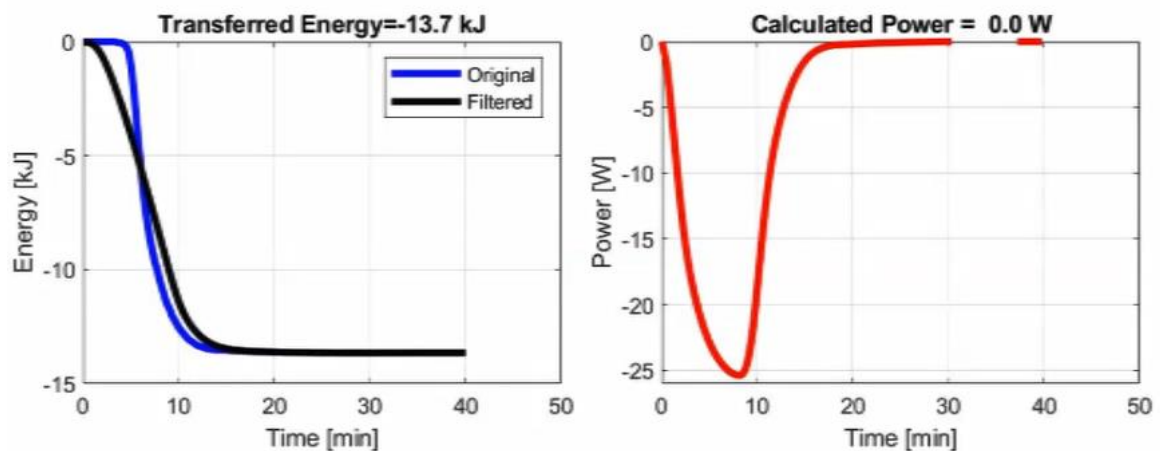


Figure 40: Released energy and required power for the 1 cm sample with fins

**Results for samples with 3 cm distance between MPE-tubes:**

**VISUAL MONITORING OF THE DISCHARGING FOR THE 3 CM SMALL SAMPLES**

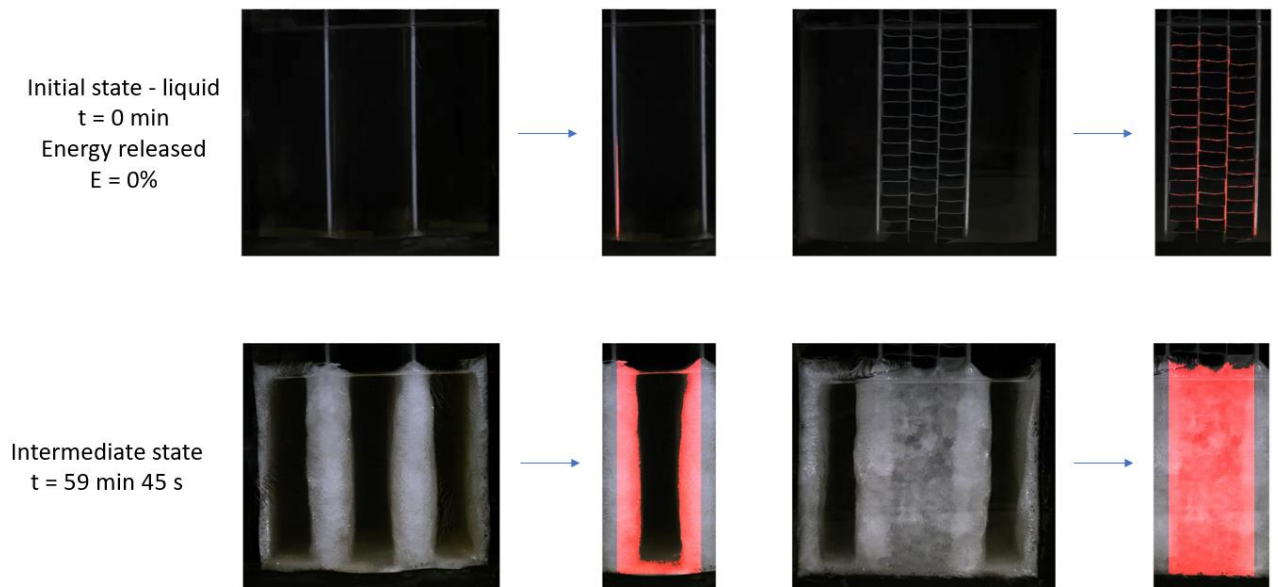


Figure 41: Image processing of solidifying for the 3 cm separation samples - Initial and intermediate state.

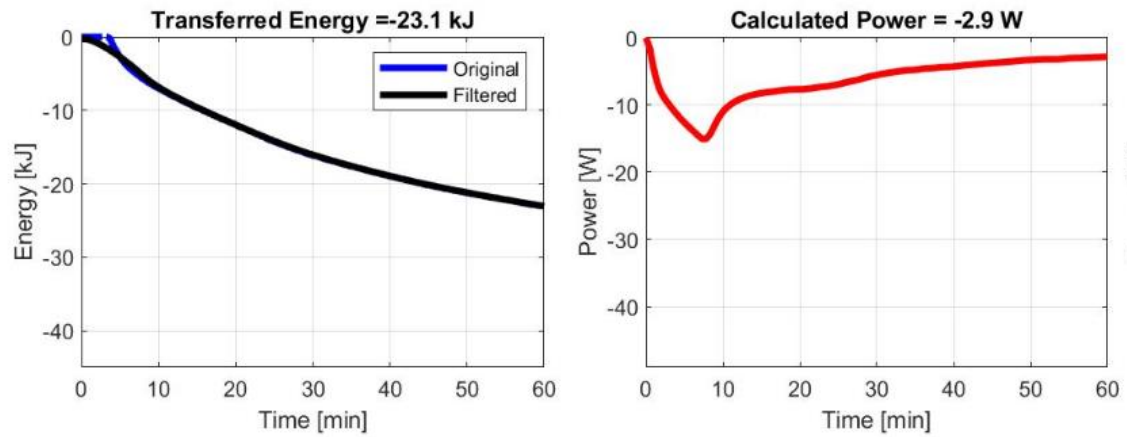


Figure 42: Released energy and required power for the 3 cm separation and no fin sample

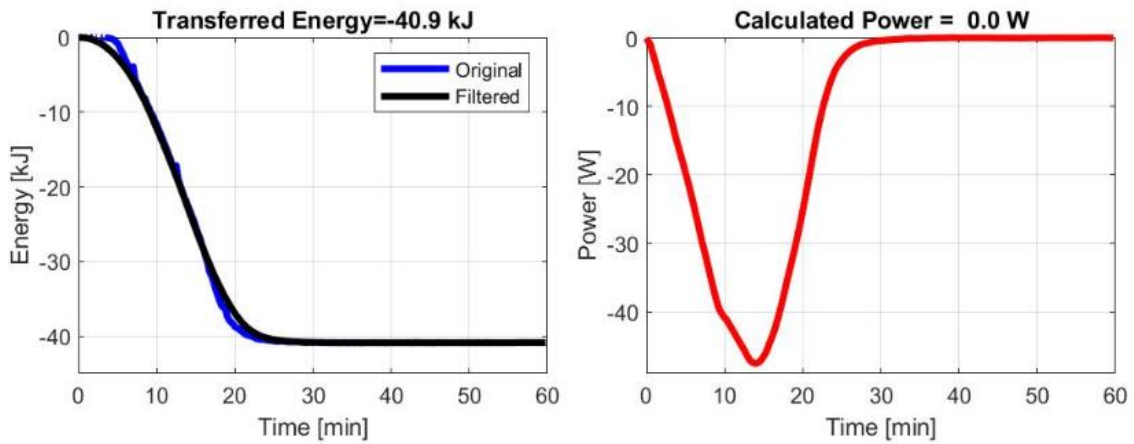


Figure 43: Released energy and required power for the 3 cm separation sample with fins

In Figure 44, the plot representing the maximum power for each of the samples and processes is shown. In addition, error bars have been applied in order to take into account the error when calculating the power from the filtered energy signal.

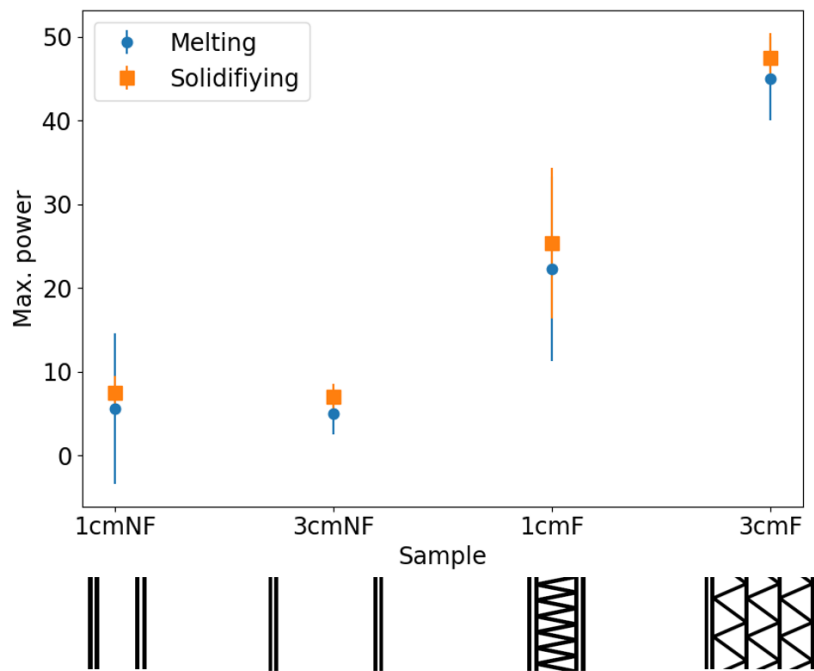


Figure 44: maximum power for each configuration tested.

As expected, using fin configuration considerably improves the maximum power the storage is going to be able to give or require. On the other side, focusing the attention into the no fin configuration, can be seen how having smaller separations between water channels improves the maximum power that can be achieved, i.e. it is almost the same as for the 3cm sample but the studied zone is smaller and therefore the PCM contained inside is also lower.

As shown in the experimental results, image processing techniques offer a good approach to the state of charge monitoring and the expected behaviours of different designs have been detected experimentally.

## 2-fluid W/PCM storage

The W/PCM storage is a small-sized analogue of the continental prototype with water as heat transfer fluid. As for the small test samples, the water provides or receives the temperature to or from the PCM, it flows unidirectional through the storage. The storage has been used to carry out experiments to characterize the charging and discharging with different PCMs, the temperature profiles developed inside the storage and water outlet temperatures.

The following figure and table show the relevant information regarding the dimensions and design parameters:

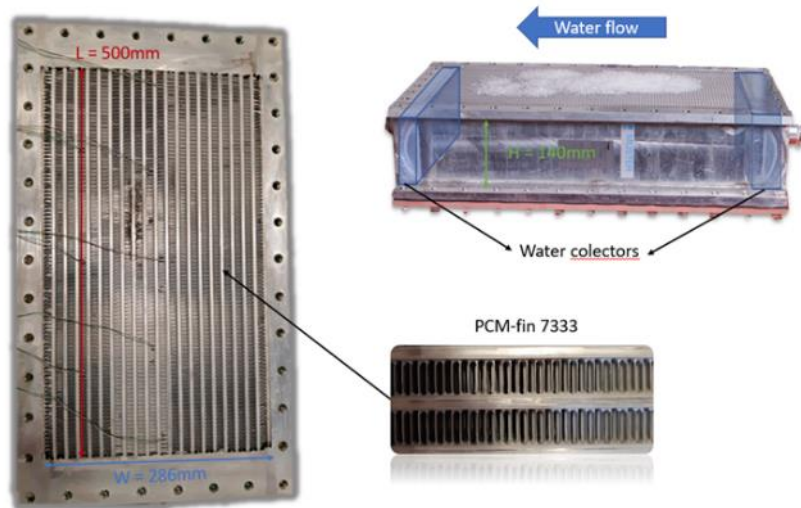


Figure 45: Design of the 2-fluid W/PCM storage filled with PCM RT64HC.

Table 21: Design parameters of the 2-fluid W/PCM storage.

Storage internal design		
Length	L	500 mm
Width	W	286 mm
Height	H	140 mm
Aluminium mass	M	9.25 kg
Total aluminium mass	M <sub>t</sub>	42 kg
Water passage		
Number of passages	n <sub>w</sub>	19
Heat transfer area	A <sub>w</sub>	5 m <sup>2</sup>
Total free volume	V <sub>w</sub>	2.70 L
Mass of aluminium	m <sub>Al_w</sub>	2.6 kg
<b>Fin type</b>	<b>AKG 43</b>	
Height	h <sub>w</sub>	3.00 mm
Fin spacing	s <sub>w</sub>	1.95 mm
Thickness	t <sub>w</sub>	0.30 mm
PCM passage		
Number of passages	n <sub>p</sub>	20
Heat transfer area	A <sub>p</sub>	13.3 m <sup>2</sup>
Total free volume	V <sub>p</sub>	11.4 L

Mass of aluminium	mAl_p	6.65 kg
<b>Fin type</b>	<b>AKG 33</b>	
Height	hp	10.0 mm
Fin spacing	sp	2.4 mm
Thickness	tp	0.3 mm
<b>Collectors</b>		
Number of collectors	nc	2
Total free volume	Vc	4.23 L
Mass of aluminium	mAl_c	4.6 kg

**Experimental setup:** To simulate storage charging and discharging operation, e.g. generation of domestic hot water, two thermal water bath temperature control units of type Julabo FP51 were used to circulate water through the storage. This way, different temperatures can be set up in them in order to be able to generate step temperature changes. The connection of these temperature control units to the storage is made by a small hydraulic circuit capable to control the source of water, i.e. which of the two units provides the water fed to the storage. In Figure 46 a scheme of the water circuit is shown, where the picture is taken from the B&R automation control interface. Through this graphical interface, it is possible to monitor different sensor measurements, as mass flow, temperatures or pressures.

The storage was thermally insulated, as well as the pipes used for connecting the mentioned hydraulic circuit to the storage. Finally, for monitoring different temperatures along the storage, PT100 temperature sensors have been positioned in different places. Two of them have been located in line to measure the water flow entering or leaving the storage (Figure 47) and 8 have been placed inside the storage to measure PCM temperatures in different positions (Figure 48).

The experiments have been made with a volumetric water flow of 90 l/h. Due to the heating and cooling capacity of the Julabos, this value has been chosen because it is inside the range of permissible water flows where the Julabo is able to compensate the cooled or heated streams when charging and discharging.

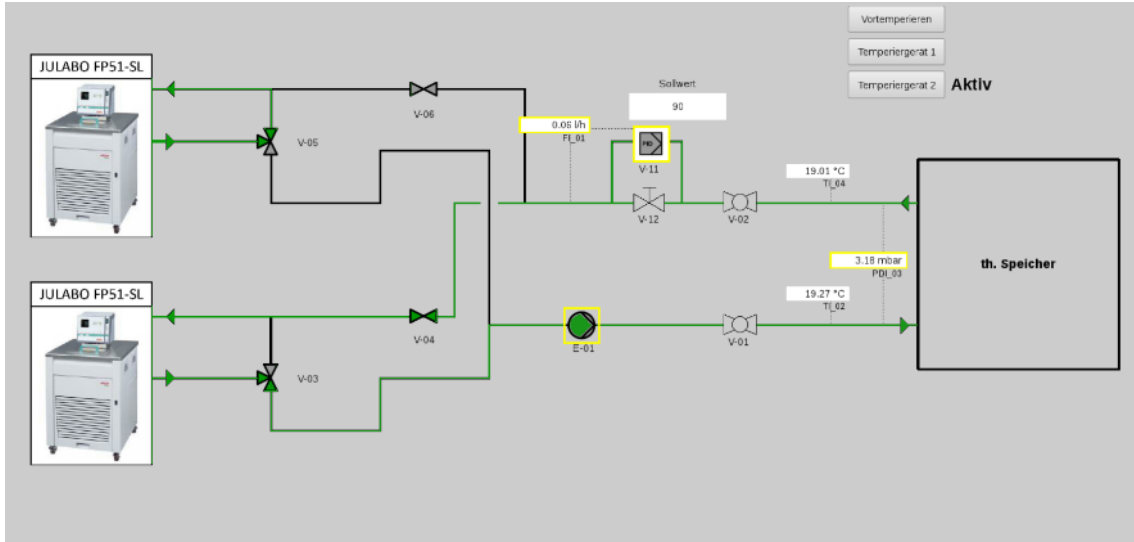


Figure 46: Scheme of the hydraulic circuit for controlling water flow for the 2-fluid W/PCM storage.

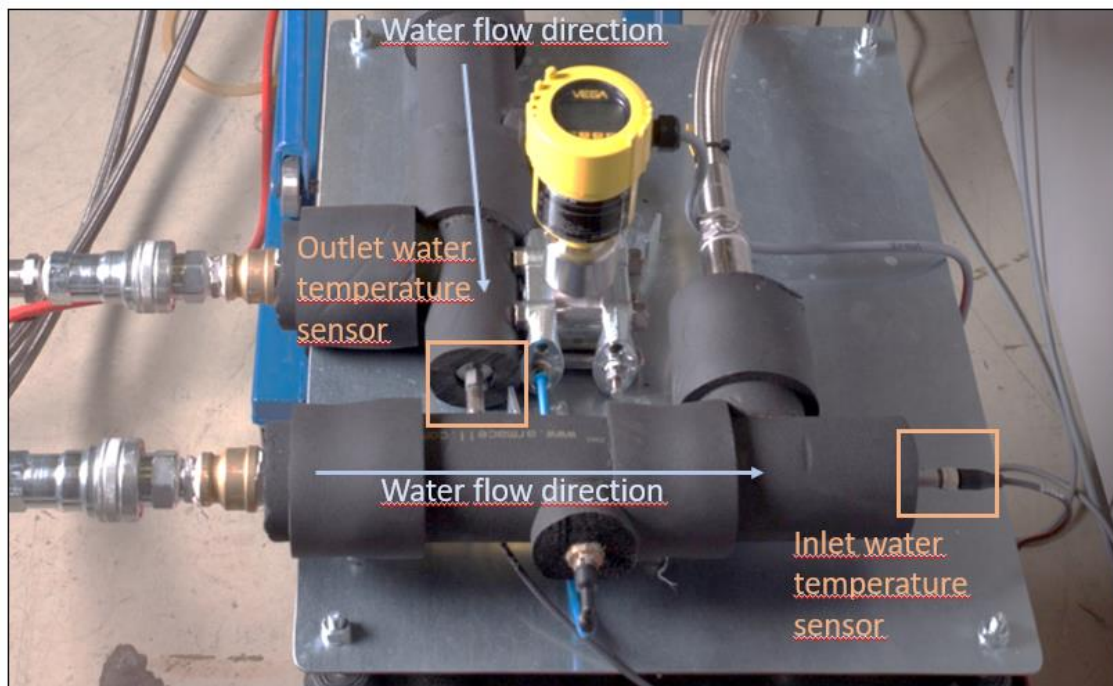


Figure 47: Two temperature sensors for inlet and outlet water temperature monitoring.

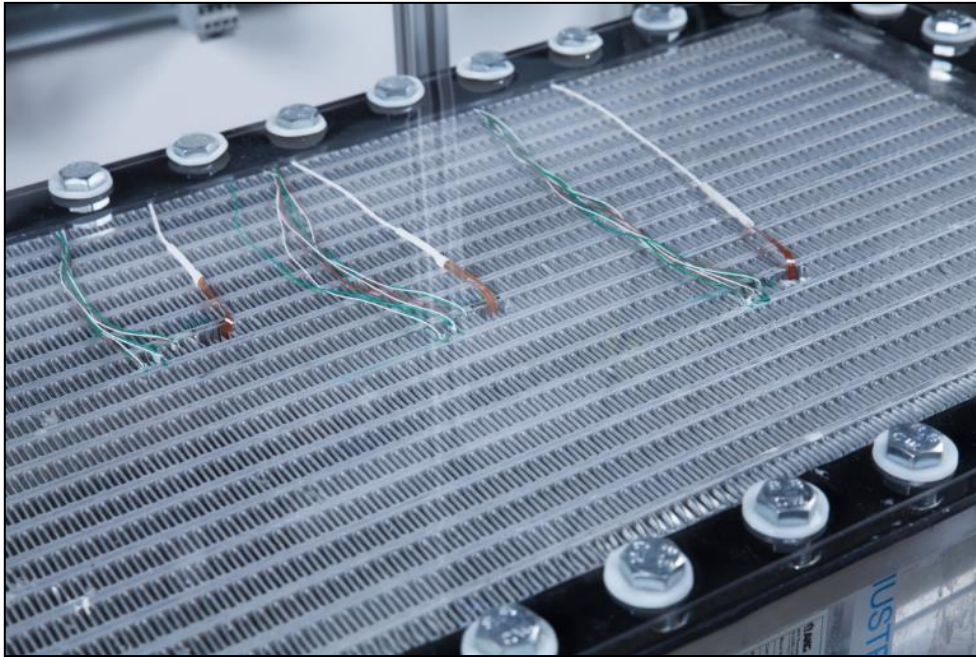


Figure 48: Temperature sensors with different locations inside 2-fluid W/PCM storage for monitoring PCM temperatures.

#### Results for the operation of the 2-fluid W/PCM storage:

After trying different temperature ranges for carrying out the experiments, it has been seen that the best results are obtained considering the range between +/- 6°C from the melting/solidification temperature. This range is wide enough to be able to see the effect the latent heat of the PCMs generate in the temperature measurements recorded and is not too large, as to produce a problem to the Julabo for compensating the incoming streams.

The PCMs used to experiment with this prototype have been RT55 and RT64HC. In addition to that, experiments with the empty storage have been carried out in order to get a better view of what is going on in the process.

At first, the results obtained with the empty storage can be seen in Figure 49. The temperature range is the same as the one used with RT55 due to the chronological order in which the experiments were performed. As was expected, the energy stored corresponds to the energy needed to heat up all the aluminium and the water inside the storage.

Energy needed to heat up the water and aluminium inside:

$$E = (m_w c_p(W) + m_{Al} c_p(Al)) \cdot \Delta T = 670.82 \text{ kJ} = 186.34 \text{ Wh}$$

Where:

- $m_w = 4.23 \text{ kg}$
- $m_{Al} = 42 \text{ kg}$
- $c_p(W) = 4.18 \text{ kJ/kg} \cdot K$
- $c_p(Al) = 0.91 \text{ kJ/kg} \cdot K$

Considering the heat losses that occur during the process, the results obtained seem to fit the theoretical assumption.

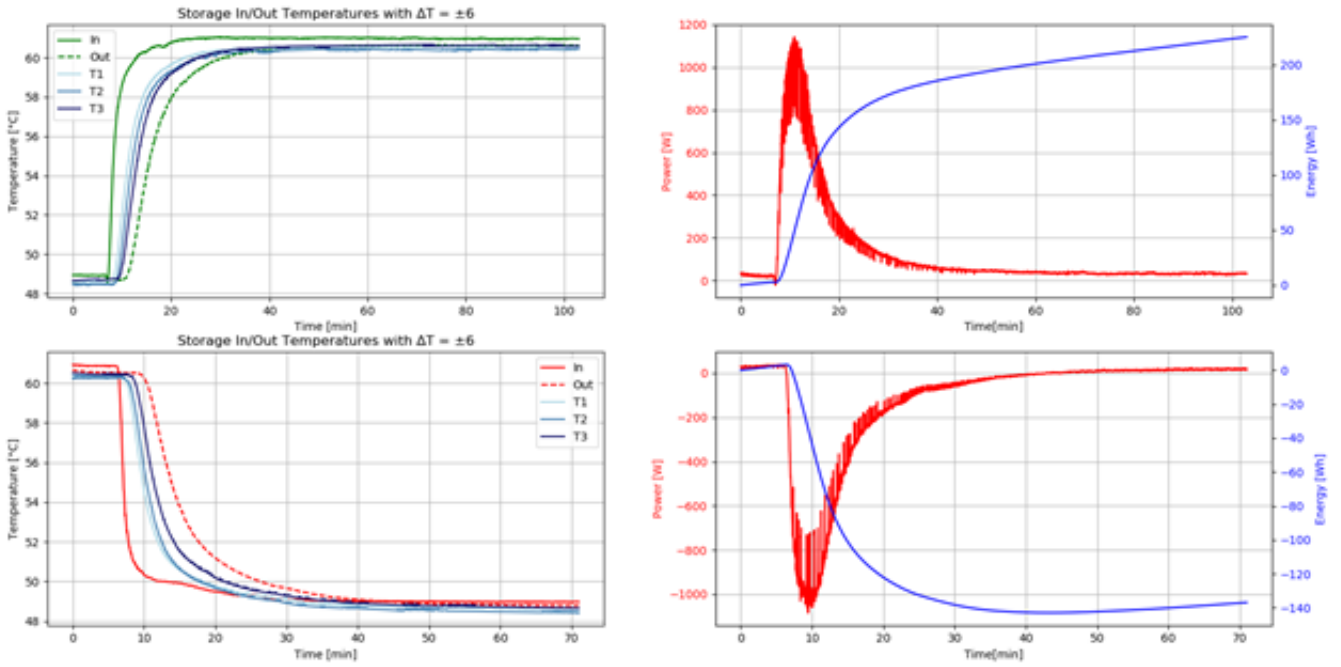


Figure 49: Experimental results obtained with the empty storage

The experimental results obtained for RT55 are shown in Figure 50. Both charging and discharging operations can be seen. In the left part, partial enthalpy distributions for both heating and cooling are shown, where the data provided by the manufacturer has been used; the middle part corresponds to the sensor data recorded, where water inlet and outlet temperatures are plotted in combination with the PCM temperatures along different positions in the storage; finally, energy and power calculations are shown, where data from the water mass flow, the temperature dependent PCMs partial enthalpy and the difference between the water temperature for the inlet and outlet have been used.

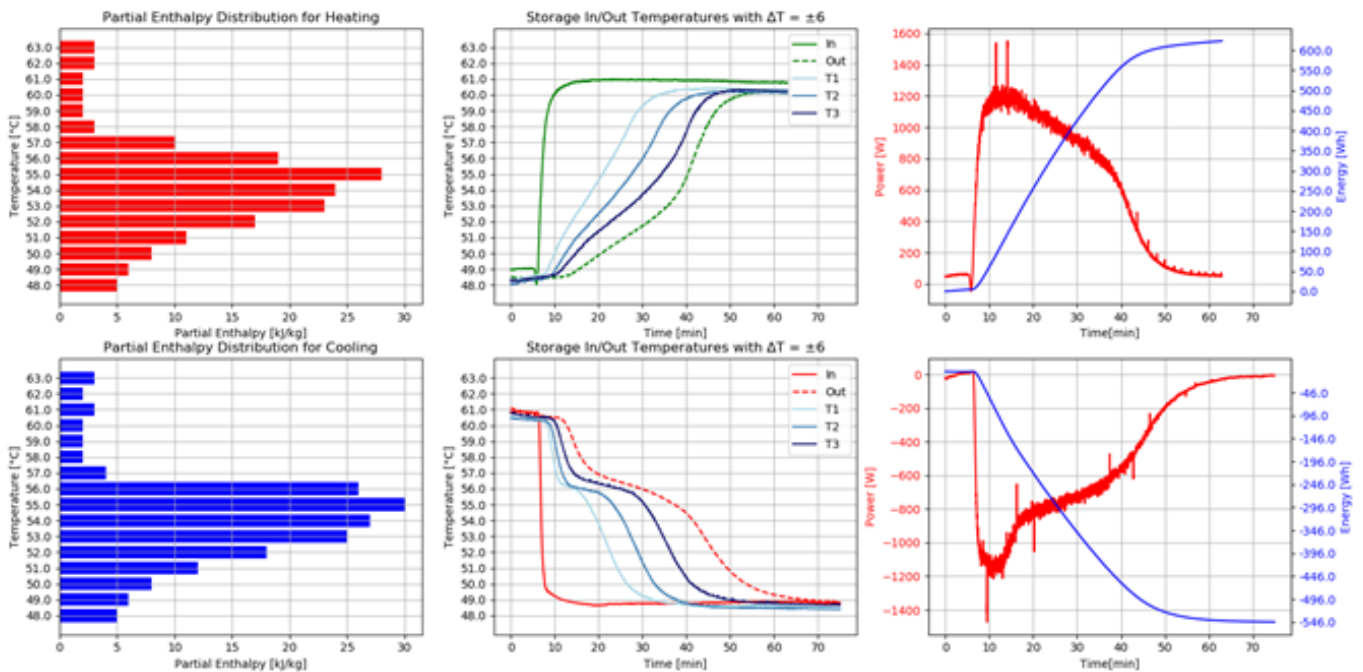


Figure 50: Experimental results for RT55

The influence of the PCM on the temperature profiles along the storage is conspicuous when compared to the results obtained for the empty storage. The sensors measuring the temperature in the PCM and the outlet temperature of the water are considerably affected by the shape of the partial enthalpy distribution of the used material and, as can be seen, this is intensified when the sensor is farther from the inlet water source.

The results obtained with RT64HC as filling material for the storage are shown in Figure 51 [28]. This material is the most performing due to the shape of its partial enthalpy distribution. As can be seen, both heating and cooling enthalpies contain very sharp latent heat peaks and, in addition, the distribution for cooling has two visible peaks in the range of study. Looking to the temperature profiles generated by this material for both processes, a clearer picture of how the PCM is affecting the output can be obtained.

As the aim of the continental design is providing domestic hot water, the discharging process is the most interesting one to consider for choosing the correct material. Focusing the attention on the results for the discharging with RT64HC, a completely flat outlet temperature profile can be noticed when the solidifying temperature is reached. Concretely, a 40-minute stationary temperature is maintained in the output water flow, which is interesting for the current application.

As a conclusion, it can be said that the partial enthalpy of the material used has a great impact on the outlet water temperature and has to be chosen in order to fulfil the requirements of the

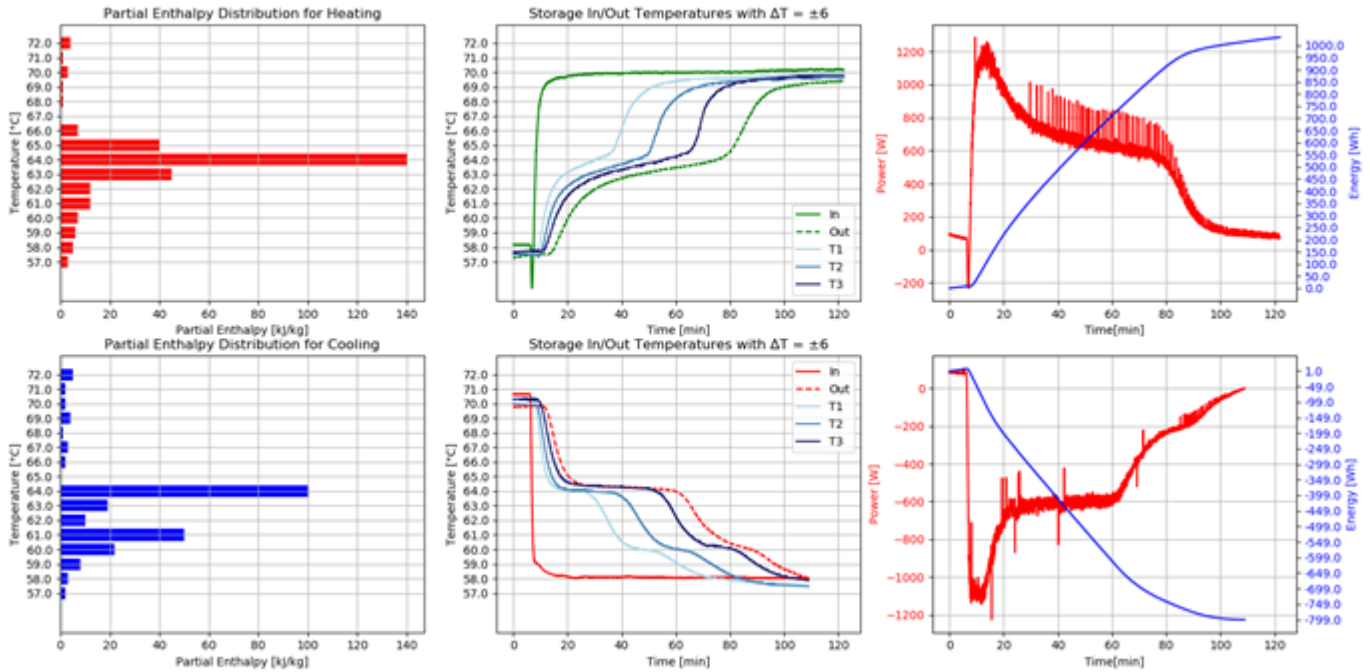


Figure 51: Experimental results for RT64HC

application. In the case of the continental prototype, materials with a very sharp and large peak for the enthalpy of the cooling process would be the most suitable and, as seen, in the case of the studied PCMs RT64HC would be preferred. On the other side, having information about water mass flow and inlet/outlet temperatures of it is enough to monitor the charging process of the storage with quite a good precision, as have been seen with the very simplified theoretical calculation for the empty storage.

## 5 Full-scale latent storages design and manufacturing

### 5.1.1 Low temperature full-scale latent storage design

The design of the full-scale latent storage was mainly driven by the storage capacity required by the system simulations. For the low temperature version, a storage capacity of 2.0 kW was agreed upon. Manufacturing and building space limitations then led to the maximum core dimensions. For the Mediterranean design a direct neighbourhood of the coolant and refrigerant passages is preferred. Since the coolant flow rate in the Mediterranean system is rather high the number of coolant passages had to be increased to 20 to stay within acceptable pressure losses on the coolant side. The refrigerant flow was arranged as U-flow to achieve higher flow velocities and better flow distribution in the heat exchanger. Within that limit it was possible to reach the storage capacity by having two PCM-passages per coolant-refrigerant-couple (Figure 52). The other main characteristics of the heat exchanger are listed in Table 22 and the drawing is shown in Figure 53.

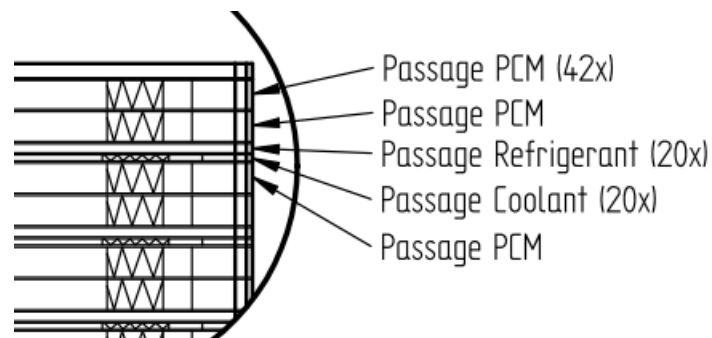


Figure 52. Arrangement of the PCM-passages in the full-scale RPW-HEX for NTUA

Table 22: Characteristics of low temperature full-scale latent storage design (NP 4013353)

	refrigerant	coolant	PCM (RT4)
Number of passages	20	20	42
Fin #	73	18	33
Fluid volume in ltr	5.34	4.6	46
core length x width x depth in mm	1000 x 585 x 160		
empty weight in kg (Al)	190		

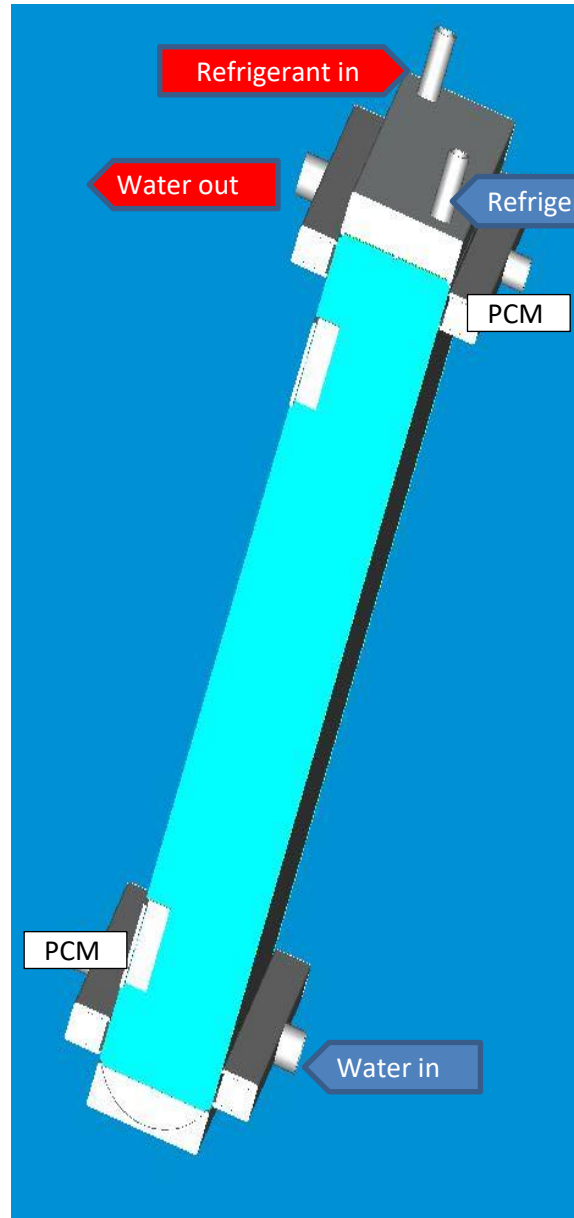


Figure 53. Drawing of low temperature full-scale latent storage for NTUA (NP 4013353)

### 5.1.2 High temperature full-scale latent storage design

Also the design of the full-scale latent storage for the Continental system was mainly driven by the storage capacity required by the system simulations. For the high temperature version a storage capacity of 2.5 kW was agreed upon. Manufacturing and building space limitations led to the maximum core dimensions. For the Continental design the PCM-passages are located between the coolant and refrigerant passages. The arrangement of the passages is shown in Figure 54. Since the coolant flow rate in the Continental system is lower than for the Mediterranean system the coolant was arranged in U-flow to achieve higher flow velocities and thus better heat transfer without violating the maximum allowed pressure loss on the coolant side. As for the Mediterranean system the refrigerant flow was arranged as U-flow to achieve higher flow velocities and better flow distribution in the heat exchanger. As for the low temperature RPW-HEX two PCM-passages are integrated per coolant-refrigerant-couple. The other main characteristics of the heat exchanger are listed in Table 23 and the drawing is shown in Figure 55.

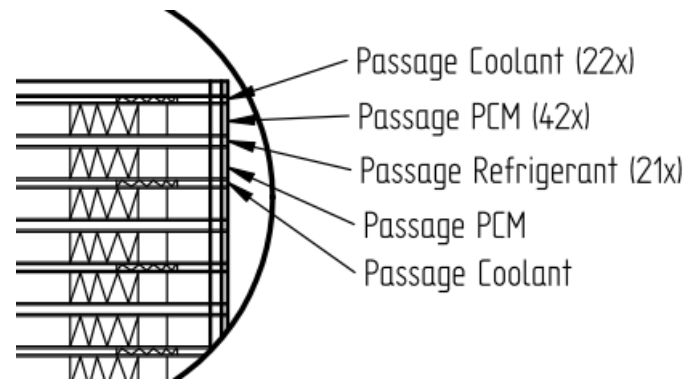


Figure 54. Arrangement of the PCM-passages in the full-scale RPW-HEX for AIT

Table 23: Characteristics of high temperature full-scale latent storage design (NP 4012812)

	refrigerant	coolant	PCM (RT64HC)
Number of passages	21	22	42
Fin #	73	18	33
Fluid volume in ltr	5,6	5	46
core length x width x depth in mm	1000 x 594 x 160		
Empty weight in kg (Al)	110		

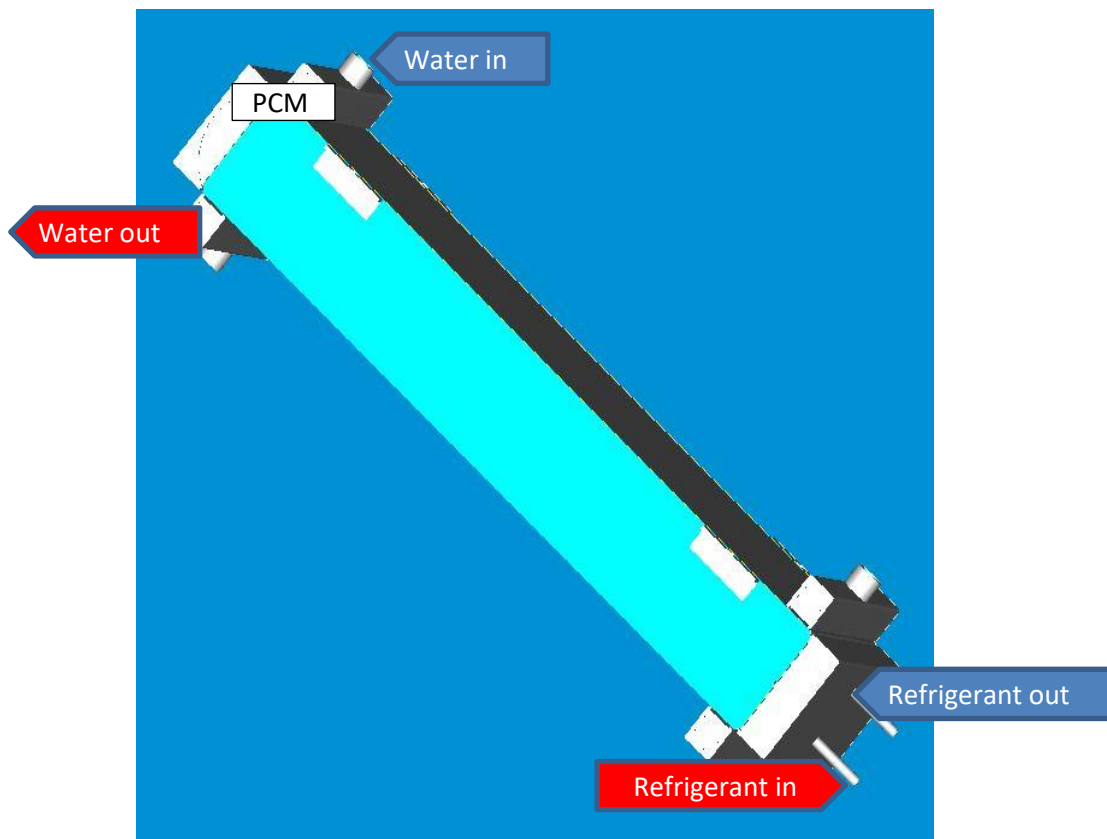


Figure 55. Drawing of high temperature full-scale latent storage for AIT (NP 4012812)

### 5.1.3 Full-scale latent storages manufacturing

The heat exchangers were then manufactured by AKG using mainly standard components and using AKG's unique dip-brazing process to braze the core. Afterwards the tanks to connect coolant, refrigerant and PCM were welded to the core together with corresponding nozzles. Also ports for connecting temperature and pressure sensors were welded to the heat exchanger. Once the RPW-HEX were leak checked under pressure they were ready to be filled with PCM.

For the low temperature RPW-HEX this was simple as RT4 is liquid at ambient temperature and it was filled in on one connector while the other one was used for de-aeration of the system securing a complete filling of the system. Figure 56 shows the finished low temperature heat exchanger with some of the ports for temperature sensors, which was shipped to NTUA in June 2019.

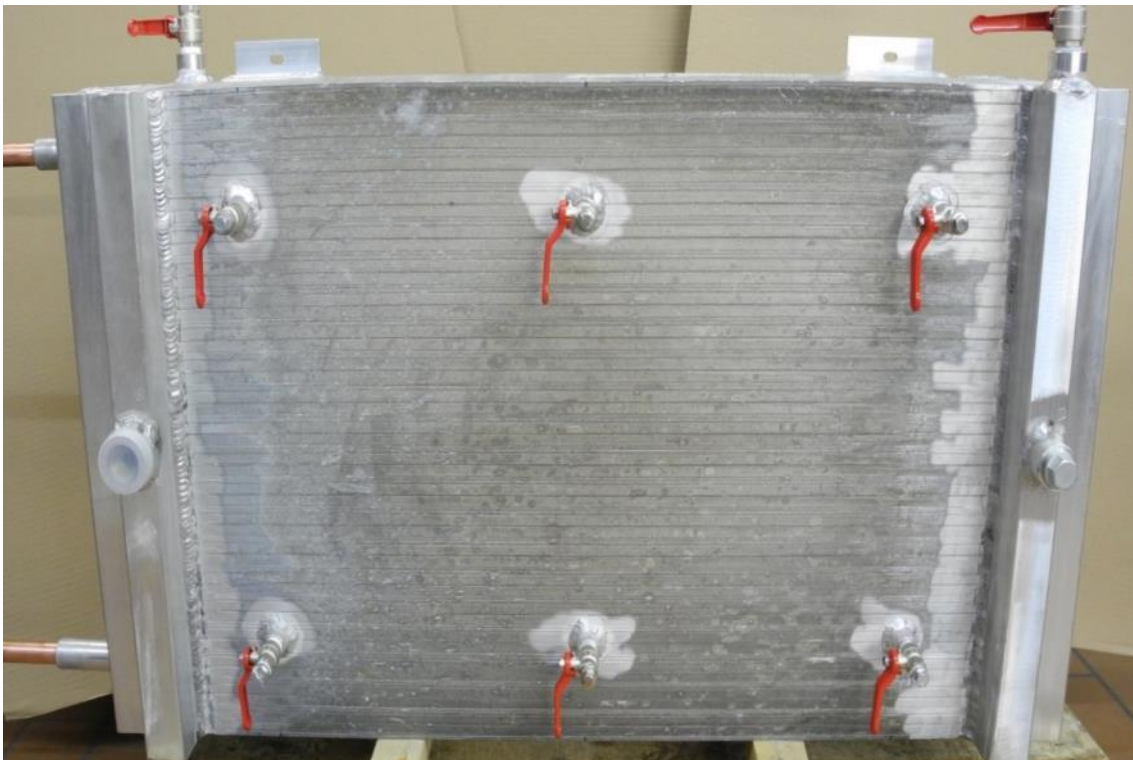


Figure 56. Photo of low temperature full-scale latent storage for NTUA (NP 4013353)

Filling the high temperature RPW-HEX for AIT was more complicated as the PCM RT64HC melts at around 64°C and thus is solid at ambient temperature.

For that purpose the RPW-HEX was connected to on the coolant side to one of AKG's test devices and hot coolant of 90°C was circulated through the heat exchanger to heat it up well above the melting temperature of the PCM. A part of the hot fluid was circulated through a tube-in-tube heat exchanger manufactured for this purpose to heat the filling pipe and the funnel, where the PCM-powder was filled in. The complete setup is shown in Figure 57.

After filling the RPW-HEX was closed and shipped to AIT in February 2019 (Figure 58).

Filling the 2,5 kWh RPW-HEX with PCM RT64 HC



Funnel filled with PCM



Tube-in-tube HEX to melt PCM

water/glykol  
inlet temperature 90 °C  
mass flow 2900 kg/h

Figure 57. Photo from setup for filling the high temperature RPW-HEX with molten PCM



Figure 58. Photo of high temperature full-scale latent storage for AIT (NP 4012812)

Thanks to valuable manufacturing experience during the production of the lab-scale samples both full-scale RPW-HEX were successfully manufactured at first go.

However further ideas for process and design improvements were gathered during manufacturing of the full-scale PRPW-HEX. Especially with respect to future production costs some of these findings shall be implemented in the production of the next RPW-HEX for the remaining demo sites. The main change will be trying to braze the cores in vacuum instead of the dip-brazing process. The process is more expensive but the finishing work on the cores was more than expected and should be significantly reduced by using AKG's vacuum brazing process. In order to manufacture the cores in that process a new stacking device was already prepared, which is shown in Figure 59.

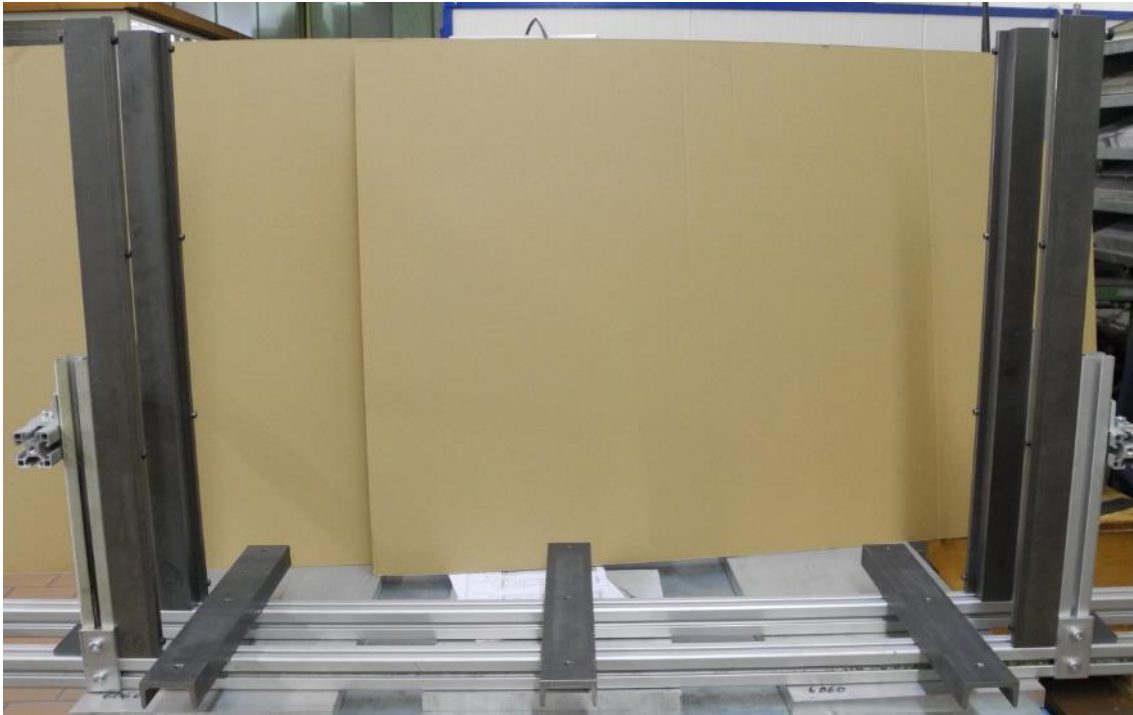


Figure 59. Stacking frame for brazing a core of an RPW-HEX in AKG'S vacuum furnace

## 6 Latent storage advanced monitoring algorithms

An important aspect related to the use of TES systems to determine the amount of energy available in the TES at any instant, which is best characterized by the state-of-charge (SOC) parameter. The consequences of operating in partial load conditions in a latent thermal energy storage tank were analysed in [32]. There are different methods reported in the literature for the determination of the SOC of an energy storage system based on the use of PCM, such as the use of electrical conductivity sensors [33], the use of pressure sensors to detect changes in the volume of the PCM [33,34], the use of temperature sensors located in the phase change material [35–43], the use of energy flow sensors able to measure the amount of heat supplied to and dissipated by the storage system [34,44], the use of image sensor or camera [40,41,43,45,46], the use of level sensors [47,48], the propagation of sound [34], PCM viscosity measurement [33], impedance spectroscopy [33], neutron diffractometer [49], light transmission measurements [33,40], and/or reaction measurements [44].

In the case of this study, four different methods were used to calculate the SOC of the latent energy storage, as described below:

1. Average PCM temperature ( $SOC_{T,PCM}$ ).
2. Average specific PCM enthalpy ( $SOC_{h,PCM}$ ).
3. Energy balance of the HTF ( $SOC_{HTF}$ ).
4. Pressure inside the PCM cavity ( $SOC_p$ ).

In each case, the PCM was considered to be 100% charged when it reached the minimum or maximum level of energy, when the purpose of the PCM was to store cold or heat, respectively. The PCM was considered to be totally discharged when it reached the maximum or minimum level of energy for cold or heat storage, respectively. According to this criterion, the first two methods will directly depend on the PCM temperature. Regarding the third method, the SOC is obtained in terms of the heat extracted from or supplied to the HEX by the HTF, depending on whether the HEX is charging or discharging. The fourth method is based on the fact that the pressure inside the PCM cavity is expected to vary when the PCM is changing phase because of its different densities in the liquid and solid states.

Focusing on the low-temperature latent storage, the analytical equations that define the SOC according to the four abovementioned methods are shown in Eq. 1 to Eq. 4:

$$SOC_{T,PCM} = \frac{T_{max} - \frac{\sum_i T_i(t) \cdot m_i}{M_{PCM}}}{T_{max} - T_{min}}$$

$$SOC_{h,PCM} = \frac{h_{max} - \frac{\sum_i h_i(t) \cdot m_i}{M_{PCM}}}{h_{max} - h_{min}}$$

$$SOC_{HTF} = \begin{cases} \frac{\int_0^t (T_{HTF,out}(\tau) - T_{HTF,in}(\tau)) \cdot d\tau}{\int_0^{t_f} (T_{HTF,out}(\tau) - T_{HTF,in}(\tau)) \cdot d\tau}, & \text{for charging} \\ 1 - \frac{\int_0^t (T_{HTF,in}(\tau) - T_{HTF,out}(\tau)) \cdot d\tau}{\int_0^{t_f} (T_{HTF,in}(\tau) - T_{HTF,out}(\tau)) \cdot d\tau}, & \text{for discharging} \end{cases}$$

$$SOC_p = \frac{p_{max} - p(t)}{p_{max} - p_{min}}$$

where  $T_i(t)$  is the temperature of the PCM compartment  $i$  at time instant  $t$ ,  $T_{min}$  and  $T_{max}$  are the minimum and maximum PCM temperature along the entire process, respectively,  $m_i$  is the mass of the PCM associated to the PCM compartment  $i$ ,  $M_{PCM}$  is the total mass of PCM inside the HEX,  $h_i(t)$  is the specific enthalpy of the PCM compartment  $i$  at temperature  $T_i$  at time instant  $t$ , being  $h_{min}$  and  $h_{max}$  the specific PCM enthalpy corresponding to  $T_{min}$  and  $T_{max}$ , respectively,  $p(t)$  is the pressure inside the PCM cavity at time instant  $t$ , being  $p_{min}$  and  $p_{max}$  the minimum and the maximum pressure corresponding to  $T_{min}$  and  $T_{max}$ , respectively,  $T_{HTF,in}$  and  $T_{HTF,out}$  are the HTF temperature at the inlet and outlet of the HEX, respectively, and  $t_f$  is the total duration of the charging/discharging process.

## 6.1 Analysis of RPW-HEX storage capacity as a function of its charging/discharging operating range

The RPW-HEX storage capacity mostly depends on the phase transition enthalpy of the PCM (or simply its latent enthalpy), the PCM sensible enthalpy and the sensible enthalpy of the storage case and internals made from aluminium.

### 6.1.1 PCM solid/liquid phase transition temperature range

The PCM solid/liquid phase transition temperature range describes the temperature range where the PCM changes its state from solid to liquid or vice-versa. It is characterized by the liquid mass phase fraction,

$$\xi = \frac{m^l}{m^l + m^s}$$

where  $m^s$  and  $m^l$  are the masses of solid and liquid phase, respectively. From the analysis of the peak shape of PCM specific heat capacity data, e.g. generated by DSC, the phase transition temperature range can be identified, see Figure 60.

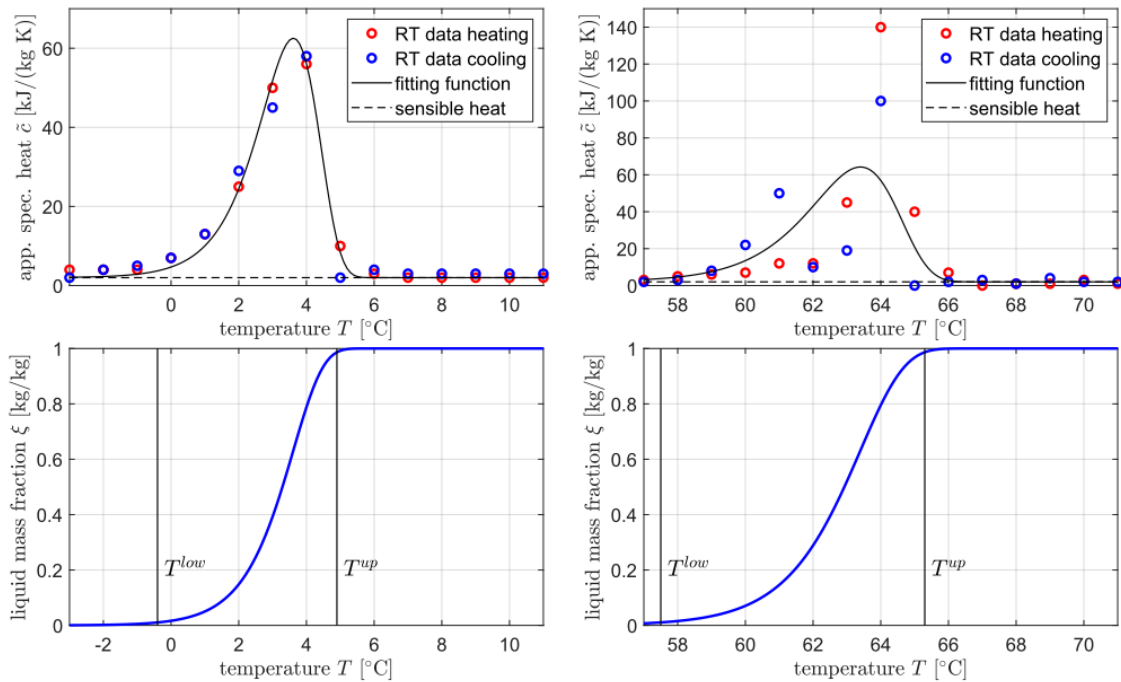


Figure 60. Peak identification in heat capacity data provided by manufacturer Rubitherm for PCM RT4 (left above), and RT64HC (right above). Corresponding baseline-corrected and normalized cumulative peaks are used to model changes of the liquid mass phase fraction  $\xi$  (below).

The lower and upper limits of the phase transition temperature ranges in Figure 60 (below) are identified as  $T^{low} = T(\xi = 0.01)$  and  $T^{up} = T(\xi = 0.99)$ .

### 6.1.2 RPW-HEX energy absorption/release

The following assumptions are made

- homogeneous temperature in the RPW-HEX, in the aluminium casing and internals as well as in the PCM,
- water and refrigerant in the RPW-HEX do not contribute to the internal energy,
- RPW-HEX is filled with 35 kg PCM,
- empty RPW-HEX weights 130 kg.
- The energy absorbed and released results from contributions from
- PCM latent heat (145 and 220 kJ/kg for RT4 and RT64HC, respectively),
- PCM sensible heat (2 kJ/kg/K for RT4 and RT64HC for solid and liquid state),
- aluminium RPW-HEX casing and internals (0.978 kJ/kg/K).

A simple integration of the sensible and latent enthalpies over a relevant temperature range yields the results for the CONT and MED RPW-HEX shown in Figure 61.

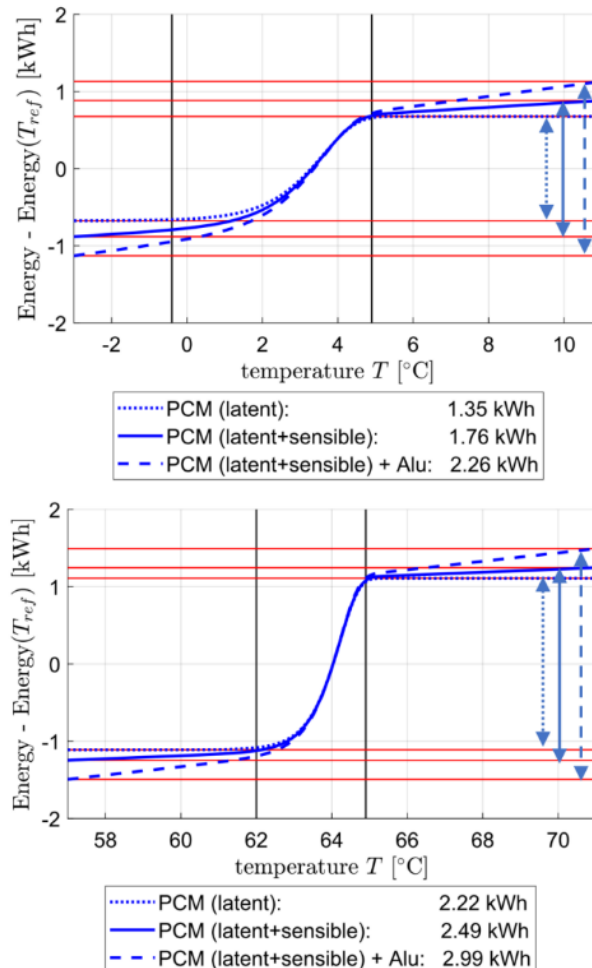


Figure 61. Contributions to energy absorption/release for RPW-HEX filled with 35 kg PCM RT4 (left) and RT64HC (right). Reference temperatures  $T_{ref}$  for calculation of energies are defined by peak temperatures in the PCM heat capacity data in Figure 60.

It is noted that for both, MED and CONT system, equal storage geometry and PCM mass is assumed. In other words, the results shown in Figure 61 show the thermal capacity of one storage prototype filled with different PCM. It turns out, that especially for the current RPW-HEXS design of the MED system, these assumptions are rather conservative (mass ratio PCM/Al rather small). AKG is considering several measures for further optimization of the RPW-HEX geometry (using less aluminium for the same amount of PCM in the storage) in order to reduce the contributions from aluminium sensible heat. These measures are reduction of the number of refrigerant passages, reduction of the volume of the collectors for water and refrigerant, using PCM passages with increased thickness (or a double PCM passages).

### 6.1.3 PCM density changes

Rubitherm PCM data sheets give constant values for solid and for liquid PCM densities  $\rho$ . Therefore, it seems reasonable to assume that PCM density changes during phase transition range (defined by  $T^{low}$  and  $T^{up}$ ) and that outside of this range the PCM density is constant (changes are not significant). Density changes are computed as

$$\rho = \xi \rho^l + (1 - \xi) \rho^s$$

where  $\rho^s$  and  $\rho^l$  are solid and liquid densities taken from Rubitherms data sheets.

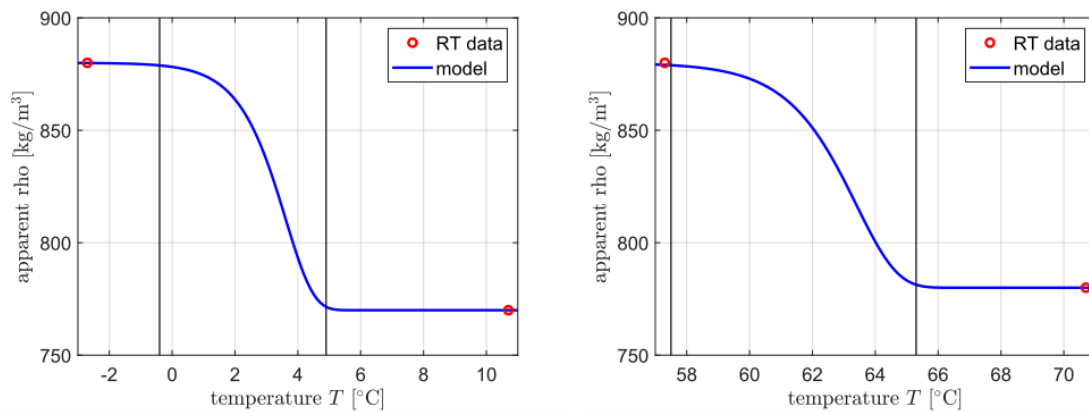


Figure 62. Prediction of density changes for RT4 (left) and RT64HC (right) over the phase transition temperature range identified in Figure 61.

The following conclusions can be drawn from the theoretical analysis of the RPW-HEX storage capacity:

- For the considered RPW-HEX design,
  - for the operation inside of the phase transition temperature range ( $T^{low} \dots T^{up}$ ), the RPW-HEX aluminium contributes little to the total storable energy;
  - for the operation outside of the phase transition temperature range, significant additional amounts of (sensible) storage capacity might be levered (depending on the selected “extended” temperature range), see Figure 61.
- The most realistic monitoring device to assess the charging state (SoC) of the RPW-HEX is a sensor measuring the pressure in the PCM passages.

*Ideally, this sensor is independent of the measurement position, i.e. the pressure in the PCM is homogenous. (This is a big advantage compared to temperature sensors, taking into account that temperature is likely not homogenous.)*

- Such a pressure sensor is sensitive to changes in the PCM density. These changes occur only within the phase transition temperature range. Outside the pressure sensor is “blind”, see Figure 61.
- Such a pressure sensor can be used even when PCM phase transition temperature range is different for melting (heating) and solidification (cooling).

#### 6.1.4 Experimental tests for the monitoring of the SOC with the low temperature lab-scale 2-fluid HEX

The results of the experimental tests performed with the low temperature lab-scale 2-fluid HEX are shown in this section, for the four methods for determining the SOC investigated in this study (equations 1 to 4) [29]. Figure 63 shows that, during charging, a consistent relationship exists between the methods based on PCM enthalpy estimation and energy balance of the HTF, which follow similar trends along most of the process duration for each of the flow rates. The method based on PCM average temperature measurements shows a faster increase during the first part of the process, and when the SOC reaches a value around 50% there is a clear reduction in the increasing rate and it adjusts to the previous two curves when the SOC is around 80%. Finally, the method based on pressure measurements shows a different behavior with respect to the other three methods. At the beginning of the process, it increases at similar rates as the other methods but, unlike the other curves, in this case the increase is maintained at a level similar to the one at the beginning until it reaches values almost as high as 90%.

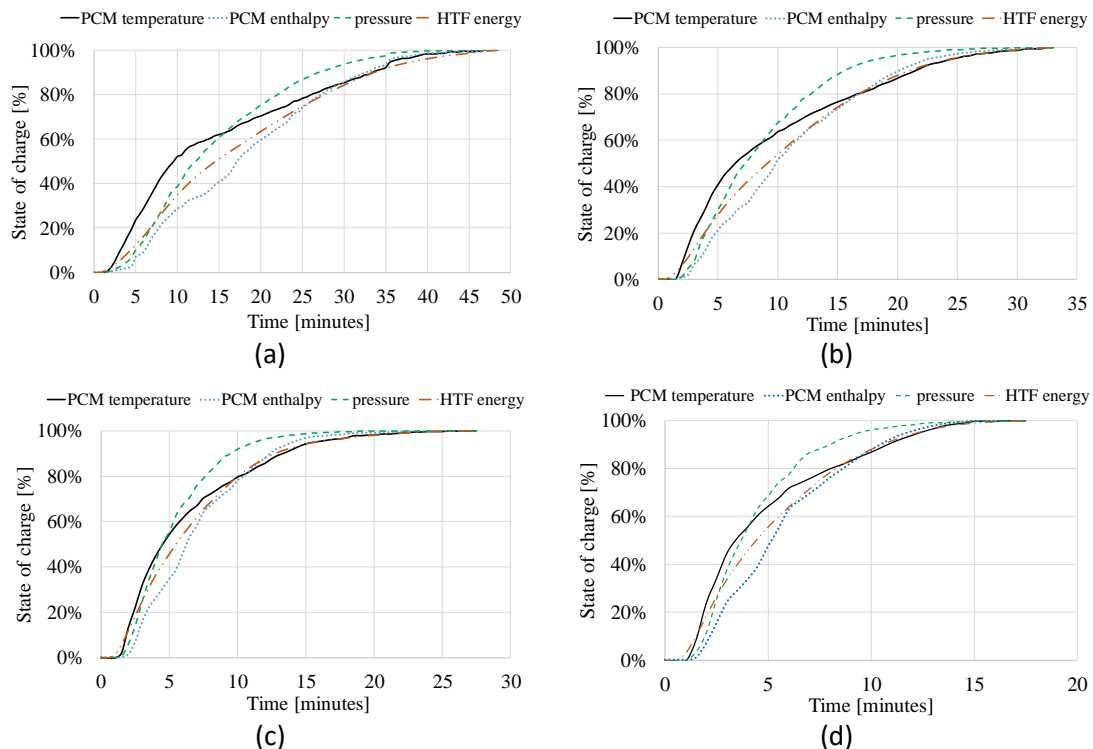


Figure 63. Comparison between the four methods for determining the SOC during charging at a HTF flow rate of (a) 0.5 L/min, (b) 1.0 L/min, (c) 1.5 L/min, and (d) 2 L/min [29].

Figure 64 [29] shows the evolution of the SOC determined according to different methods during the charging process at a flow rate of 0.5 L/min and at different temperature ranges. The

behavior of each of the four curves does not change significantly by changing the temperature range applied during the process.

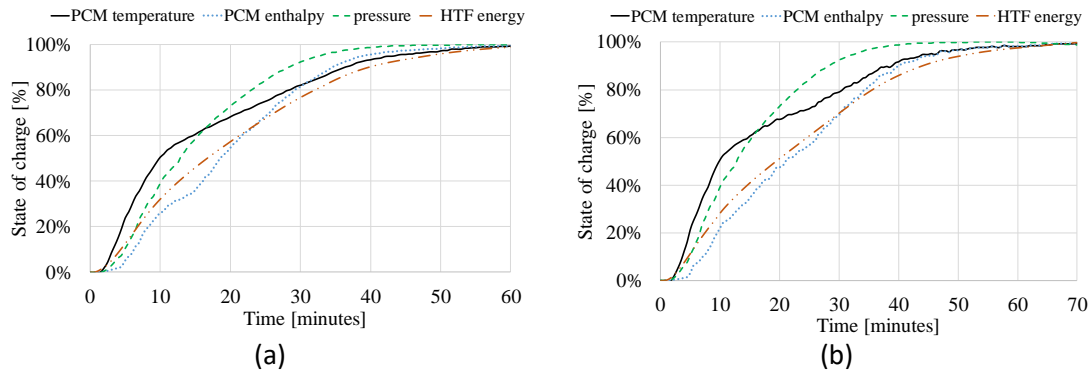
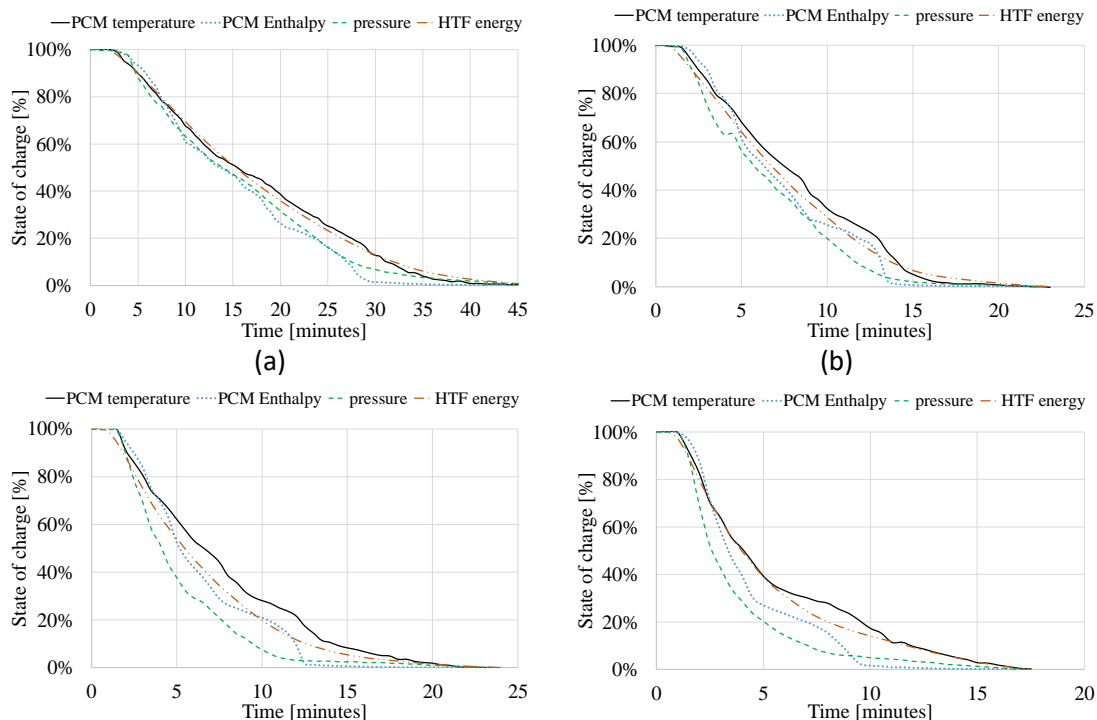


Figure 64. Comparison between the four methods for determining the SOC during charging at a flow rate of 0.5 L/min and two different temperature ranges at (a)  $\pm 8^\circ\text{C}$  and (b)  $\pm 4^\circ\text{C}$  [29].

The evolution of the SOC according to the different methods during discharging at different HTF flow rates is shown in Figure 65 [29]. Unlike the charging process, the methods based on PCM enthalpy and energy balance of the HTF give quite different curves during discharging. The curve based on HTF energy balance is decreasing smoothly towards its minimum value, while the curve based on PCM enthalpy shows large slope variations along the entire process, especially for higher HTF flow rates. Like in the charging process, the curve based on pressure measurements has the highest variation rate during the first part of the process, being therefore the method that gives the lowest values for the SOC along most part of the entire process. On the other hand, the curve based on the average PCM temperature has a different profile as compared to the charging profile, being in this case more similar to the profile of the curve based on the HTF energy balance.



(c) (d)

Figure 65. Comparison between the four methods for determining the SOC during discharging at a HTF flow rate of (a) 0.5 L/min, (b) 1.0 L/min, (c) 1.5 L/min, and (d) 2 L/min [29].

The evolution of the SOC obtained by the different methods during discharging at different temperature ranges at a flow rate of 0.5 L/min is shown in Figure 66 [29]. There is no significant difference between the discharging processes at the two different temperature ranges, and discharging at  $\Delta T \pm 8$  °C seems to occur slightly faster. It can also be noticed that in the  $\Delta T \pm 8$  °C case the pressure undergoes a short fluctuation at around 7 minutes after the start of the process, after which it continues to drop until the HEX is almost completely discharged. Here again, the curves corresponding to the average PCM temperature and HTF energy balance are quite similar, while fluctuations in the curve based on the average PCM enthalpy can also be observed.

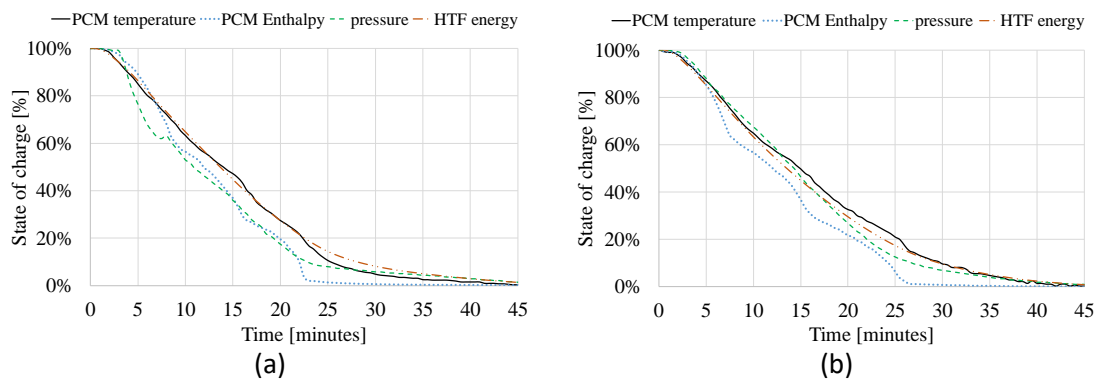


Figure 66. Comparison between the four methods for determining the SOC during discharging at a flow rate of 0.5 L/min and two different temperature ranges at (a)  $\pm 8$  °C and (b)  $\pm 4$  °C [29].

### 6.1.5 Experimental tests for the monitoring of the SOC with the full-scale lab prototype for the CONT system

A transferability study was carried out to assess the performance of the “Average PCM temperature ( $SOC_{T,PCM}$ )” (method 1) and “Pressure inside the PCM cavity ( $SOC_p$ )” (method 4) monitoring method for a full-scale lab prototype, in other words the full-scale latent storage of the CONT system operated at AIT’s thermal labs.

**Methodology:** To capture the charging of the PCM inside the RPW-HEX two approaches have been used: pressure measurements (method 4) and surface temperature measurements (adapted method 1). As discussed before, the pressure measurement approach is based on the displacement of gas in the PCM-section of the RPW-HEX by the expanding PCM during heating. It is anticipated that a great portion of the volumetric expansion of the PCM is attributed to melting (Figure 62) and may result in a significant pressure increase when the PCM section of the RPW-HEX is sealed. However, the gas needed to cover the volumetric expansion of the PCM is considered dead space as it doesn’t contribute to the storage capacity of the RPW-HEX.  $\epsilon$  is the specific dead space and is the ratio between gas-volume  $V_{gas}$  and total PCM-section-volume  $V_{PCM-section}$  – the gas-volume and the PCM-volume  $V_{PCM}$  – at a reference temperature  $\vartheta_{ref}$ .

$$\epsilon = \frac{V_{gas}}{V_{PCM-section}} \Big|_{\vartheta_{ref}} = \frac{V_{gas}}{V_{gas} + V_{PCM}} \Big|_{\vartheta_{ref}}$$

The pressure increase due to expansion of the PCM strongly depends on  $\epsilon$  where  $\epsilon_{critical}$  is the minimal dead space needed to capture the expanding PCM where the pressure increases to infinite. Considering air as gas and an incompressible PCM  $\epsilon_{critical}$  is approx. 11.36% for the used

PCM (RT64HC) when the PCM is heated from reference temperature 20°C to 80°C. The pressure inside the gas quickly decreases with dead space reaching a mere of 2.5bar at  $\epsilon=20\%$  (cf. Figure 67).

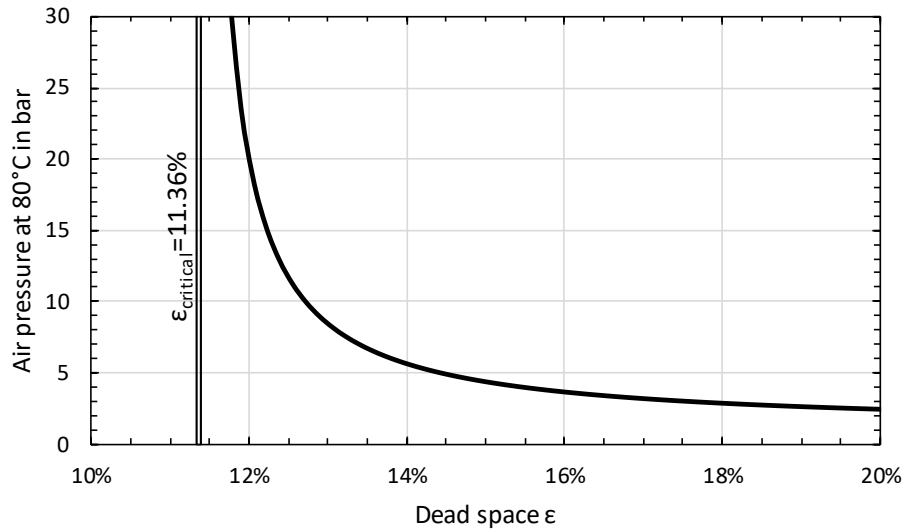


Figure 67. Pressure in the PCM section of the RPW-HEX depending on the dead space considering heating from 20°C to 80°C.

On the other hand, the pressure measurement approach might build on the direct identification of PCM temperatures and the correlation to the known phase transition behaviour of the PCM with a discriminant enthalpy peak at melting and solidification respectively (cf. Figure 68).

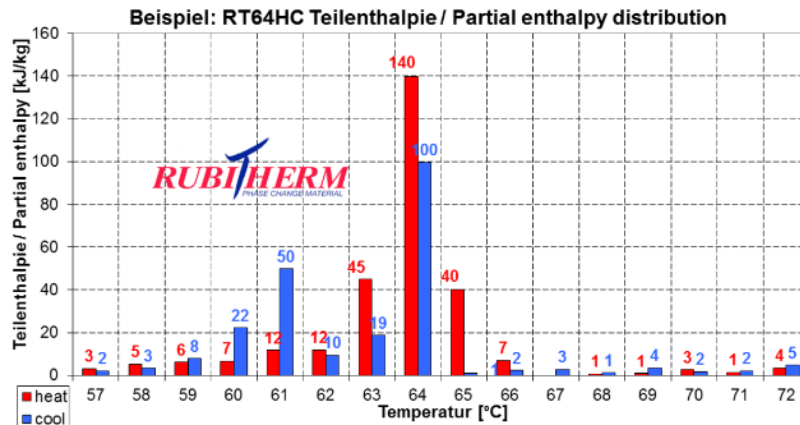


Figure 68: Partial enthalpy distribution of the used PCM (RT64HC).<sup>5</sup>

**Measurement setup:** To measure the temperature a pressure transmitter from EMERSON Type 3051CD was connected to the PCM section of the RPW-HEX using adequate fittings and a flexible house. The pressure transmitter was integrated into the industrial PLC system and data were

<sup>5</sup> Rubitherm (2018). Data sheet – RT64HC. Rubitherm Technologies GmbH. Retrieved on August 27, 2019, from [https://www.rubitherm.eu/media/products/datasheets/Techdata\\_-RT64HC\\_EN\\_06082018.PDF](https://www.rubitherm.eu/media/products/datasheets/Techdata_-RT64HC_EN_06082018.PDF).

transferred using the HART communication protocol. Pictures of the pressure measurement is given in Figure 69.



Figure 69: RPW-HEX PCM pressure measurement.

To measure the temperatures the RPW-HEX was equipped with 14, class A, 2x10mm PT-100 temperature sensors from RS PRO type 362-9799. The positioning of the sensors is given in Figure 70.

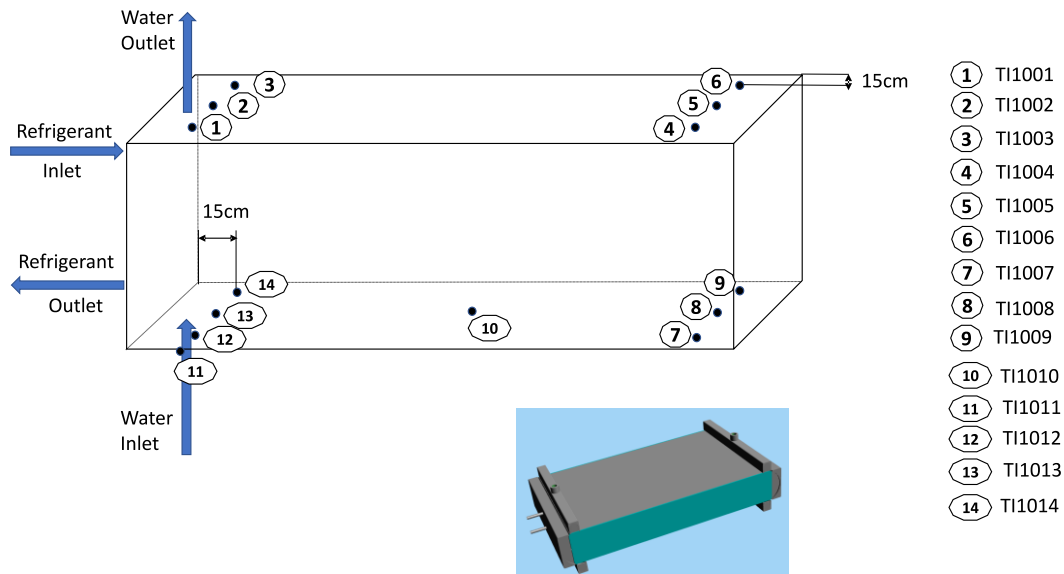


Figure 70: RPW-HEX surface temperature measurements positions.

Heat-conducting paste was used to avoid measurement errors and adhesive tape was used to fix the sensors to the RPW-HEX. The sensors were connected using 4-wires to the PT-100 inputs of the PLC system (Bernecker und Rainer, Type X20ATA312). The temperature sensor application process is illustrated in Figure 71.

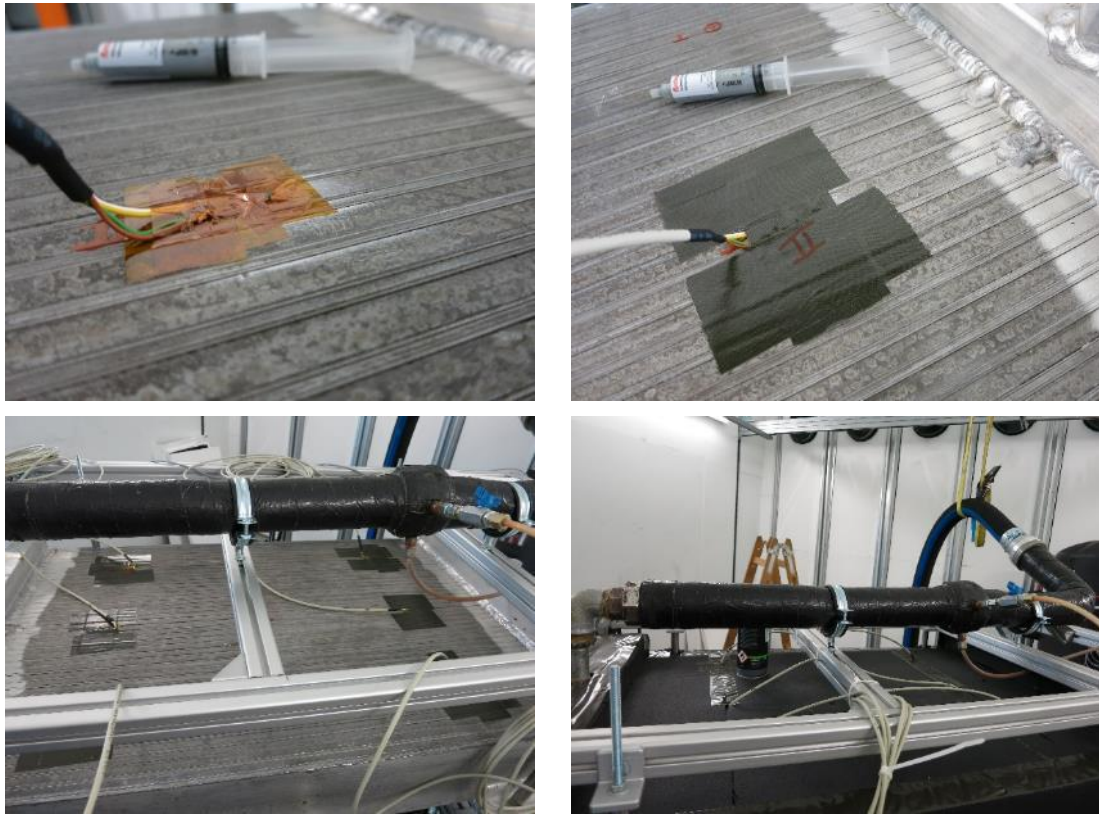


Figure 71: RPW-HEX surface temperature measurements.

**Results:** The measurement setup was operated for several weeks where the expanding PCM reflected a challenge. PCM leaked through the screws and was also found in the pressure hose blocking the pressure measurement (see Figure 72).

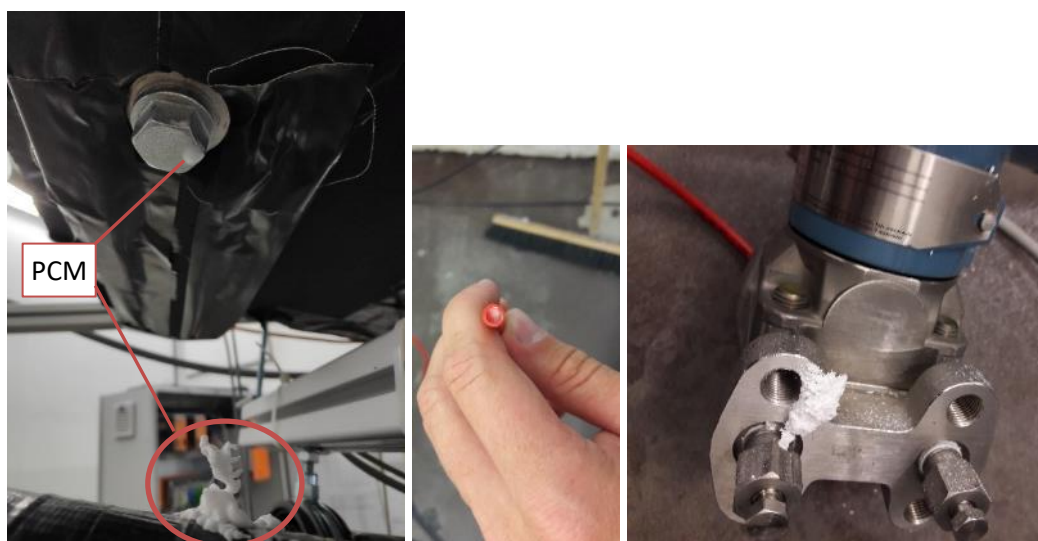


Figure 72: Leaking PCM and blocked pressure hose.

However, for several charging and discharging cycles temperatures and pressure were successfully measured. Temperature measurements for one RPW-HEX discharging cycle is given

in Figure 73. Two distinct temperature plateaux have been observed corresponding to the enthalpy peaks during solidification (cf. Figure 68). The first plateau is at about 64-66°C and the second between 56-58°C.

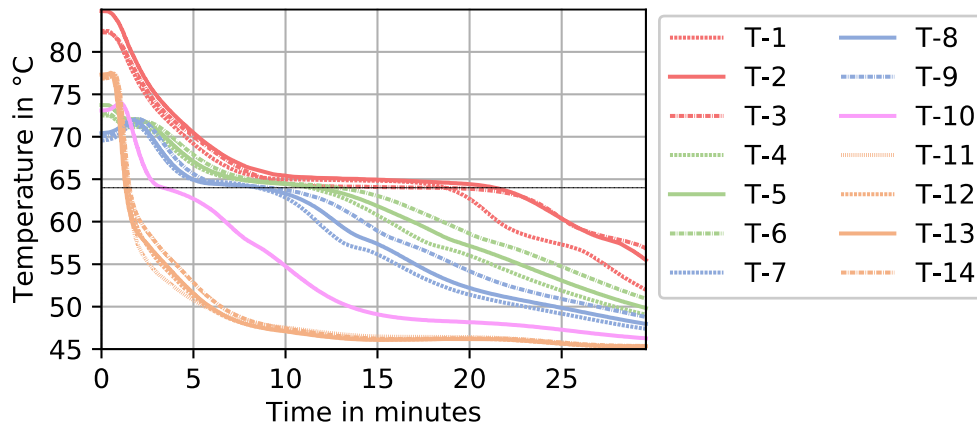


Figure 73: RPW-HEX surface temperature measurements for discharging operation.

The pressure measurement for discharging is given in Figure 74. The first order time-dependent derivative of the pressure  $\dot{p}$  ( $dp/dt$ ) as well as the moving average of  $\dot{p}$  is also given. The measurements reveal that after about 17 minutes there is a sharp decline in  $\dot{p}$  which levels off after about 22 minutes (cf. zoom in Figure 74). The onset (17 minutes) of this step in  $\dot{p}$  corresponds well with the time when T-3 passes 64°C and the end of the step (19 minutes) corresponds well with the time when T-2 passes 64°C.

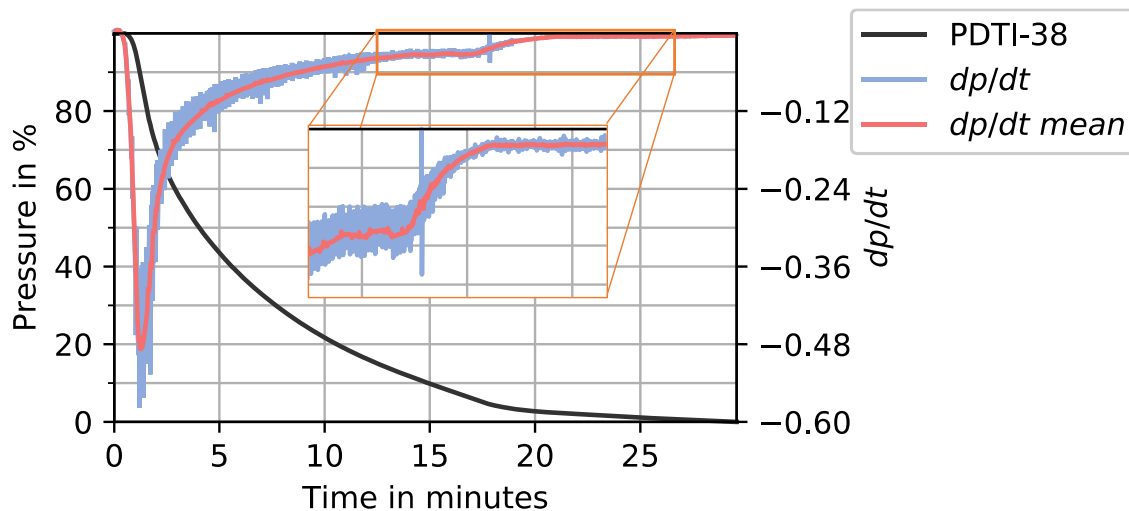


Figure 74: RPW-HEX PCM pressure measurement and including the first order time-dependent derivative of the pressure. A detailed first order time-dependent derivative between 12-27 minutes is also shown.

The measurements reveal that there is evidence that the pressure and its first order time-dependent derivative is a discriminant of the solidification of the PCM inside the RPW-HEX.

### 6.1.6 Conclusions/ recommendations

For thermal energy storage systems based on the use of PCM, the information regarding the SOC is very important from the control strategy point of view. Therefore, a reliable method is deemed necessary to accurately determine the SOC of the PCM at any time. Different methods for SOC determination were previously investigated and are available in the literature, such as

the use of temperature, pressure, level, or electrical conductivity sensors, optical and acoustic properties measurements, or by applying an energy balance.

In this study, four different methods for the determination of the SOC of different prototypes of a latent heat TES tank filled with commercial PCM for HVAC and DHW applications in residential buildings were investigated, based on: (1) average PCM temperature; (2) average specific PCM enthalpy; (3) energy balance of the HTF; and (4) pressure inside the PCM cavity. The results show that each of these methods can be used to estimate the SOC, depending on the level of accuracy required as well as the amount or quality of the instrumentation available.

The four methods for determining the SOC of the PCM tank investigated in this study have both advantages and disadvantages. A good strategy in practical applications could be to combine two or more of these methods and take profit of the advantages of each of the methods. For instance, one could use the method based on pressure measurements combined with the average temperature method, which would not require any information on the PCM properties or TES tank characteristics. The temperature measurements could be used to determine the SOC outside the PCM phase changes range, i.e. when the tank is completely charged or discharged, while the pressure measurements could be used during the phase change. The transition from one method to the other would be dictated by the point when temperature measurements indicate the beginning or the end of the phase change process. Temperature measurements could also be used to calibrate the pressure measurements before each of the phase change process. Therefore, in this case one should be able to distinguish between the sensible and latent contributions to the pressure measurements. The sensible contribution is mainly due to the volume change of the air inside the cavity, and possibly from PCM expansion or contraction when it is totally liquid or solid. The latent contribution only comes from density variation of the PCM during phase change.

To quantify the magnitude of both sensible and latent contributions, an additional experiment was performed with the low-temperature 2-fluid HEX at a flow rate of 0.5 L/min in the sensible temperature range between 12°C and 26 °C to compare it to the temperature range of the same amplitude but between -2 °C and 12 °C, which includes the latent temperature range of the PCM.

Figure 75 shows the pressure variation in both sensible and latent temperature ranges. The temperature at the center of the HEX ( $T_3$ ) is also shown in the graph to give a rough indication of the average PCM temperature and, therefore, of the SOC. During the first 40 minutes of the experiment, the PCM is cooled down in the sensible range from 26 °C to 12 °C. The pressure drop in this range is 0.17 bar, from 1.08 bar to 0.91 bar, due to the sensible contribution only. During the next 40 minutes, the PCM is further cooled down from around 13 °C to -1 °C, and the pressure drops 0.36 bar, from 0.94 bar to 0.58 bar, due to both the sensible and latent contributions. Therefore, by subtracting the sensible contribution one can get the latent contribution of 0.19 bar, which is almost the same as the sensible contribution. At around 120 minutes the discharging process is initiated. The PCM is heated from -2 °C to 12 °C during 40 minutes, and the pressure increases 0.37 bar in this temperature range, from 0.59 bar to 0.96 bar. Finally, the PCM is heated in the sensible range from 13 °C to 26 °C, and the pressure increases 0.11 bar, from 0.97 to 1.08 bar. Thus, the pressure variation in the latent range is very similar for charging and discharging processes (0.36 bar vs. 0.37 bar), while there is a slight difference in the sensible range, being the variation during discharging less than during charging (0.11 bar vs. 0.19 bar). This may happen because the discharging process started immediately after the end of the charging process, and the temperature distribution inside the HEX could probably not have been uniform, which might have caused a deviation of the pressure inside the air cavity with respect to the expected value.

Figure 75 also shows an estimation of the latent contribution to the total pressure (denoted as 'Pressure\_lat') that was obtained by subtracting the sensible contribution term, which was assumed to be a linear function of  $T_3$ , from the total pressure. It can be noticed how the latent

contribution is kept constant around 0.75 bar outside the phase change range, and it decreases to a minimum around 0.58 bar when the HEX is supposed to be completely charged (no contribution from the sensible term). A slight deviation from the expected value of around 0.75 bar occurs just after the discharging process, where the latent term contribution increases to around 0.80 bar during 30 minutes, after which it slightly decreases towards 0.75 bar.

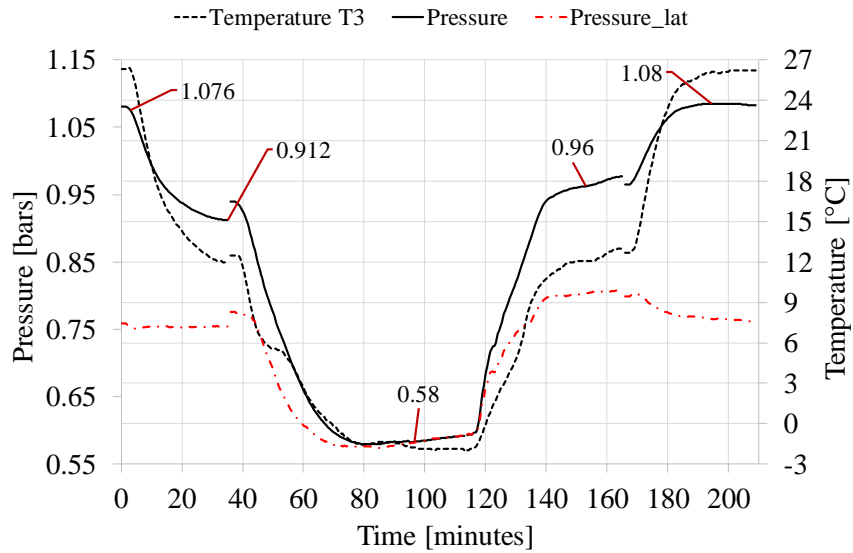


**Figure 75. Pressure and temperature evolution in the sensible and latent temperature ranges for both charging and discharging processes at 0.5 L/min.**

In view of the above analysis, the method based on pressure measurements inside the PCM cavity can be applied to estimate the SOC of the HEX because there is a direct relation between the pressure and the state of the PCM.

## 7 Conclusions

The present deliverable reports the activity on the development of high and low temperature heat storages for the Continental and Mediterranean HYBUILD systems. The activity was mainly divided in three sub-tasks:

- At first, a selection process based on process requirements, as well as safety and economic constraints, allowed the identification of the PCMs to be employed in the storages;
- Lab-scale storages were designed, manufactured and tested in laboratory (AIT for the Continental storage, UDL for the Mediterranean one). The effect of PCM features and operating parameters on the behavior of the storage was evaluated.
- Based on experimental results, full-scale storages were designed and manufactured;
- Finally, different techniques for the monitoring of the SOC of the storage were evaluated and the most promising one was identified.

## 8 References

- [1] Pardiñas ÁÁ, Alonso MJ, Diz R, Kvalsvik KH, Fernández-Seara J. State-of-the-art for the use of phase-change materials in tanks coupled with heat pumps. *Energy Build* 2017;140:28–41. <https://doi.org/10.1016/J.ENBUILD.2017.01.061>.
- [2] Kapsalis V, Karamanis D. Solar thermal energy storage and heat pumps with phase change materials. *Appl Therm Eng* 2016;99:1212–24. <https://doi.org/10.1016/J.APPLTHERMALENG.2016.01.071>.
- [3] Zou D, Ma X, Liu X, Zheng P, Cai B, Huang J, et al. Experimental research of an air-source heat pump water heater using water-PCM for heat storage. *Appl Energy* 2017;206:784–92. <https://doi.org/10.1016/J.APENERGY.2017.08.209>.
- [4] Song M, Deng S, Dang C, Mao N, Wang Z. Review on improvement for air source heat pump units during frosting and defrosting. *Appl Energy* 2018;211:1150–70. <https://doi.org/10.1016/J.APENERGY.2017.12.022>.
- [5] Cabeza LF, Castell A, Barreneche C, de Gracia A, Fernández AI. Materials used as PCM in thermal energy storage in buildings: A review. *Renew Sustain Energy Rev* 2011;15:1675–95. <https://doi.org/10.1016/J.RSER.2010.11.018>.
- [6] Emhofer J, Barz T, Marx K, Hochwallner F, Cabeza, L.F., Zsembinski, G, Strehlow A, Nitsch B, et al. Integration of a compact two fluid PCM heat exchanger into the hot superheated section of an air source heat pump cycle for optimized DHW generation. 2019.
- [7] Gasia J, Miró L, de Gracia A, Barreneche C, Cabeza L. Experimental Evaluation of a Paraffin as Phase Change Material for Thermal Energy Storage in Laboratory Equipment and in a Shell-and-Tube Heat Exchanger. *Appl Sci* 2016;6:112. <https://doi.org/10.3390/app6040112>.
- [8] Miró L, Barreneche C, Ferrer G, Solé A, Martorell I, Cabeza LF. Health hazard, cycling and thermal stability as key parameters when selecting a suitable phase change material (PCM). *Thermochim Acta* 2016;627–629:39–47. <https://doi.org/10.1016/J.TCA.2016.01.014>.
- [9] Oró E, de Gracia A, Castell A, Farid MM, Cabeza LF. Review on phase change materials (PCMs) for cold thermal energy storage applications. *Appl Energy* 2012;99:513–33. <https://doi.org/10.1016/j.apenergy.2012.03.058>.
- [10] Veerakumar C, Sreekumar A. Phase change material based cold thermal energy storage: Materials, techniques and applications - A review. *Int J Refrig* 2016;67:271–89. <https://doi.org/10.1016/j.ijrefrig.2015.12.005>.
- [11] Rubitherm. Rubitherm 2019.
- [12] PCMproducts. PCM Products 2019.
- [13] PCES. Phase Change Energy Solutions 2019.
- [14] RGEES. RGEES LLC 2019.
- [15] PLUSS. PLUSS® 2019.
- [16] Shengli T, Dong Z, Deyan X. Experimental study of caprylic acid/lauric acid molecular alloys used as low-temperature phase change materials in energy storage. *Energy Conserv* 2005;6:45–7.
- [17] PureTemp. PureTemp LLC 2019.

- [18] Jankowski NR, McCluskey FP. A review of phase change materials for vehicle component thermal buffering. *Appl Energy* 2014;113:1525–61. <https://doi.org/10.1016/j.apenergy.2013.08.026>.
- [19] Zsembinszki G, Fernández AG, Cabeza LF. Selection of the appropriate phase change material for two innovative compact energy storage systems in residential buildings. *Appl Sci* 2020;10:2116. <https://doi.org/10.3390/app10062116>.
- [20] Pereira J, Cunha D, Eames P. Thermal energy storage for low and medium temperature applications using phase change materials – A review. *Appl Energy* 2016;177:227–38. <https://doi.org/10.1016/j.apenergy.2016.05.097>.
- [21] Pielichowska K, Pielichowski K. Phase change materials for thermal energy storage. *Prog Mater Sci* 2014;65:67–123. <https://doi.org/10.1016/j.pmatsci.2014.03.005>.
- [22] Mehling H, Cabeza LF. Heat and cold storage with PCM. An up to date introduction into basics and applications. 1st ed. Springer-Verlag Berlin Heidelberg; 2008. <https://doi.org/10.1007/978-3-540-68557-9>.
- [23] Zalba B, Marín J, Cabeza L, Mehling H. Review on thermal energy storage with phase change: materials, heat transfer .... vol. 23. 2003.
- [24] Climator. Climator 2019.
- [25] Kenisarin M, Mahkamov K. Salt hydrates as latent heat storage materials: Thermophysical properties and costs. *Sol Energy Mater Sol Cells* 2016;145:255–86. <https://doi.org/10.1016/j.solmat.2015.10.029>.
- [26] Sharma A, Tyagi V V, Chen CR, Buddhi D. Review on thermal energy storage with phase change materials and applications n.d. <https://doi.org/10.1016/j.rser.2007.10.005>.
- [27] Rohsenow WM, Hartnett JP (James P., Cho YI. Handbook of heat transfer. McGraw-Hill; 1998.
- [28] Barz T, Emhofer J. Paraffins as phase change material in a compact plate-fin heat exchanger - Part I: Experimental analysis and modeling of complete phase transitions. *J Energy Storage* 2021;33:102128. <https://doi.org/10.1016/j.est.2020.102128>.
- [29] Zsembinszki G, Orozco C, Gasia J, Barz T, Emhofer J, Cabeza LF. Evaluation of the State of Charge of a Solid/Liquid Phase Change Material in a Thermal Energy Storage Tank. *Energies* 2020;13:1425. <https://doi.org/10.3390/en13061425>.
- [30] The Dow Chemical Company. Dowtherm SR-1 n.d.
- [31] Mselle BD, Vérez D, Zsembinszki G, Borri E, Cabeza LF. Performance Study of Direct Integration of Phase Change Material into an Innovative Evaporator of a Simple Vapour Compression System. *Appl Sci* 2020;10:4649. <https://doi.org/10.3390/app10134649>.
- [32] Gasia J, de Gracia A, Peiró G, Arena S, Cau G, Cabeza LF. Use of partial load operating conditions for latent thermal energy storage management. *Appl Energy* 2018;216:234–42. <https://doi.org/10.1016/j.apenergy.2018.02.061>.
- [33] Paberit R, Öjertborn J. Detecting State of Charge in PCMs - Experimental investigation of changes in chemical and physical properties during phase transitions. Chalmers University of Technology, Gothenburg, Sweden, 2016.
- [34] Steinmaurer G, Krupa M, Kefer P. Development of sensors for measuring the enthalpy of PCM storage systems. *Energy Procedia* 2014;48:440–6. <https://doi.org/10.1016/j.egypro.2014.02.052>.

- [35] Grama, S., Dorson, M. H., Christianson R. Thermal energy battery with enhanced heat exchange capability and modularity. WO2014059163, 2013.
- [36] Dixler, K., Kwok W. Active and passive cooling for an energy storage module. US20140158340, 2012.
- [37] Barz T, Seliger D, Marx K, Sommer A, Walter SF, Bock HG, et al. State and state of charge estimation for a latent heat storage. *Control Eng Pract* 2018. <https://doi.org/10.1016/j.conengprac.2017.11.006>.
- [38] Kazuhiro, D., Tetsuya, I., Yasuyuki, U., Yuka, U., Takashi Y. Cooling equipment, temperature control system, air conditioning system, and hot water supply system for the same. US2014124158A1, 2014.
- [39] Barz T. Method for determining the charge level of a latent heat storage device. EP3336473, 2017.
- [40] Beaupere, N., Soupremanien, U., & Zalewski L. Solidification monitoring of supercooled phase change materials. 12th IIR Conf. Phase-Change Mater. Slurries Refrig. Air Cond. (PCM 2018), Orford (Quebec), Canada: International Institute of Refrigeration (IIR); 2018, p. 166–73. <https://doi.org/10.18462/iir.pcm.2018.0022>.
- [41] Charvát P, Štětina J, Mauder T, Klimeš L. Visual monitoring of the melting front propagation in a paraffin-based PCM. *EPJ Web Conf* 2017;143:02042. <https://doi.org/10.1051/epjconf/201714302042>.
- [42] Zhou G, Zhu M, Xiang Y. Effect of percussion vibration on solidification of supercooled salt hydrate PCM in thermal storage unit. *Renew Energy* 2018:537–44. <https://doi.org/10.1016/j.renene.2018.03.077>.
- [43] Wang Y, Amiri A, Vafai K. An experimental investigation of the melting process in a rectangular enclosure. *Int J Heat Mass Transf* 1999;42:3659–72. [https://doi.org/10.1016/S0017-9310\(99\)00024-1](https://doi.org/10.1016/S0017-9310(99)00024-1).
- [44] Fischer UR, Maschke U, Schneider J. Entwicklung eines Messverfahrens zur Bestimmung des thermischen Beladungsgrades von PCM-Paraffin-Speichern : Schlussbericht zum BMWi-Projekt 0327370F; Verbundprojekt Energie Optimiertes Bauen (EnOB), Thematischer Verbund LowEx. Cottbus: 2008. <https://doi.org/https://doi.org/10.2314/GBV:590236296>.
- [45] Klimeš L, Mauder T, Charvát P, Štětina J. A Front Tracking Method Accelerated by Graphics Processing Units for Phase Change Modelling in Latent Heat Thermal Energy Storage: A Comparison with Interface Capturing Methods. *Chem. Eng. Trans.*, vol. 61, 2017. <https://doi.org/10.3303/CET1761171>.
- [46] Klimeš L, Mauder T, Charvát P, Štětina J. Front tracking in modelling of latent heat thermal energy storage: Assessment of accuracy and efficiency, benchmarking and GPU-based acceleration. *Energy* 2018;155:297–311. <https://doi.org/10.1016/j.energy.2018.05.017>.
- [47] Chazelle, B., Couturier, R., Martinelli M. System and method for determining the charge level of a latent heat store. EP3201555, 2014.
- [48] Henze, G. P., Kalz, D. E., Liu, S., Felsmann C. Experimental analysis of model-based predictive optimal control for active and passive building thermal storage inventory. *HVAC&R Res* 2005;11:189–213. <https://doi.org/10.1080/10789669.2005.10391134>.
- [49] Sugo H, Kisi E, Bradley J, Fiedler T, Luzin V. In situ neutron diffraction studies of operating MGA thermal storage materials. *Renew Energy Environ Sustain* 2017;2:34.

<https://doi.org/10.1051/rees/2017023>.